The Pennsylvania State University

The Graduate School

Department of Mechanical and Nuclear Engineering

CHEMICAL SIGNATURES FOR UNKNOWN AND INTERDICTED SAMPLES IN THE ENVIRONMENT FOR NUCLEAR FORENSIC ANALYSIS

A Dissertation in

Nuclear Engineering

by

Chad Bredthauer Durrant

Submitted in Partial Fulfillment
of the Requirements
for the Degree of

Doctor of Philosophy

August 2017

The dissertation of Chad Bredthauer Durrant was reviewed and approved* by the following:

Dr. Kenan Ünlü
Professor of Nuclear Engineering
Director of the Radiation Science and Engineering Center
Dissertation Advisor
Chair of Committee

Dr. Jack Brenizer
Emeritus Professor of Mechanical and Nuclear Engineering

Dr. Marek Flaska
Professor of Nuclear Engineering

Dr. Peter Heaney
Professor of Geosciences

Dr. Annie Kersting
Director, University Relations and Science Education,
Lawrence Livermore National Laboratory, Livermore CA 94550
Laboratory Mentor

Dr. Dawn Shaughnessy
Group Leader, Nuclear and Radiochemistry,
Lawrence Livermore National Laboratory, Livermore CA 94550
Laboratory Mentor

Karen A. Thole
Professor of Mechanical and Nuclear Engineering
Chair of the Mechanical and Nuclear Engineering Department

*Signatures are on file in the Graduate School

ABSTRACT

Irradiation of materials may produce unique signatures that can be measured and identified through the various types of radiation particles emitted from the materials. The emitted particles may be characteristic to specific radioisotopes thereby allowing the identification and characterization of the irradiated material. The characterization of a potentially radioactive material and then determining its origin is useful in diverse applications including nuclear forensics samples. This thesis investigates problems associated with two areas, improving the understanding of radionuclide transport in the environment and improving the speed with which samples can be chemically separated. Both topics are relevant to increasing the ability to apply nuclear forensics techniques to unknown samples in the environment.

Understanding sorption and desorption processes is essential to predicting the mobility of radionuclides in the environment. Typically, such sorption reactions are studied in single mineral binary systems. This work investigates adsorption/desorption of cesium (Cs) in both binary and two-mineral "ternary" systems in order to study component additivity, desorption kinetics and sorption reversibility in the presence of two competing minerals. First, binary Cs sorption experiments were performed with the clay minerals, illite, montmorillonite, and kaolinite, in a $NaHCO_3$ solution over a Cs concentration range of 10^{-3} to 10^{-11} M to quantify the non-linear (illite) and linear (kaolinite and montmorillonite) sorption behavior. The binary sorption experiments were followed by desorption experiments to test for sorption reversibility. Cesium exhibits partial irreversible sorption to illite whereas Cs sorption to kaolinite and montmorillonite is reversible. In the ternary experiments, Cs was separately sorbed to illite,

montmorillonite or kaolinite for ~14 days, and then Cs-free illite was place inside a dialysis bag (Float-a-lyzer®) inside the beaker with the pre-sorbed clays to induce desorption of the originally adsorbed Cs. Results from these ternary experiments show significantly greater Cs desorption compared to the binary desorption experiments. The ternary experiments confirm batch desorption findings of irreversible sorption of some Cs to illite and reversible sorption of Cs to kaolinite and montmorillonite.

Plutonium (Pu), which has significantly more complex aqueous chemistry than Cs, is another radionuclide of chief concern in environmental contamination and transport scenarios. The dialysis bag experimental setup and procedure, which was designed and tested in the Cs experiments, was then applied to experiments using Pu to investigate the sorption and long-term desorption behavior of Pu in the presence of two minerals. These experiments were specifically designed to look at the long-term (7 months) reversibility of Pu sorption to montmorillonite in the presence of goethite, both common minerals in a variety of geologic environments. The distribution coefficient, K_d, of Pu sorption to montmorillonite continued to increase over the duration of the experiment, indicating that equilibrium in a ternary system is a long process occurring over several months to years. Results suggest that Pu on montmorillonite is reversible at pH 8, with up to 14 percent of the Pu desorbing from the montmorillonite and sorbing to the goethite. This would suggest that goethite may be the more important mineral influencing long-term colloid-facilitated transport of Pu.

Additional studies were undertaken to explore the development and testing of an automated chemical separation system for post-detonation nuclear forensic related samples. The development of this chemical separation system entailed identifying a

suitable chemical separation sequence to sequentially separate eight elements; europium (Eu), gadolinium (Gd), neptunium (Np), plutonium (Pu), promethium (Pm), terbium (Tb), uranium (U), and zirconium (Zr), elements that may be of interest for post-detonation nuclear forensic analysis. A likely post-detonation situation could be in an urban environment where many samples could have a significant cement matrix associated with the sample. The chemical separation scheme would need to account for this given matrix and the large mass of associated material. To this end, batch sorption and separation experiments were conducted to examine the sorption behavior of Pu and U on AG 1x8 resin in varying concentrations of hydrochloric acid (HCl) and dissolved cement. These batch experiments were used to determine possible interferences or adverse separation effects that may result from a high concentration cement matrix. Similar batch sorption experiments with varying acid and cement concentrations were also conducted with Eu and Eichrom's LN® and TRU® resins in order to determine possible adverse consequences as a result of interferences caused by the cement.

The hardware for the separation system consisted of several pumps, valves, ion-exchange columns, and a fraction collector. A software program written in LabVIEW was developed to control the hardware. A test separation experiment was conducted with uranium (U), lead (Pb), and tin (Sn) isotopes to troubleshoot and test the ability of the system to sequentially separate elements. The trial run successfully separated the elements; however, several changes were made afterwards including the addition of an injection loop, a fraction collector, and changing the tubing such that eluents flowed through a more chemically inert material that was less susceptible to corrosion.

After developing the chemical separation scheme and system design was finished, it was tested with five surrogate samples. The purpose of using the automated chemical separation system was to shorten the time necessary to effectively separate the eight elements of interest. The total run-time for the system was 160 minutes including sample injection, sequential separation, and wash/regeneration steps. Four of the samples had a known composition, including one that had a cement-like matrix. The elemental fractions recovered were consistent across each sample including the cement-like sample. This consistency is indicative of the robustness of the system and its ability to handle even samples with significant background mass. The final sample was of unknown composition and used to demonstrate the ability of the automated chemical separation system to sequentially separate the elements of interest and accurately determine the initial sample composition. This automated chemical separation system was a proof of concept that the eight specified elements could successfully be separated using automation and used to determine the composition of an unknown sample. Actinide recoveries were around 90% and lanthanide recoveries were around 30%.

TABLE OF CONTENTS

LIST OF FIGURES

LIST OF TABLES

LIST OF ABBREVIATIONS

α-HIBA	Alpha-hydroxyisobutyric acid
ACS	American Chemical Society
AG 1x8	Analytical Grade ion exchange resin
AW	Atomic Weight
CEC	Cation Exchange Capacity
Ci	Curies
CMPO	Octylphenyl-N,N-di-isobutyl carbamoylphosphine oxide
CPM	Counts Per Minute
CPS	Counts Per Second
eV	Electronvolt
FEP	Fluorinated Ethylene Propylene
FES	Frayed Edge Sites
FIR	Far Infrared Spectroscopy
HDEHP	Di-2-ethylhexylorthophosphoric acid
HPGe	High Purity Germanium
HPLC	High performance/pressure liquid chromatography
ICP-MS	Inductively Coupled Plasma Mass Spectrometry
K_d	Distribution Coefficient
K_{SEL}	Selectivity Coefficient
LaF_3	Lanthanum Fluoride
LLNL	Lawrence Livermore National Laboratory
LSC	Liquid Scintillation Counting
meq	Milliequivalent
MQ	Milli Q water
MW	Molecular Weight
MWCO	Molecular Weight Cut-Off Size
NMR	Nuclear Magnetic Resonance Spectroscopy
PBq	Petabecquerel
PEEK	Polyetheretherketone

PPM	Parts Per Million
PTFE	Polytetrafluoroethylene
PUREX	Plutonium Uranium Redox Extraction
RDD	Radiation Dispersal Device
SDK	Software Development Kit
TBP	Tributyl Phosphate
TOT	Tetrahedral Octahedral Tetrahedral
tSIE	Transform Spectral Index of the External Standard
XRD	X-Ray Diffraction

ACKNOWLEDGEMENTS

At the close of this journey I would be remiss if I did not acknowledge and thank by name some of the many individuals who supported me through this process. I want to start by thanking my wife, Sojin, because without her patience, support and encouragement, this journey would have been that much more difficult. Thank you for your patience, especially towards the end, as I spent many long hours at work either in the lab or writing. Also, I want to thank my daughters, Hana and Halyn, who may not realize the sacrifices they made or how much strength and resolve I received each time I saw their smiling faces and all the hugs and kisses they gave each morning as I left to go work. I want to thank my parents for teaching me from a young age to have determination and to finish things that I start. Their continued support and love motivated me when I was tired at night and wanted to push the tasks off to the next day. Thank you for teaching me the value of education and seeking after knowledge. I want to thank my father and mother-in-law as well. My father-in-law made a concerted effort to become knowledgeable about anything nuclear related and hearing his support for my studies was very inspiring. My mother-in-law also made many a great sacrifice of her time to come and help us during the birth of our two daughters, which allowed me to quickly return to work and focus on my studies and research. Without each of my family members and their backing and encouragement earning a PhD would have been a much more difficult challenge to overcome.

Professionally I am indebted to numerous individuals as well. First, I would like to thank Professor Kenan Ünlü, my advisor, for his mentorship and support as I took a somewhat circuitous path from Penn State to Lawrence Livermore National Laboratory

in pursuit of my PhD. Dr. Amanda Johnsen's exceptional mentorship and guidance particularly with respect to lab work and safety left an indelible impression and her meticulous approach and perseverance will no doubt be an example for me throughout the rest of my career. Also thank you to Dr. Sarah Bender, one of my peers at Penn State, for being a sounding board for ideas, concerns, preventing me from overstressing during the candidacy exam period, and most of all for being a friend. I also want to acknowledge the Penn State Breazeale Reactor staff, without whose help conducting research at the reactor would have been most difficult. I want to thank all of the other many friends and families from State College who are too numerous to count, for your friendship during this journey.

I want to thank fantastic mentors and peers from my time at Lawrence Livermore National Laboratory. I was fortunate enough to work with two outstanding groups and have Drs. Annie Kersting and Dawn Shaughnessy as mentors. I want to thank them for their graciousness in mentoring and supporting me and the research projects that I worked on. They were both extremely busy, yet they also made time for me whenever I asked and were also always quick with words of advice and encouragement. I want to thank Dr. Mavrik Zavarin for his advice and counsel and the copious time spent reviewing much of my work before presenting including papers, posters, and presentations. Thanks are also due to all of the members of the subsurface biogeochemical group and experimental nuclear and radiochemistry groups. Their advice and input was essential for the preparation and carrying out of all the experiments I conducted while at Lawrence Livermore National Laboratory. Last but certainly not least I wish to thank Dr. James Begg. His patience to let me struggle to find answers and draw

conclusions on my own is primarily responsible for the growth I have experienced as a scientist. His thoughtful evaluation of all aspects of my work, from experimental design to data analysis to writing, provided the necessary critiques I needed in order think more concisely and critically about my work. I am deeply indebted to him for the time and attention that he so willingly gave during my time working on this thesis.

Finally, I want to thank the Nuclear Forensics Graduate Fellowship program and the Lawrence Graduate Scholar program for their sponsorship and financial support in my endeavor to earn a doctoral degree. These programs provided me not only with financial support, but with unique opportunities to visit numerous national labs, meet experts in technical nuclear forensics analysis, and make connections that will be invaluable in my career going forward.

Academic Disclaimer

The author wrote this dissertation in support of requirements for the degree Doctor of Philosophy in Nuclear Engineering at The Pennsylvania State University, University Park, PA. The research is funded in part by the LLNL Graduate Scholars Program, and is not a deliverable for any United States government agency. The views and opinions expressed are those of the author, and do not state or reflect those of the United States government or Lawrence Livermore National Security, LLC.

LLNL Disclaimer

Neither the United States government nor Lawrence Livermore National Security, LLC, nor any of their employees makes any warranty, expressed or implied, or assumes any legal liability or responsibility for the accuracy, completeness, or usefulness of any information, apparatus, product, or process disclosed, or represents that its use would not

infringe privately owned rights. Reference herein to any specific commercial product, process, or service by trade name, trademark, manufacturer, or otherwise does not necessarily constitute or imply its endorsement, recommendation, or favoring by the United States government or Lawrence Livermore National Security, LLC, and shall not be used for advertising or product endorsement purposes.

NFGF Disclaimer

Part of this research was performed under the Nuclear Forensics Graduate Fellowship Program, which is sponsored by the U.S. Department of Homeland Security, Domestic Nuclear Detection Office and the U.S. Department of Defense, Defense Threat Reduction Agency. This material is based upon work supported by the U.S. Department of Homeland Security under Grant Award Number, 2012-DN-130-NF0001-02. The views and conclusions contained in this document are those of the authors and should not be interpreted as necessarily representing the official policies, either expressed or implied, of the U.S. Department of Homeland Security.

Chapter 1

Introduction

The discovery of nuclear fission was the fundamental driving force behind numerous advances in the fields of nuclear chemistry and nuclear physics and many corresponding engineering achievements during the past century. Some of these achievements, such as nuclear weapons, have had devastating consequences. Other achievements, such as nuclear power or medical isotope production for various medical treatments, have provided many benefits to society. However, even these generally positive achievements have been the source of accidents and catastrophes with severe consequences. Effectively managing these crises can help to mitigate both immediate and long-term effects. Sometimes the sites of these radioactive events can be managed quickly and efficiently preventing significant long-term consequences to the public, such as the Three Mile Island incident. Oftentimes these nuclear/radioactive events, whether from nuclear weapons testing and the resulting fallout, or power plant accidents such as Chernobyl and Fukushima, result in environmental impacts that must be monitored and managed for decades and perhaps even centuries.

In order to effectively manage the consequences of these events, it is important to understand the origin of these events, their transport mechanisms, and to try and assess the impact that each incident may have. In the United States protocols and guidelines have been established to respond to a catastrophe caused by nature, accident, or acts of

terror [1] and more specifically for radiological events [2]. The US Department of Defense (DOD), Department of Energy (DOE), and Department of Homeland Security (DHS) are the primary coordinating agencies who then interact with many other entities within the US government depending on the type of incident [2]. Depending on the type of radiological incident, one or more response teams from the primary coordinating agencies may be deployed to assess hazards or threats posed to the community and/or gather information regarding the causation of the radiological event [3] [2]. The study of these radioactive events and determining their origins is a subset of forensic science entitled, nuclear forensics.

1.1 Nuclear Forensics

Forensic science at the most fundamental level is any science that can be used in, or is suitable for, a court of law. The science pertaining to the legal matter should be unbiased and objective [4]. Nuclear forensics is a subset of the forensic sciences focused specifically on characterizing radioactive materials with respect to the material, both radioactive and non-radioactive, its origin, how the material was obtained, and who was involved or responsible [5].

With the increased awareness of terrorism over the last few decades, most nuclear forensics cases typically relate to the proliferation or smuggling of nuclear materials. It is hoped that individuals who attempt to transport nuclear materials or sell these materials on the black market are caught and the material is confiscated before the transaction can take place. The confiscated material can then be analyzed to determine what it is and

where it came from [6] [7] [8] after which law enforcement agencies determine how the material came to be in the possession of those persons and how to prosecute them.

Nuclear forensics is an important focus for the United States. Domestically there are numerous sites that have been contaminated as a result of weapons testing and production. Understanding how the various radionuclides interact and can or cannot be transported in the environment is crucial to determining potential health and environmental effects on nearby populations. As the only country ever to use an atomic weapon on another country, the US is also acutely aware of the destructive impact as well as the need to quickly analyze debris in order to make proper attribution and develop an appropriate response. In order to achieve these goals, numerous research programs at both national laboratories and universities spend a significant amount time developing models and programs that can help achieve these goals.

1.2 Environmental Radiochemistry

Tracing the transport of radioactive material through the environment is an important aspect of nuclear forensics as it can help determine the origin of the material. Environmental nuclear forensics is less concerned with attributing the material to persons with criminal intent, but rather to study the social and environmental impacts and then draw conclusions about possible actions that can be taken to mitigate any potential detrimental consequences. Since the advent of nuclear weapons and nuclear power, a diverse array of radionuclides has been introduced into the environment, both intentionally and unintentionally. When radioactive material is found in the environment, it is important to determine what the material is, the origin of the material, and how the

material got there. After this information is determined, the environmental and health impacts of the radioactive material, as well as any necessary remediation actions, can be decided.

While there are many environmentally important radionuclides, this work focuses on radionuclides of two elements, cesium (Cs) and plutonium (Pu). Nuclear weapons testing, nuclear power accidents, leaks and intentional discharges at high level waste storage sites, have all contributed large quantities of these radionuclides to the environment. The fast and thermal neutron fission reactions for most common nuclear fuels produces ^{137}Cs with a fission product yield greater than six percent [9]. The relatively high fission product yield of ^{137}Cs combined with its half-life of 30.17 years make ^{137}Cs one of the more common radionuclides found to persist in the environment. The total ^{137}Cs released from nuclear weapons testing is estimated to be nearly 950 PBq [10] and the total ^{137}Cs released from the Chernobyl, Fukushima, and Hanford sites is nearly 500 PBq [11] [12] [13] [14] [15]. Hundreds of PBq of radioactive Cs have been introduced to the environment; however, in order to minimize exposure to the carcinogenic effects of radiation from ^{137}Cs, the United States Environmental Protection Agency (US EPA) has put a limit on ^{137}Cs in drinking water of 7.4 Bq/L or 1.7×10^{-14} M assuming no other radionuclides are present [16]. Understanding where ^{137}Cs exists and how it can be transported in the environment is important for maintaining safety and developing remediation strategies for affected communities.

The sorption characteristics of Cs to various minerals have been extensively studied through batch sorption and desorption experiments. Clay minerals found ubiquitously in the environment have shown a propensity for the rapid sorption of

significant quantities of Cs [17] [18] [19] [20]. However, in the environment, Cs associated with one mineral does necessarily remain stagnant. As the Cs bearing mineral is transported in groundwater, it is probable that it will encounter different minerals and sorption conditions that can affect how the Cs will behave. This work investigates the behavior of Cs sorption in complex, multi-mineral systems. These results are then used to refine environmental transport models and make more accurate public health risk assessments. A more comprehensive description of Cs sorption behavior and results of the Cs sorption in multi-mineral conditions can be found in Chapter 2.

Since the discovery of Pu, more than 2000 MT has been released into the environment as a result of nuclear weapons testing, accidents and discharges [21]. Plutonium is very toxic chemically as well as being radioactive with a long half-life (>24,000 years for ^{239}Pu). It is estimated that the LD_{50}(30), or lethal dose to 50 percent of the population after 30 days, is less than 100 mg of Pu inhaled and less than 25 mg of Pu injected intravenously [22]. As a result of these adverse health effects, the EPA has established very low limits for Pu in drinking water of 15 pCi/L or 0.55 Bq/L. On a molar basis this is equivalent to 1×10^{-12} M ^{239}Pu, 3×10^{-13} M ^{240}Pu, or 4×10^{-15} M ^{238}Pu. For comparison, the EPA acceptable limits for other trace elements such as arsenic, lead, and uranium are 13×10^{-8} M, 7.2×10^{-8} M, and 13×10^{-8} M respectively [23]. Thus, Pu in the environment poses many unique challenges and concerns for those living near sites where Pu contamination exists. Understanding how Pu is transported or immobilized in the subsurface is essential for developing environmental transport models for Pu migration.

In the subsurface, Pu exists with multiple minerals and oftentimes organic matter in the groundwater, thereby creating tertiary, ternary, quaternary, etc. molecular systems. Each mineral and organic phase can cause the Pu to react in a different way within the environment. However, all current environmental reactive transport models for Pu are based exclusively on binary mineral systems, i.e., one mineral interacting with Pu, but these binary systems are too simplistic to represent what is actually happening in the environment. Using a methodology developed to study Cs in multi-mineral systems; this work discusses the results of Pu behavior in two-mineral systems. A more thorough description of Pu sorption behavior in the subsurface as well as results of Pu sorption in multi-mineral conditions can be found in Chapter 3.

1.3 Post-Detonation Nuclear Forensics

There is poignant evidence of the tragic destruction that can come from the detonation of a nuclear device as evidenced by the two bombs dropped on Nagasaki and Hiroshima during World War II. Over 100,000 people perished immediately from the bomb blasts and approximately an equal number died over the next several months and years from burns, radiation sickness and other injuries. Thousands of acres of city and farmland were demolished [24]. If a nuclear weapon or radiation dispersal device (RDD) were used today, one of the principal primary objectives would be to determine what the source material for the device was and who was responsible for its use. Samples from the surrounding areas would undergo a suite of chemical separations and analyses to determine various characteristics of the device. For a fission device, first the fuel type is

identified to determine the sophistication of the device. Next, fission products and various trace elements are identified in order to develop a set of isotopic signatures that determine characteristics such as device yield and the material's origin. This process is very labor intensive and the chemical analyses of the samples can take several weeks.

The very high radiation field of the sample area and gamma ray interferences caused by the fission products drastically limit the ability to discriminate between individual radionuclides. This in turn inhibits the effectiveness of portable detectors. Instead, the samples must be analyzed at a laboratory. The samples, which could be any number of matrices including cement, glassy beads and various organic matter, must then be prepared for analysis. This likely means a complete dissolution of the sample will be required which can be time consuming. Next, a procedure for separating a majority of the matrix components from the radioactive components is carried out. Then the actinides, in particular neptunium, plutonium and uranium are separated [5]. In addition, all workers will be potentially exposed to significant does of radioactivity, especially during dissolution and separation procedures, due to the large amount of fission products that would be present in these samples.

An automated chemical separation system would reduce the potential dose to the worker. This work describes the development of a system to automate the chemical separation of up to eight elements, europium (Eu), gadolinium (Gd), neptunium (Np), plutonium (Pu), promethium (Pm), terbium (Tb), uranium (U), and zirconium (Zr) in a cement type matrix. The development of this automation system and the separation results of a surrogate sample are described further in Chapter 4.

Chapter 2

Cesium Sorption and Desorption

Significant quantities of radioactive Cs have been released to the environment. These releases have occurred as a result of nuclear weapons testing [25], nuclear accidents at Chernobyl, Russia and Fukushima, Japan [26] [27], and leaks from high level waste storage sites such as Hanford, USA [11] and Mayak, Russia [28]. Total ^{137}Cs released from nuclear weapons testing is estimated to be 948 PBq [10]. Total ^{137}Cs released from the Chernobyl and Fukushima accidents and at the Hanford site is estimated to be ~85 PBq [12], 13-36 PBq [13] [14] [15], and 370 PBq [11] , respectively. The ^{137}Cs decays to stable barium by beta minus decay according to the following equation,

$$^{137}_{55}Cs \rightarrow {}^{137}_{56}Ba + e^{-} + \overline{\nu} \qquad \text{Equation 2-1}$$

where an electron, e^-, and an antineutrino, $\overline{\nu}$, are emitted from the radioactive ^{137}Cs nucleus. The decay scheme for ^{137}Cs is shown in Figure 2-1.

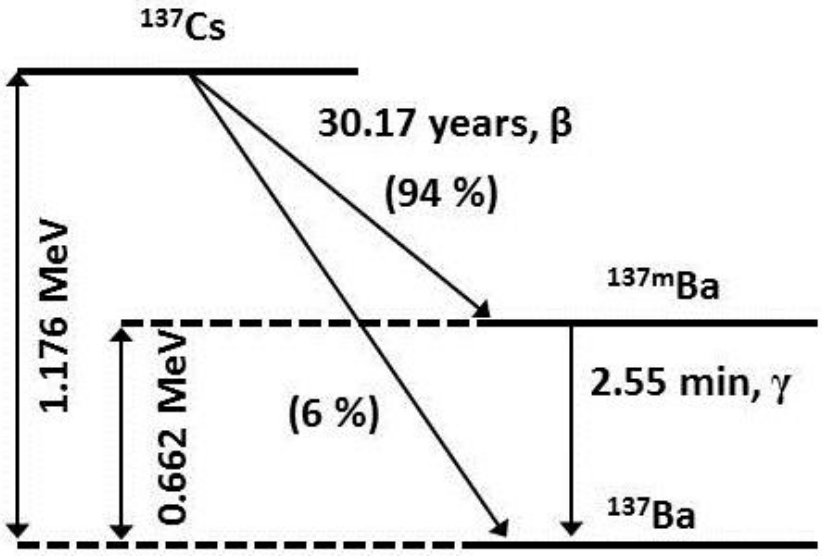

Figure 2-1. The decay scheme for ^{137}Cs as it decays by beta decay to stable ^{137}Ba.

The persistence of ^{137}Cs ($t_{1/2}$ 30.1 y) in the environment can pose substantial health concerns. The US EPA regulates the amount of beta emitting radionuclides in drinking water such that the equivalent dose is less than 4 mrem per year [16]. This dose corresponds to a maximum ^{137}Cs concentration of 7.4 Bq/L or 1.7×10^{-14} M. Thus, ^{137}Cs is a drinking water hazard even at trace concentrations. Cesium is distributed uniformly throughout the body with a slightly higher concentration in muscle tissue. The irradiation effects can lead to cancer and genetic damage in the individual [29]. Cesium is found in Group I on the periodic table. Cesium is an alkali metal and has a melting point of 28.4°C. Cesium is the most electro-positive element and readily oxidizes in water to form highly soluble Cs^+ ions [9], though it does not hydrolyze or complex with other ions easily. Released ^{137}Cs readily dissolves and can be absorbed by plants as an analog of K^+, Na^+ and other mono valent cations, or ^{137}Cs can enter the groundwater and thereby enter

the food chain [30] [31] [32]. The widespread contamination and potential health risks of ^{137}Cs have led to extensive study of its interactions in the environment.

The environmental contamination and potential health risks associated with ^{137}Cs make understanding its transport behavior in the environment an important area of investigation. Understanding the conditions that control Cs transport may also guide remediation strategies for Cs clean-up in the environment and help to design strategies for the safe storage of radionuclides present in spent nuclear fuel.

To date, a large number of experiments aimed at studying the mobility of Cs have focused on the sorption and desorption of Cs to specific minerals and host rock material [20] [33] [34]. Typically, Cs displays a high affinity for clay minerals, such as micas, illite, vermiculites, and montmorillonite, and a low affinity for iron oxide minerals, quartz, calcite and gibbsite [35] [36]. This has been attributed to the cation exchange properties of clay minerals and the propensity for Cs^+ to undergo cation exchange.

Due to their high sorption capacity and their ubiquity in nature, aluminosilicate clays are particularly important in controlling Cs behavior in the environment. Cs sorption to clays takes place via a cation exchange process [17] [20] [37] [38] [39] [40]. The total number of cations that can exchange on a mineral surface is referred to as the cation exchange capacity, CEC. Typically as the CEC increases, the extent of Cs sorption to the mineral increases [33]. However, some minerals, such as illite and vermiculite have low CEC values yet demonstrate a high Cs sorption affinity [20]. This has been attributed to unique properties of certain sorption sites on clays that have high selectivity for the Cs^+ cation. Cs sorption to illite, montmorillonite, and kaolinite clays was the focus of this

study. Each of these clay minerals has a different elemental composition and structure giving rise to different Cs sorption behavior.

Illite $(K, H_3O)(Al, Mg, Fe)_2(Si, Al)_4O_{10}[(OH)_2(H_2O)]$ is a non-expanding 2:1 (two tetrahedral silica layers sandwiching an octahedral alumina layer, TOT) aluminosilicate micaceous clay. Cesium sorption to illite has been described as a cation exchange process on either the basal/planar, edge, or interlayer sites [41]. The interlayer sites are located between two 2:1 TOT layers. Weathering near the edges of the illite expands the interlayer producing wedge or frayed edge sites (FES) [42]. These FES sites are highly selective for Cs [38] [43] [44]. As a result, while illite has much lower CEC than montmorillonite, at Cs concentrations below 10^{-7} M, illite will sorb more Cs than montmorillonite [37] [45]. Cs sorption to the various illite sorption sites has been confirmed by nuclear magnetic resonance (NMR) spectroscopy and far infrared (FIR) spectroscopy [46] [47] [48].

Montmorillonite, $(Na,Ca)_{0.3}(Al,Mg)_2Si_4O_{10}(OH)_2 \bullet n(H_2O)$, is a 2:1 aluminosilicate clay in the smectite group. Montmorillonite has an expanding interlayer [42] that allows for increased interaction between cations in solution and those in the clay interlayer. The expanded interlayer results in a high CEC and capacity to sorb large quantities of Cs [17] [37] [49] [50].

Kaolinite, $Al_2Si_2O_5(OH)_4$, is a 1:1 aluminosilicate, non-expanding clay. Sorption of Cs to kaolinite occurs by cation exchange at permanently charged sites on the basal surfaces of the mineral [47] [49] [51] [52] [53]. Due to its low CEC and absence of FES sites, kaolinite will sorb Cs less effectively than montmorillonite or illite.

The cation composition of the electrolyte can affect Cs sorption to clays as the cations compete with Cs for available sorption sites [20] [54] [55]. Cations with low hydration energy are preferentially sorbed to minerals [56] [57] [58], thus it follows that monovalent cations such as, Cs^+, Na^+, K^+, NH_4^+, will be selectively sorbed over divalent cations, such as Ca^{2+} and Mg^{2+}, due to lower hydration energies [17] [20] [59] [60].

The extent of Cs sorption to illite, montmorillonite, and kaolinite is also affected, to some extent, by pH. In solution, Cs takes the form of Cs^+, and does not normally form complexes, especially in the pH range of most groundwater (5-9). Previous work has shown that Cs sorption to illite is independent of pH in this range [38] [39] [41]. However, there exists a pH dependency below pH 5 [40] [49] [55]. This pH dependence has been attributed to the competition of hydronium ions (H_3O^+) for cation exchange sites at low pH. Studies have found a small pH dependency on sorption at pH 5-9 for montmorillonite [20] [36] [61] and kaolinite [20] [36] [62]. No explanation was given for the small overall variation in Cs sorption to montmorillonite and kaolinite.

While a substantial number of sorption experiments have been reported in the literature [20] [33] [34], significantly fewer desorption data are available. Shultz et al. (1960) showed that Cs sorbed to the montmorillonite interlayer can exchange with other cations in solution and desorb. The Cs that sorbs to kaolinite planar sites can also readily exchange with other cations and desorb [63]. However, the behavior with illite is more complex. At trace concentrations, Cs is almost entirely sorbed on the high affinity FES sites. When Cs sorbs to these sites, it causes the FES sites to collapse. Batch sorption experiments attribute irreversible Cs sorption because of this collapse, primarily due to size effects preventing other cations access to the collapsed sites [17]. As the Cs

concentration increases, so does sorption to edge and planar sites of illite. These sites are accessible to other cations in solution and Cs desorption from these sites is similar to desorption from montmorillonite [37] [50] [59]. However, more recently, high concentrations of Cs have been shown to exacerbate interlayer collapse and, thus, lead to irreversible sorption behavior even at high Cs concentrations [64].

The contact time between Cs and the mineral has been shown to affect Cs desorption. For illite, as Cs sorption period increases, the amount of Cs that is retained by illite during desorption can also increase [65]. The effect of Cs-illite contact time on desorption is especially pronounced at trace Cs concentrations. The effect of contact time on Cs desorption has not been observed in montmorillonite or kaolinite. The Cs-illite behavior is explained by the slow (weeks to months) diffusion of Cs into the illite interlayer [36] [37] [66] [67]. Some studies with short contact times, (5 minutes to a few hours), did not show a decrease in desorption with contact time. [39] [64]. This may have been because the contact time was too short to observe significant Cs interlayer diffusion.

Wauters et al. (1994) and De Koning and Comans (2004) examined Cs desorption behavior using the "infinite bath method". The infinite bath method uses an ammonium hexacyanoferrate which has a high selectivity and capacity for Cs as a means for driving desorption of Cs from a mineral. These two papers introduced the concept of partial irreversibility of Cs sorption to illite, or the idea that due to the interlayer collapse and irrespective of the desorption time, at least a portion of the initially sorbed Cs will be retained, especially in the presence of Cs concentrations $>8\times10^{-7}$ M and alkali metal concentrations greater than 10^{-4} M [64] [68]. De Koning and Comans (2004) propose Cs reversibility for concentration below those listed above or in an infinite bath scenario

[64]. Importantly, these studies were performed on the scale of hours to weeks; whereas, the time scale for transport in the environment is on the scale of years. Thus, apparent irreversibility on short timescales may, in fact, appear as reversible at longer timescales. Quantification of the desorption rates is essential to answering the question of Cs sorption irreversibility at environmentally relevant timescales.

Most sorption/desorption studies are conducted as single mineral binary batch experiments. However, in the environment, Cs will interact with multiple minerals simultaneously. There have been few studies that have looked at the combined effect of multiple minerals on the sorption of Cs. Yanagi et al. (1989) conducted Cs sorption experiments in the presence of montmorillonite, sand and loams individually and as composite mixtures. The sorption of Cs in these experiments was reported in terms of a distribution coefficient K_d (mL/g). The K_d values of the mixtures were evaluated based on the component additivity approach [69] as described by;

$$K_{d,m} = K_{d,A}w_A + K_{d,B}w_B \qquad \text{Equation 2-2}$$

where $K_{d,m}$ is the K_d of the mixture, A and B represent components A and B and w is the weight fraction of each component in the mixture. The predicted K_d of the mixture was compared to the measured K_d value of the mixture [70]. Palmer et al. (1981) also used a component additivity approach to study the sorption of Cs to individual minerals and mixtures using, montmorillonite, illite, zirconium oxide, alumina, and quartz. Palmer et al. and Yanagi et al. conclude that the distribution coefficient of a mixture could be estimated to within a factor of 2 to 4 using the component additivity approach. However,

a more accurate determination would require testing each nuclide over a range of mixture compositions, pHs, and solution compositions [70] [71].

The evaluation of Cs sorption to illite, montmorillonite, and kaolinite over a wide range of initial Cs concentration that extends to low, environmentally relevant concentrations not evaluated previously is discussed. Data is presented for binary batch Cs sorption to, and desorption from illite, montmorillonite, and kaolinite across an initial Cs concentration range of 10^{-3} to 10^{-11} M. Cesium sorption/desorption behavior in two-mineral ternary systems is also examined. By keeping the two mineral phases physically separated by a "Float-A-Lyzer" dialysis bag, the individual contribution of each mineral to the overall sorption is demonstrated and the competitive sorption and desorption of Cs in a ternary system over a period of nearly 17 months is evaluated. This method provides a rich dataset to evaluate component additivity, reversibility, and desorption kinetics in the presence of clay minerals. The results indicated that apparent sorption irreversibility at short timescales (days to weeks) may, in fact, be the result of kinetically slow but reversible processes that are revealed in experiments performed over longer, environmentally relevant, timescales (months to years).

2.2 Cs Sorption Preliminary Experiments

Prior to investigating the sorption of Cs on mineral surfaces, preliminary experiments were conducted to understand how dialysis bags with varying pore sizes may affect sorption of Cs minerals. Also experiments were conducted that examined the

quenching or matrix interference effects that may manifest due to the presence of a mineral, such as illite in the scintillation cocktail.

Dialysis Bag Pore Size Experiments

In our multi-mineral experiments, a permeable membrane dialysis bag was used to separate the different mineral phases while allowing the Cs to interact with both mineral phases. In order to determine an appropriate membrane size that would maintain a separation of the mineral phases without restricting the movement of Cs^+ ions, a set of experiments was conducted with three different molecular weight cut-off (MWCO) sizes of 5 mL permeable membranes (Spectra/Por Float-A-Lyzer® G2) hereafter referred to as Float-A-Lyzers or dialysis bags. The three MWCO sizes tested were 100-500 Dalton, 500-1k Dalton, and 3.5k-5k Dalton, with the largest Float-A-Lyzer corresponding to a pore size of <2 nm in diameter and the smallest Float-A-Lyzer corresponding to approximately 0.3-0.5 nm in diameter. A graphical pore size chart for the Float-A-Lyzers is included in Appendix A1. The Float-A-Lyzer membrane is made of biotech grade cellulose ester, the top and bottom pieces are made of sealed polycarbonate and the screw-on-cap is made from polypropylene with a leak proof and re-sealable silicon O-ring. Each Float-A-Lyzer was prepared by removing the cap and submerging in MQ H_2O for at least 30 minutes to remove the glycerine coating used to preserve the membrane. Next the Float-A-Lyzers were rinsed with MQ H_2O. Five mL of buffer solution was added to each of the Float-A-Lyzers follow by 10 µL of ^{137}Cs stock solution with an activity of ~0.155 µCi. Each Float-A-Lyzer was then placed in 250 mL polyethylene centrifuge tube containing 150 mL of buffer solution. The 250 mL centrifuge tubes were placed in the dark on the orbital shaker and aliquots of the buffer solution were taken

after 1, 4 and 14 days. Aliquots were counted on the Liquid Scintillation Counter (LSC) to determine the extent of Cs diffusion through the Float-A-Lyzer. After 14 days a 1 mL aliquot was taken from inside the Float-A-Lyzers and compared with results from outside the Float-A-Lyzers. Complete diffusion would result in ~42 cpm/mL in both the centrifuge tube and inside the Float-A-Lyzer. The results of Cs diffusion outside the Float-A-Lyzer are shown in Figure 2-2. The size comparison shows that the largest pore size membrane allows for complete diffusion within one day (3500-5000 Dalton), the middle pore size reaches complete diffusion within two weeks and that after two weeks the smallest pore size still has yet to reach 50 percent diffusion. The difference between the ^{137}Cs inside and outside the Float-A-Lyzer after 14 days was less than 2 percent for the two larger pore size membranes. The 3500-5000 Dalton size membrane was used for all future experiments.

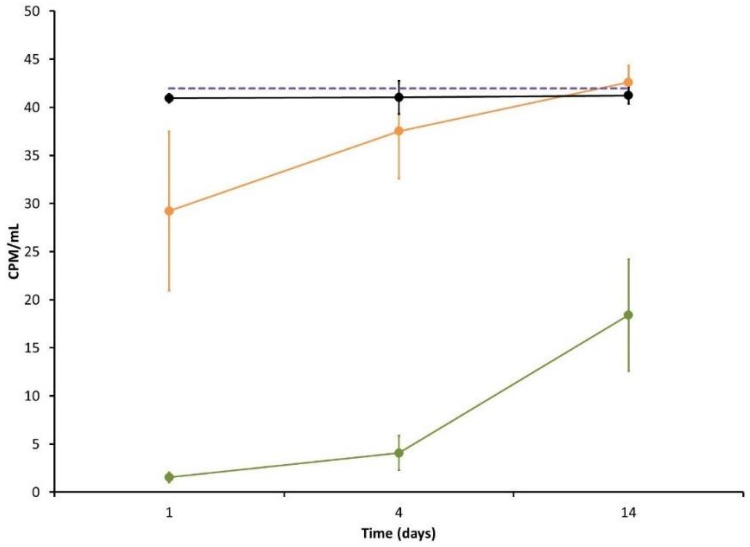

Figure 2-2. A comparison of the diffusion of Cs through different pore size Float-A-Lyzers (dialysis membranes). The different pore sizes are (●) 3500-5000 Dalton, (●) 500-1000 Dalton and (●) 100-500 Dalton. Perfect diffusion of the ^{137}Cs added to each Float-A-Lyzer is represented by the dotted horizontal line. The error bars represent the standard deviation of triplicate samples.

Measuring ^{137}Cs radioactivity can be achieved by gamma counting on a high purity germanium (HPGe) detector or by LSC. In order ensure counting results would not be affected by acid concentration or mineral interference, a quench curve for Cs in Ultima Gold scintillation cocktail was obtained and mineral interference experiments were conducted. If by chance either of these affected the measurement of Cs this information could be used to correct the measured values.

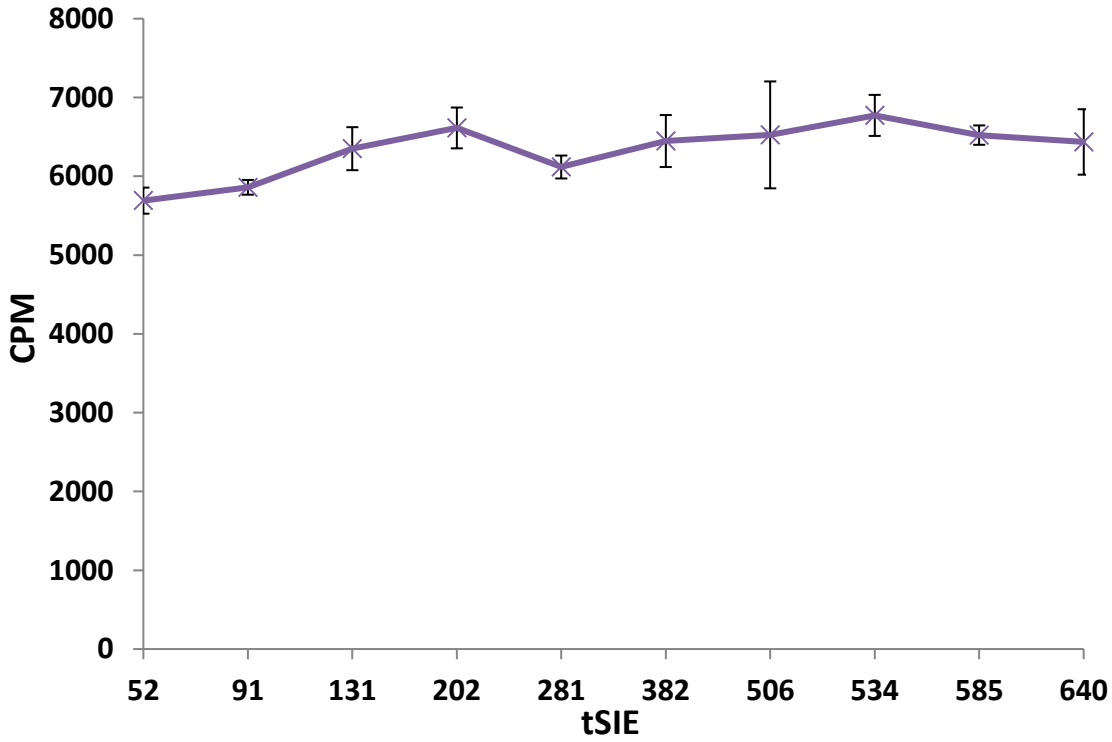

Figure 2-3. The quench curve for ^{137}Cs in Ultima Gold scintillation cocktail. The measured CPM of each sample plotted against tSIE. Error bars represent the standard deviation of triplicate samples.

The LSC quench curve for Cs in Ultima Gold scintillation cocktail was obtained by following a procedure recommended by the Packard Instrument company [72] [73]. Ten samples with a known amount of ^{137}Cs were prepared with progressively more nitromethane added to each sample with time. The nitromethane acts as a chemical

quenching agent, decreasing the light detected by the LSC. The samples were prepared in triplicate and the average CPM detected was plotted against the transformed Spectral Index of the External standard (tSIE) as shown in Figure 2-3. The tSIE is a measure of the amount of light detected by the LSC where higher values represent less interference and low tSIE values indicate significant quenching that may suppress the count rates of the measured radionuclide. The average counts per minute (CPM) of triplicate samples is plotted against the tSIE measured by the LSC. Lower tSIE values correspond to higher volumes of added nitromethane. The results of the average detected CPM of ^{137}Cs is mostly independent, with perhaps a slight dependence at values, below 100 tSIE. The CPM expected from each sample was within 1-2% of the measured values except for the low tSIE samples where expected versus measured CPM differed by as much as 5%. Samples with tSIE values lower than 300-400 were rare. As a result, the measured ^{137}Cs CPM was assumed to be the actual value throughout the rest of this work, and no corrections were applied.

When measuring Cs sorbed to the surface of a mineral, there will be some mass of mineral present in the Cs-scintillation cocktail solution that may interfere with the measurement. Most experiments where Cs was measured with a mineral in the scintillation cocktail had mineral concentrations of 1 g/L. In order to determine any possible interferences, different amounts of ^{137}Cs were added to either a 1 g/L suspension or a 5 g/L suspension of illite. The Cs and illite suspension were equilibrated for a few days and then measured by LSC. The results are given in Table 2-1 and show that the 5 g/L illite suspension resulted in slightly higher measured Cs than the 1 g/L suspension. From the results, it appears that the presence of solid material has a small effect (~5 %)

on the measured Cs for the higher count rates, but after reaching a threshold of around 15 CPM/mL the effect of the mineral becomes more pronounced. Nearly all samples from this work had mineral suspension compositions of 1 g/L or less and an expected CPM/mL of Cs greater than 60. Therefore, it was expected that there would be no need to correct for the mineral suspension.

Table 2-1. The measured counts versus the expected counts of Cs in 1 and 5 g/L illite suspensions.

Solid/Solution g/L	CPM/mL	Standard Deviation	Expected CPM/mL	% difference
1	59.6	1.3	60	0.7
5	62.9	2.2	60	4.9
1	29.9	0.1	30	0.4
5	31.7	0.6	30	5.5
1	14.1	0.2	15	5.8
5	17.4	3.2	15	15.9

2.3 Materials and Methods

Materials

All solutions were prepared using ACS grade chemicals without further purification and ultrapure water (Milli-Q Gradient System, > 18 MΩ.cm). Fithian Illite from Rochester, NY (Ward's Science), SWy-1 montmorillonite (Clay Minerals Repository), and KGa-1b Kaolinite (Clay Minerals Repository) were used in this study. Preparation for SWy-1 Na-montmorillonite has been previously reported [74] and the same method was also used for the preparation of illite and kaolinite. The minerals were prepared individually by mixing 100 g L^{-1} of the mineral in 0.001 M HCl for 30 minutes in order to remove soluble salts and impurities. Next 0.03 M H_2O_2 was added for 30

minutes to minimize the oxidative and reductive potential of any remaining impurities as well as removing trace organic material. The clay suspensions were then centrifuged for six hours at 2500 g and the supernatant (calculated to contain particles < 50 nm diameter) was discarded. The wet solids were transferred to 6000-8000 molecular weight cut off (MCWO) dialysis bags and suspended in a 0.01 M NaCl electrolyte solution and dialyzed for seven days to homo-ionize the minerals. The minerals were extruded from the dialysis bags into Milli-Q H_2O. The suspension was then centrifuged (sedimentation for 1 hour was used for illite and kaolinite) at 100 g for five minutes and the supernatant, which contained particles >2 µm was discarded. The remaining solids (50 nm < - < 2 µm) were dried at 60 °C. A portion of the dried minerals was resuspended in a 5 mM NaCl and 0.7 mM $NaHCO_3$ solution (pH 8) with an ionic strength of 0.0057 M. The solid:solution ratio of the mineral suspensions were 1 g/L unless otherwise noted. The mineral suspensions were allowed to equilibrate for several days.

Binary Sorption Experiments

Ten mL of each mineral suspension was added to 15 mL polyethylene centrifuge tubes. A total of 17 different initial Cs concentrations ranging from 10^{-3} to 10^{-11} M were prepared. A combination of stable CsCl and ^{137}Cs was added to samples with Cs concentrations of 10^{-9} M and higher. The centrifuge tubes were placed on an orbital shaker at 0.4 g at room temperature and kept in the dark for the duration of the experiment. The samples were shaken continuously for at least two weeks to allow sufficient time for Cs to sorb to the mineral [39]. Mineral blanks were also performed to test for any sorption to container walls. At the end of the sorption period, each tube was centrifuged for two hours at 3600 g to obtain a <50 nm particle size cut off in the

supernatant. An aliquot of the supernatant was taken from each sample and the ^{137}Cs measured by LSC (Packard Tri-Carb TR2900 LSA and Ultima Gold cocktail). The distribution coefficient, K_d, for each sample was calculated as follows:

$$K_d = \frac{[Cs]_i - [Cs]_{eq}}{[Cs]_{eq}} \times \frac{1}{[mineral]} \quad \text{Equation 2-3}$$

where $[Cs]_i$ is the initial concentration of Cs, $[Cs]_{eq}$ is the equilibrium concentration of Cs in the aqueous phase, and [mineral] is the solid:solution ratio in g mL^{-1}. The units of K_d are mL g^{-1}.

Binary Desorption Experiments

Binary desorption experiments were performed at the conclusion of the sorption experiments. At the end of the 14 day sorption period and after centrifugation, a total of 9.5 mL of the supernatant was quantitatively removed and replaced with 9.5 mL of Cs-free buffer solution. The centrifuge tubes were placed in the dark on the orbital shaker and shaken continuously for at least two weeks. The centrifuge tubes were then spun for 2 hours at 3600 g to reach the <50 nm particle size cut off. An aliquot of the supernatant was removed and ^{137}Cs measured by LSC. The measured ^{137}Cs was used to determine the total fraction of Cs desorbed from each of the samples. One or two sequential batch exchanges were carried out for each mineral by repeating the steps listed previously.

Ternary Sorption/Desorption Experiments

In the two-mineral ternary Cs sorption/desorption experiments, 150 mL of each clay suspension (dry clay mass of 0.15 g total) was added to 250 mL centrifuge tubes. ^{137}Cs was added as a tracer to stable Cs before being added to each of the mineral suspensions. Cesium concentrations were chosen such that Cs sorption to illite is

dominated by the high affinity FES sites (low Cs) and the edge or planar sites begin to contribute to total Cs sorption (high Cs). Three illite suspensions with Cs concentrations of 10^{-6}, 5×10^{-7} and 10^{-7} M were prepared. Three montmorillonite suspensions with Cs concentrations of 5×10^{-7}, 10^{-7}, and 5×10^{-8} M were prepared, and two kaolinite suspensions with Cs concentrations of 5×10^{-7} and 10^{-7} M were prepared. Lastly, solutions with Cs concentrations of 10^{-6}, 5×10^{-7}, 10^{-7}, and 5×10^{-8} M (and no minerals) were used as controls. All samples were placed on an orbital shaker in the dark and allowed to equilibrate for two weeks. After the equilibration period, 5 mL of a 60 g/L illite suspension (0.3 g total) was loaded into 3500-5000 MWCO Spectra/Por Float-A-Lyzers. The Float-A-Lyzers with the illite suspensions (see Figure 2-4) were then inserted into each of the centrifuge tubes. The centrifuge tubes were then returned to the dark on the

Figure 2-4. A picture of the Spectra/Por Float-A-Lyzer filled with illite mineral suspension before it was added to the flotation cell.

orbital shaker. The suspensions outside the Float-A-Lyzers were periodically sampled over the duration of the experiment, a period of nearly 17 months. The experimental

setup is shown in Figure 2-5. A 1 mL aliquot of the suspension was taken and counted by LSC.

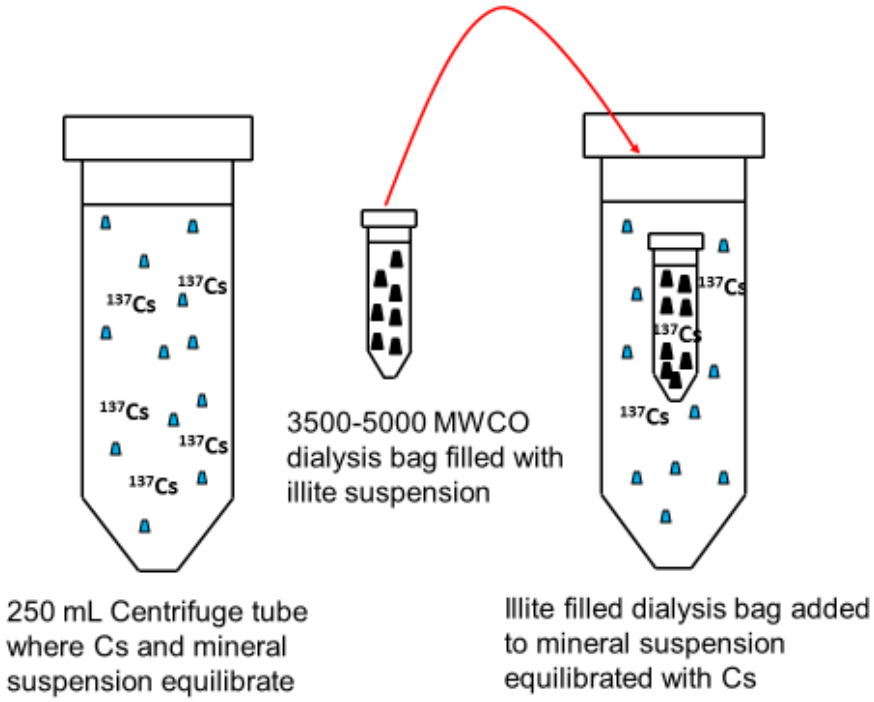

Figure 2-5. A diagram of the experimental setup for the multi-mineral experiments.

Then a 1.2 mL aliquot of the suspension was removed and centrifuged for 2 hours at 3600 g to achieve a particle size cutoff of 50 nm. A 1 mL aliquot of the supernatant was removed and counted by LSC to determine the aqueous Cs concentration. Separate experiments were performed to verify that the suspensions were sufficiently stable to allow for quantitative and reproducible measurement of the total Cs activity in the suspensions. Characterization of sample blanks indicated that negligible Cs sorbed to the either the membrane or walls of the centrifuge tube. Therefore, it can be assumed that the decrease in total Cs outside the Float-A-Lyzer corresponds to a proportional increase in

the total Cs sorbed to illite inside the Float-A-Lyzer. The amount of Cs sorbed to the illite inside the Float-A-Lyzer was calculated as follows:

$$Cs_{id,n} = Cs_0 - Cs_{bulk,n} \quad \text{Equation 2-4}$$

where $Cs_{id,n}$ is the amount of Cs (moles) on the illite inside the Float-A-Lyzer after n days, Cs_0 is the amount of Cs in the suspension before the Float-A-Lyzer was added and $Cs_{bulk,n}$ is the amount of Cs in the bulk suspension outside the Float-A-Lyzer after n days. After the last sampling time point, the Float-A-Lyzer was removed from the centrifuge tube and rinsed several times with Milli-Q water to remove any residue from the outside of the Float-A-Lyzer. The Cs activity in the Float-A-Lyzer was then measured by gamma spectroscopy to determine the total amount of Cs sorbed to the illite inside the Float-A-Lyzer.

Modelling

The ion exchange reaction between Cs and each of the Na-homoionized clay minerals can be defined as follows:

$$\text{Na-Clay} + Cs^+ \leftrightarrow \text{Cs-Clay} + Na^+ \quad \text{Equation 2-5}$$

Based on this reaction, a cation exchange model was developed to describe Cs sorption to each mineral using the FIT4FD code [75]. The FIT4FD code adjusts the selectivity coefficient and CEC parameters to simulate Cs sorption for each of the Cs mineral sorption isotherms. The selectivity coefficients are usually described by one of two conventions: the Gaines-Thomas convention or the Vanselow convention. However, for the case of monovalent exchange reactions, the two conventions are equivalent. The

Vanselow convention, which is used in the model for this work, defines the selectivity coefficient for the reaction as follows:

$$ {}^{Cs}_{Na}K_{SEL} = \frac{(M_{Cs})^{Z_{Na}}(a_{Na})^{Z_{Cs}}}{(M_{Na})^{Z_{Cs}}(a_{Cs})^{Z_{Na}}} \qquad \text{Equation 2-6} $$

where M_{Cs} and M_{Na} are the mole fractions of Cs and Na defined as the moles of Cs or Na sorbed per mass divided by the total number of moles in the system [76].

2.4 Results and Discussion

Binary Sorption

Binary Cs sorption experiments were conducted with illite, kaolinite, and montmorillonite across an initial Cs concentration range of 10^{-3} to 10^{-11} M. Figure 2-9 presents these sorption data as the logarithm of the distribution coefficient ($\log(K_d)$) versus the logarithm of the equilibrium aqueous Cs concentration. Cs sorption to illite appears to be linear for Cs concentrations below 5×10^{-9} M with an average $\log(K_d)$ value of 4.7. At Cs concentrations greater than 5×10^{-9} M, the K_d decreases with increasing concentration. At a Cs concentration of 4×10^{-4} M, the $\log(K_d)$ was 2.4. The transition from linear sorption to non-linear sorption has previously been explained by the presence of multiple sorption sites on illite [38] [39] [40]. The Cs initially sorbs to the high affinity FES sites until filled, and then the Cs begins to sorb to the edge and planar sites. Hence, at low Cs concentrations where the FES sites are not saturated, the K_d values are high and constant. As the FES sites become saturated and the Cs begins to sorb to the less selective

edge and planar sites, the K_d begins to decrease. These experiments are consistent with behavior reported in the literature where the high affinity FES sites are saturated around 5×10^{-9} M.

Figure 2-6 shows Cs sorption isotherms onto Na-illite at varying ionic strengths. The isotherms are given as the logarithm of the distribution coefficient ($\log(K_d)$) versus the logarithm of the equilibrium concentration of Cs in solution. The units of K_d are in mL/g and the units of Cs concentration are mol/L (M). The Cs sorption to illite is non-linear. This non-linearity is indicative that illite has multiple sorption sites. Below trace initial Cs concentrations of ~10^{-7} M (corresponding to equilibrium Cs concentrations of ~10^{-8} M) the K_d values are relatively constant, consistent with previous findings of a high Cs affinity sorption site, At trace Cs concentrations, sorption to illite is controlled by the FES having ahigh selectivity for Cs. Above trace concentrations, an inflection point is reached at which point the K_d values begin to decrease with increasing Cs concentration.

A comparison of isotherms at varying ionic strengths is also plotted on Figure 2-6. As the ionic strength of the background electrolyte solution decreases, the K_d values increase because at each sorption sites there is less competition with other cations. The isotherm from this work has a background electrolyte solution with an ionic strength of 0.006 M. This is the lowest ionic strength of the isotherms and consequently it has the highest K_d values, close to 10^5 mL/g at trace concentrations. At the highest ionic strength of 0.5 M the K_d values at trace concentrations around 5 x 10^3 mL/g.

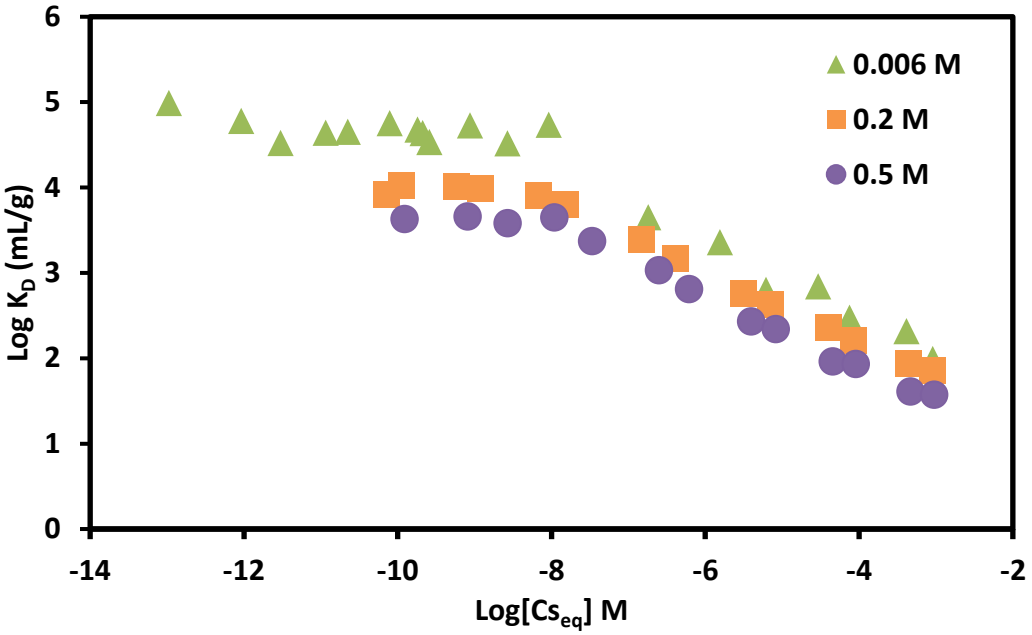

Figure 2-6. The concentration of Cs sorption to illite is plotted against the sorption Kd and compared to previously published as a function of ionic strengths. This work used 1 g/L illite and an ionic strength of 0.006 M at pH 8 (▲). Isotherm data from previous work at ionic strength = 0.2 M (■) and 0.5 M (●) are plotted for comparison **[**54**]**. Error bars based on the propagation of 2% LSC uncertainties are smaller than the symbols.

In contrast to illite, Cs sorption to montmorillonite is linear across the entire concentration range investigated with an average log(K_d) value of 2.9±0.08. Montmorillonite has previously been described as having only a single sorption site [41] and the linearity of the sorption results are consistent with that conceptual model. The sorption of Cs to kaolinite is indicative of non-linear sorption behavior at very high Cs concentrations. However, the sorption K_d is linear for Cs equilibrium concentrations less than 4×10^{-5} M with an average log(K_d) value of 2.5±0.09. Both 1-site and 2-site models have previously been used to describe the sorption of Cs to kaolinite [20] [77] [78] [79]. The 2-site models usually do not represent 2-sites on kaolinite but rather the presence of high affinity, low capacity sites attributed to trace amounts of other clay minerals such as

illite and vermiculite [78] [79] [80] [81]. For this work, X-ray diffraction (XRD) analysis (Bruker D8 X-ray diffractometer) of the montmorillonite and kaolinite showed no evidence of additional trace minerals (accurate to the 2% percent level) as seen in Figure 2-7 and Figure 2-8.

Furthermore, the presence of high affinity, low capacity sites attributed to trace phases should lead to non-linearities at low Cs concentration (Figure A-2) and this was not observed in our study. Therefore, Cs sorption to kaolinite observed here can be attributed to a single cation exchange site. Above 4×10^{-5} M Cs, the decrease in K_d is likely caused by a decrease in sorption due to saturation of planar sorption sites.

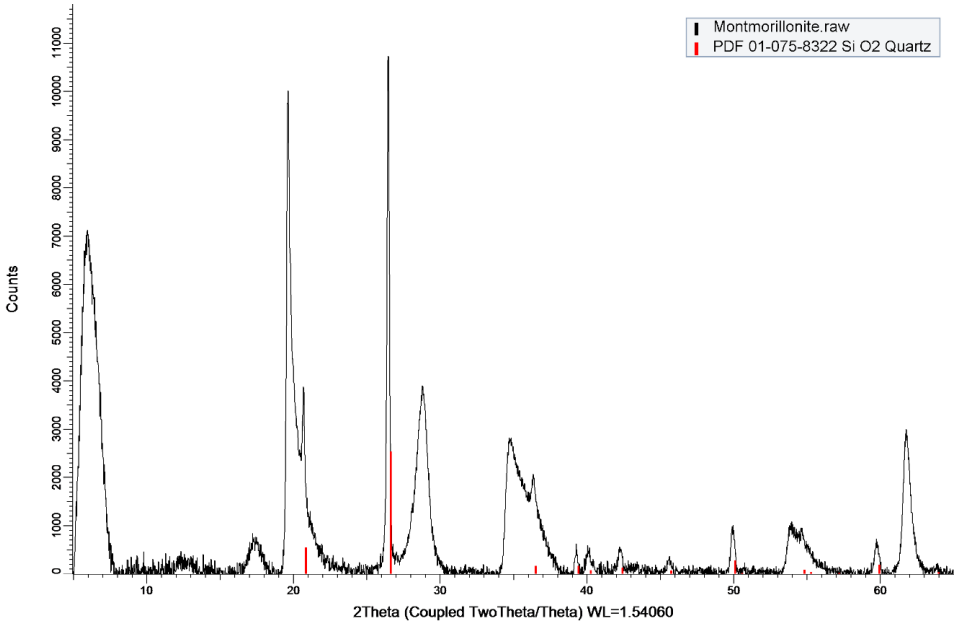

Figure 2-7. XRD analysis of montmorillonite indicating the absence of trace mineral impurities.

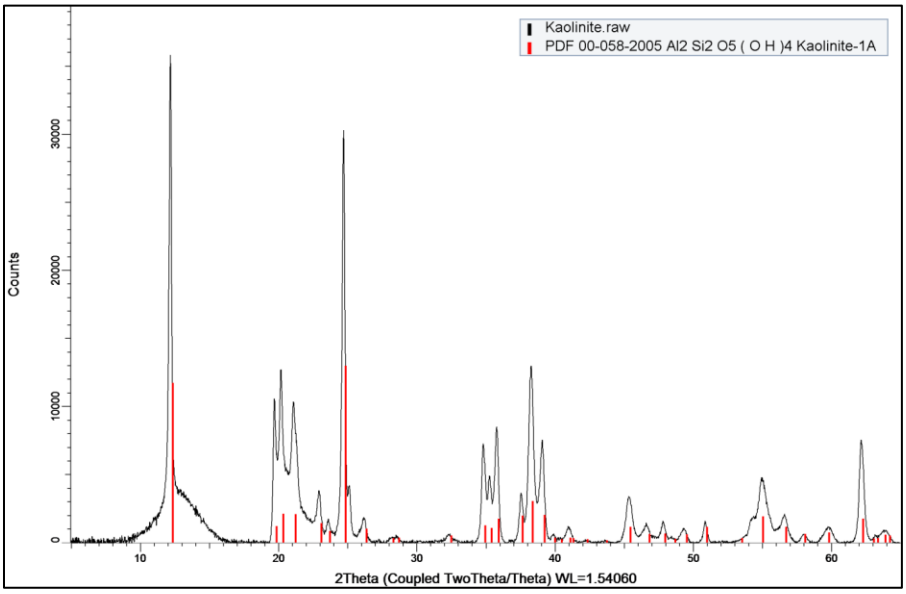

Figure 2-8. XRD analysis of kaolinite indicating the absence of trace mineral impurities.

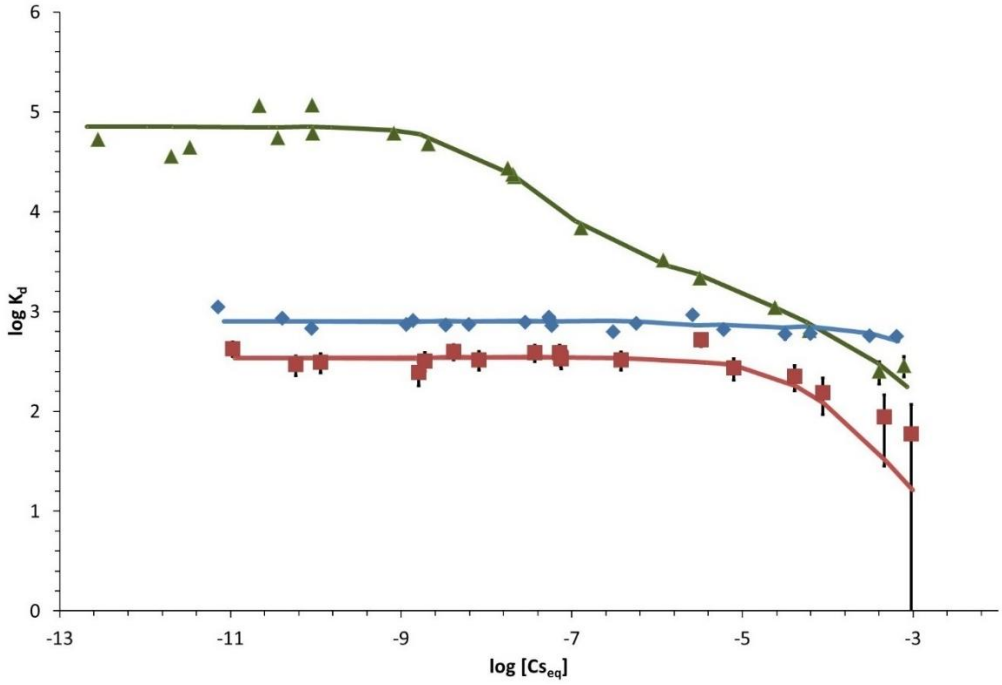

Figure 2-9. Cs sorption K_d values (mL/g) for (▲) Na-illite, (■) Na-kaolinite, and (♦) Na-montmorillonite as a function of Cs concentration in solution (mol/L). All experiments performed in 0.7 mM $NaHCO_3$, 5 mM NaCl buffer solution at pH 8. The solid solution ratio is 1 g/L for each mineral and 2 σ error bars are propagated from 2% LSC uncertainties. The solid lines represent the sorption models with parameters developed using the FIT4FD code.

At Cs concentrations below 5×10^{-9} M, there is a pronounced difference in the extent of Cs sorption between illite, montmorillonite, and kaolinite. The equilibrium K_d for illite is approximately two orders of magnitude greater than the K_d values for montmorillonite or kaolinite. These results highlight the importance of understanding the mineralogy present when predicting Cs environmental behavior. The K_d values for each of the three minerals are consistent with K_d values reported in recent literature. However, the specific K_d values are affected by the ionic strength, electrolyte composition, and the mineral source used by the various authors [53] [54] [55] [79] [80].

The FIT4FD program was used to model the sorption of Cs to each of the minerals. Selectivity coefficients and cation exchange capacities were based on values from the literature for each clay [40] [74] [79]. However, the selectivity coefficients were adjusted to improve the fits to the data, when necessary. Model fits to the data are shown as solid lines in Figure 2-9 and the fitted model parameters (selectivity coefficients and cation exchange capacities) are shown in Table 2-2. Also listed are the selectivity coefficients and cation exchange capacities from Missana et al., 2014 for comparison.

Previous evaluations of Cs sorption to illite over a wide range of Cs concentrations have used both 2-site and 3-site models [11] [40] [54] [79] [82]. The third site has been shown to contribute to sorption only at Cs concentrations $>10^{-4}$ M [54] [82]. Since the binary isotherm experiments reached Cs concentrations as high as 10^{-3} M, a 3-site model was used here. The fitted parameters are in very good agreement with the recently published values of Missana et al. 2014.

Modeling Cs sorption to montmorillonite has been simulated with both 1-site and 2-site models. Staunton and Roubaud (1997) and Iijima et al. (2010) showed that a 1-site model can describe the sorption of Cs to montmorillonite [41] [83]. When 2-site models have been used, the second site is often attributed to minerals such illite or vermiculite that are interstratified in the montmorillonite [11] [79] [84]. In this case, the presence of a second site was not observed in the data nor warranted in the modeling (Figure A-2). The fitted selectivity coefficient for this data is an order of magnitude smaller than that reported by Missana et al., (2014). This is likely the result of significant illite inclusions in the smectite used by Missana et al., (2014); however, the fitted selectivity coefficient is in good agreement with that reported by Gast et al., (1969) for the same montmorillonite used in this work. Gast et al., (1969) reported a logK of 0.79 compared to a log K of 0.69 reported in this work [85].

For Cs sorption to kaolinite, the presence of a very low concentration but high affinity site has been speculated [20] and 2-site models have been used to describe Cs sorption [79] [53]. However, this second site may also result from a trace amount of high affinity Cs sorbing mineral interstratified in the kaolinite [20] [47]. The absence of mineral impurities in this particular kaolinite has been discussed in prior work [86] and a 1-site model was sufficient to simulate the sorption behavior of Cs. The Cs-kaolinite sorption data (Figure 2-9) suggest site saturation at Cs concentrations greater than 10^{-4} M. Similar behavior was also observed by Missana et al. (2014). A second low affinity site could be used to better fit the high concentrations data. However, the CEC of this additional site would need to be more than an order of magnitude higher and this is

unreasonable when compared to CEC values reported in the literature for kaolinite. Furthermore, given the large errors associated with the high Cs concentration kaolinite data, the additional modeling complexity was not warranted in this case.

Table 2-2. Selectivity coefficient and site concentration parameters used model development of Cs sorption onto Na-clay minerals.

	$\text{Log}(^{Cs}_{Na}K_{SEL})$		Sites (mol/g)	
	[43]	This Work	[43]	This Work
Illite FES sites	6.90 ± 0.15	6.39 ± 0.1	$4.62 \times 10^{-7} \pm 0.15$	$5.92 \times 10^{-7} \pm 0.08$
Illite site 2	3.10 ± 0.15	3.02 ± 0.04	$3.88 \times 10^{-5} \pm 0.15$	$1.76 \times 10^{-5} \pm 0.13$
Illite site 3	1.75 ± 0.15	1.31 ± 0.04	$1.55 \times 10^{-4} \pm 0.15$	$1.81 \times 10^{-4} \pm 0.16$
Smectite site 1	7.59 ± 0.15	NA	$2.31 \times 10^{-8} \pm 0.15$	NA
Smectite site 2	1.68 ± 0.15	0.77 ± 0.1	$1.02 \times 10^{-3} \pm 0.15$	$1.03 \times 10^{-3} \pm 0.15$
Kaolinite site 1	5.50 ± 0.15	NA	$5.00 \times 10^{-9} \pm 0.15$	NA
Kaolinite site 2	2.10 ± 0.15	2.05 ± 0.1	$1.99 \times 10^{-5} \pm 0.15$	$2.01 \times 10^{-5} \pm 0.07$

Although the minerals used by Missana et al., (2014) come from different sources, (e.g. FEBEX bentonite vs. SWy-1 montmorillonite) the total site concentrations used in their model development and ours are similar. Published CEC values for each mineral used in this work are given as follows in meq/100 g: 19.1, 94.0 and 2.0 for Fithian illite [42], SWy-1 montmorillonite [41] and KGa-1 kaolinite [87], respectively.

Binary Desorption

Batch desorption experiments were conducted to determine Cs sorption reversibility on illite, montmorillonite, and kaolinite. In Figure 2-10, the fraction of sorbed Cs that had desorbed from each mineral after two weeks is plotted against the logarithm of the equilibrium aqueous Cs concentration. In the case of illite, at equilibrium Cs concentrations below 10^{-7} M, less than two percent of the Cs desorbed after two weeks. In contrast, at higher Cs concentrations, the percent Cs desorbed increased until it reached a maximum of 33 percent for equilibrium Cs concentrations of 4×10^{-4} to 6×10^{-5}

M. It is apparent that both the sorption and desorption behavior of Cs is non-linear. The minimal desorption observed at low Cs concentrations may be suggestive of an irreversible sorption phenomenon. However, the reversibility can only be evaluated by comparing the observed desorption behavior to predicted desorption using the equilibrium sorption constants determined in the sorption experiments.

To test sorption reversibility, the amount of Cs to desorb from illite was simulated using the same model parameters developed to describe sorption (Figure 2-10). For the majority of the samples, predicted Cs desorption is in agreements with the data. The results are generally consistent with published desorption experiments and suggest reversible sorption at these timescales. At low concentrations, below 10^{-7} M, the Cs is thought to be bound to the active FES sites that lead to collapse of the interlayer and in turn the irreversible attachment of Cs [88] to the illite. Shultz et al. (1960) showed that Cs sorbed on illite at low initial Cs concentrations (less than 10^{-7} M) exhibited the potential to irreversibly sorb some of the Cs and that 10 percent or less of the Cs was desorbed from illite even with multiple extractions [59]. In other studies, less than five percent of the Cs was desorbed from illite at concentrations below 10^{-7} M or less [78] [49] [89]. As the equilibrium Cs concentration increases and the FES sites are filled, subsequent adsorption occurs to the edge and planar sites from which Cs is more easily exchanged. Previous work has shown that at increasing Cs equilibrium concentrations, there is a concomitant increase in the amount of Cs desorbed from illite ranging from 10-50% dependent on factors including; Cs equilibrium concentration, ionic strength and solid solution ratio [39] [90]. The Cs desorption from illite behavior in Figure 2 is consistent with the presence of multiple sorption sites including high affinity FES sites where

exchange of Cs cations is likely to be rare on these time scales. The sorption model is based on reversible sorption behavior and predicts the fraction of Cs to desorb will continue to increase with equilibrium Cs concentration. This contrasts with the experimental data that shows the fraction of Cs to desorb stops increasing around a Cs equilibrium concentration of 10^{-5} M. This difference between the model, which assumes reversible sorption, and experimental data is likely a result of some irreversible sorption of Cs to the illite.

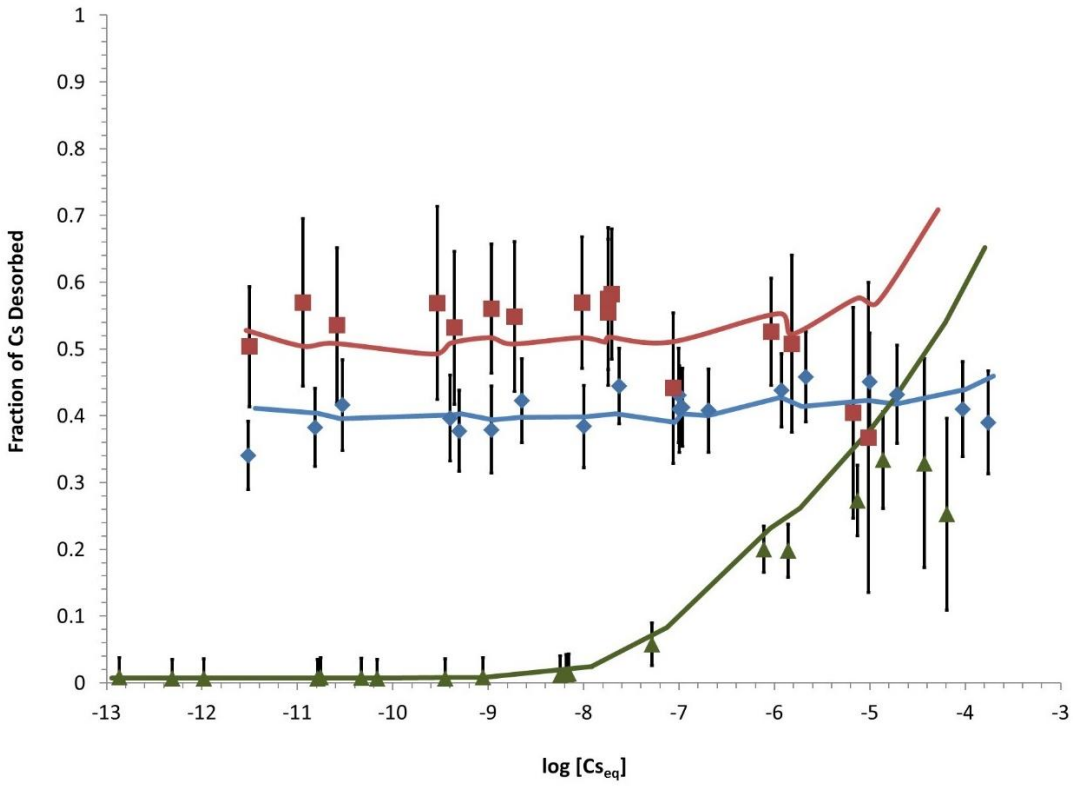

Figure 2-10. Cs batch desorption experiments showing the fraction desorbed for (▲) Na-illite, (■) Na-kaolinite, and (♦) Na-montmorillonite as a function of Cs concentration in solution (mol/L). All experiments performed in 0.7 mM $NaHCO_3$, 5 mM NaCl buffer solution at pH 8. The solid solution ratio is 1 g/L for each mineral and 2 σ error bars are propagated from 2% LSC uncertainties. The solid lines represent the predicted fraction of Cs to desorb by the sorption models.

In contrast to illite, Cs desorption from montmorillonite is relatively constant over the entire equilibrium concentration range (Figure 2-10). Approximately 40% of Cs desorbs from montmorillonite under these conditions. The amount of Cs to desorb from montmorillonite as predicted by the 1-site sorption model (Figure 2-10) is in good agreement with these desorption data. Thus, sorption reversibility of Cs from montmorillonite is clearly demonstrated under these conditions.

At concentrations of 10^{-12} to 10^{-5} M, Cs desorption behavior on kaolinite is similar to montmorillonite (Figure 2-10). Approximately 50% of Cs desorbs from kaolinite across this concentration range and the 1-site sorption model effectively predicts this behavior. Above 10^{-5} M, the experimental desorption data and desorption predicted by the 1-site model appear to diverge with the desorption data decreasing and the desorption predicted by the model increasing. While trace cations or a different sorption mechanism such as surface complexation may contribute to the increase in overall sorption at high Cs concentrations, as discussed previously the divergence between the model and data is most likely not a second cation exchange site, and the large error bars indicate that sorption is probably reversible even at higher concentrations.

Figure 2-11 shows the distributions coefficients for illite, montmorillonite and kaolinite in the sequential batch desorption experiments. Figure 2-11-B and Figure 2-11-C show the K_d values for montmorillonite and kaolinite after each batch desorption, respectively. The solid lines represent the corresponding K_d values predicted by the sorption models for montmorillonite and kaolinite. The montmorillonite desorption K_d values are linear across the range of Cs equilibrium concentrations and correspond well with both the model and sorption behavior from Figure 2-9. The similarity in K_d values

over the three extractions is consistent with reversible sorption of Cs to montmorillonite. Figure 2-11-C shows that kaolinite desorption K_d values are also linear across the range of equilibrium concentrations studied. Moreover, the similarity in K_d values obtained for the two extractions also supports reversible sorption of Cs on kaolinite.

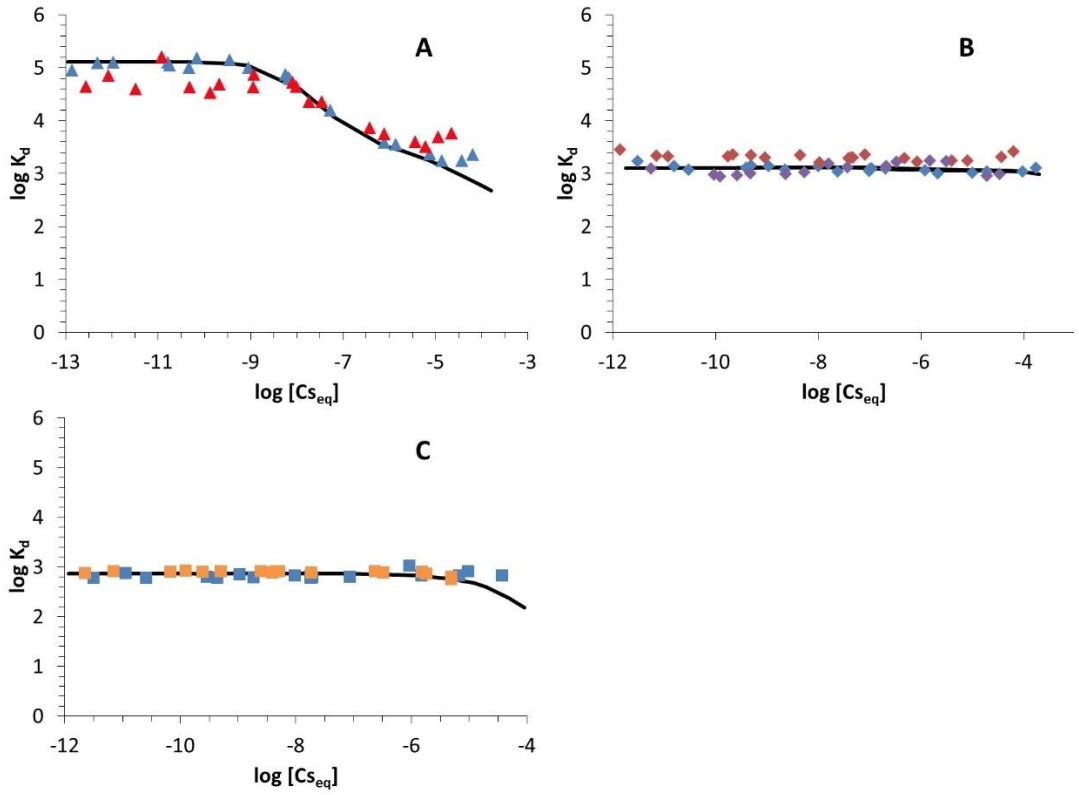

Figure 2-11. Cs batch desorption K_d values for (A) Na-illite after (▲) 14 days, (▲) 197 days, (B) Na-montmorillonite after (♦) 14 days, (♦) 142 days, (♦) 209 days, and (C) Na-kaolinite after (■) 14 days, (■) 307 days. All experiments performed in 0.7 mM $NaHCO_3$, 5 mM NaCl buffer solution at pH 8. The solid solution ratio is 1 g/L for each mineral and error bars propagated from 2% LSC uncertainties are removed for clarity. The sold lines represent predicted K_d values from sorption models.

In Figure 2-11-A the K_d values for Cs desorption from illite are constant at low Cs concentrations ($<10^{-8}$ M). The K_d values then decrease until ~10^{-5} M where they appear to plateau with increasing Cs concentration. For Cs concentrations below ~10^{-5} M the K_d

predicted by the model follow the measured desorption K_d values. Above ~10^{-5} M the predicted desorption Kd values underestimate the observed values. Furthermore, the second extraction leads to a larger deviation between predicted and measured Kd values. These results suggest that Cs sorption to illite at high Cs concentrations may be partially irreversible, consistent with the findings of De Koning et al. (2004) who attributed irreversible sorption to the collapse of FES sites caused by the presence of excess Cs cations.

Ternary sorption/desorption

Two-mineral "ternary" Cs sorption/desorption experiments were carried out to investigate the reversibility and kinetics of Cs sorption/desorption in the presence of two clay minerals. Cesium, with initial concentrations ranging from 10^{-6} to 5×10^{-8} M, was initially equilibrated with a 1 g/L mineral suspension of illite, montmorillonite, or kaolinite for two weeks in 250 mL centrifuge tubes. Then 3500-5000 MWCO Float-A-Lyzers were filled with 5 mL of 60 g/L illite mineral suspension (without Cs). The Float-A-Lyzers were inserted into the centrifuge tubes as seen in Figure 2-12. To ensure that Cs could freely diffuse across the membrane, four control experiments were performed. In the control experiments, Cs was added to the background electrolyte solution inside the centrifuge tube without a mineral present and illite suspensions were placed in the Float-A-Lyzers. Nearly all the Cs in solution was sorbed to the illite in the Float-A-Lyzers (see appendix Figure A-3) assuring that Cs could freely diffuse across the membrane.

Figure 2-12. The flotation cell showing the illite-filled Float-A-Lyzer surrounded by the bulk phase mineral suspension.

In our ternary, illite-illite, montmorillonite-illite, or kaolinite -illite experiments, mineral suspensions in the centrifuge tubes were sampled prior to adding the illite-containing Float-A-Lyzers so that the initial distribution of Cs between the aqueous and mineral phases was known. These initial conditions are reported in Table 2-3. Of the initial Cs added to each of the samples, 60, 30, and 5 % was sorbed to illite, montmorillonite, kaolinite, respectively, prior to the addition of the illite-containing Float-A-Lyzers.

Table 2-3. A table of the initial conditions for each of the ternary systems when the dialysis membranes were added to each of the centrifuge tubes.

Mineral Suspension outside Float-A-Lyzer	**Initial [Cs] M**	**[Cs_{aq}] M when dialysis membrane was added**	**% of Cs sorbed to mineral suspension when dialysis membrane was added**
montmorillonite	5×10^{-7}	3.5×10^{-7}	28
montmorillonite	1×10^{-7}	6.9×10^{-8}	29
montmorillonite	5×10^{-8}	3.5×10^{-8}	28
kaolinite	5×10^{-7}	4.7×10^{-7}	4.4
kaolinite	1×10^{-7}	9.4×10^{-8}	5.0
illite	1×10^{-6}	4.6×10^{-7}	55
illite	5×10^{-7}	1.9×10^{-7}	60
illite	1×10^{-7}	3.6×10^{-8}	61
none	1×10^{-6}	9.8×10^{-7}	0
none	5×10^{-7}	5.0×10^{-7}	0
none	1×10^{-7}	1.0×10^{-7}	0
none	5×10^{-8}	5.0×10^{-8}	0

After adding the illite-containing Float-A-Lyzers, small aliquots were taken periodically from the outer mineral suspensions and used to measure the total amount of Cs in the suspension and the supernatant. The amount of Cs sorbed to the illite in the Float-A-Lyzer was then calculated according to Equation 3. The amount Cs desorbed from the clays in the suspension was calculated from the measured suspension and supernatant Cs concentrations. Figure 2-13 is a plot of the Cs fraction desorbed from each mineral as a function of time for the suspensions of illite, montmorillonite, and kaolinite (A, B and C, respectively). For all experiments with montmorillonite and kaolinite (Figure 2-13B and Figure 2-13C, respectively), the majority of the initially sorbed Cs was desorbed from the mineral surface. Desorption of Cs appears to have occurred more quickly from kaolinite than from montmorillonite, consistent with its weaker affinity for Cs. Four hundred ninety one days after the Float-A-Lyzers were

added, an average of 85 percent of the Cs desorbed from the surface of montmorillonite and an average of 97 percent of the Cs desorbed from the surface of kaolinite. The initial Cs concentration does not appear to affect the amount of Cs desorbed from kaolinite or montmorillonite at these concentrations. This is consistent with the linear and reversible Cs sorption to these minerals. Also, the cumulative fraction of Cs desorbed from kaolinite is greater than from montmorillonite, which is expected because the sorption capacity for Cs as shown in Figure 2-9 is greater for montmorillonite than kaolinite. However, a greater total mass of Cs desorbs from montmorillonite. Importantly, the near complete desorption of Cs from both montmorillonite and kaolinite in these ternary experiments indicates that Cs sorption to these minerals is truly reversible.

For the illite experiments (Figure 2-13A), the three Cs concentrations used were 10^{-6}, 5×10^{-7}, and 10^{-7} M and correspond to equilibrium Cs concentrations around the non-linear inflection point of the K_d values from Figure 1. The fraction of Cs to desorb from the illite suspension outside the dialysis membrane begins to plateau around 300 days. The highest concentration of Cs used in this experiment also had the largest fraction of Cs to desorb, reaching 52 percent by 500 days. The middle Cs concentration experiment had 44 percent of the Cs desorbed by 500 days and the lowest Cs concentration experiment had 40 percent of the Cs desorbed by 500 days.

Compared to the batch desorption data presented in Figure 2-10, the fraction of Cs to desorb is greater in the ternary, 2-mineral systems. After a single batch desorption for kaolinite, less than 60 percent of the Cs desorbed from the mineral surface whereas in the 2-mineral system near complete desorption was observed (Figure 2-13C). For montmorillonite, less than 50 percent of the Cs is desorbed in a batch system compared

with 85 percent in the 2-mineral system. For the batch desorption experiments, multiple batch extractions were conducted, and the cumulative amount of Cs desorbed from these minerals continued to increase and approached the amount desorbed in the ternary systems. This would be expected and consistent for reversible sorption (see Appendix Figure A-6).

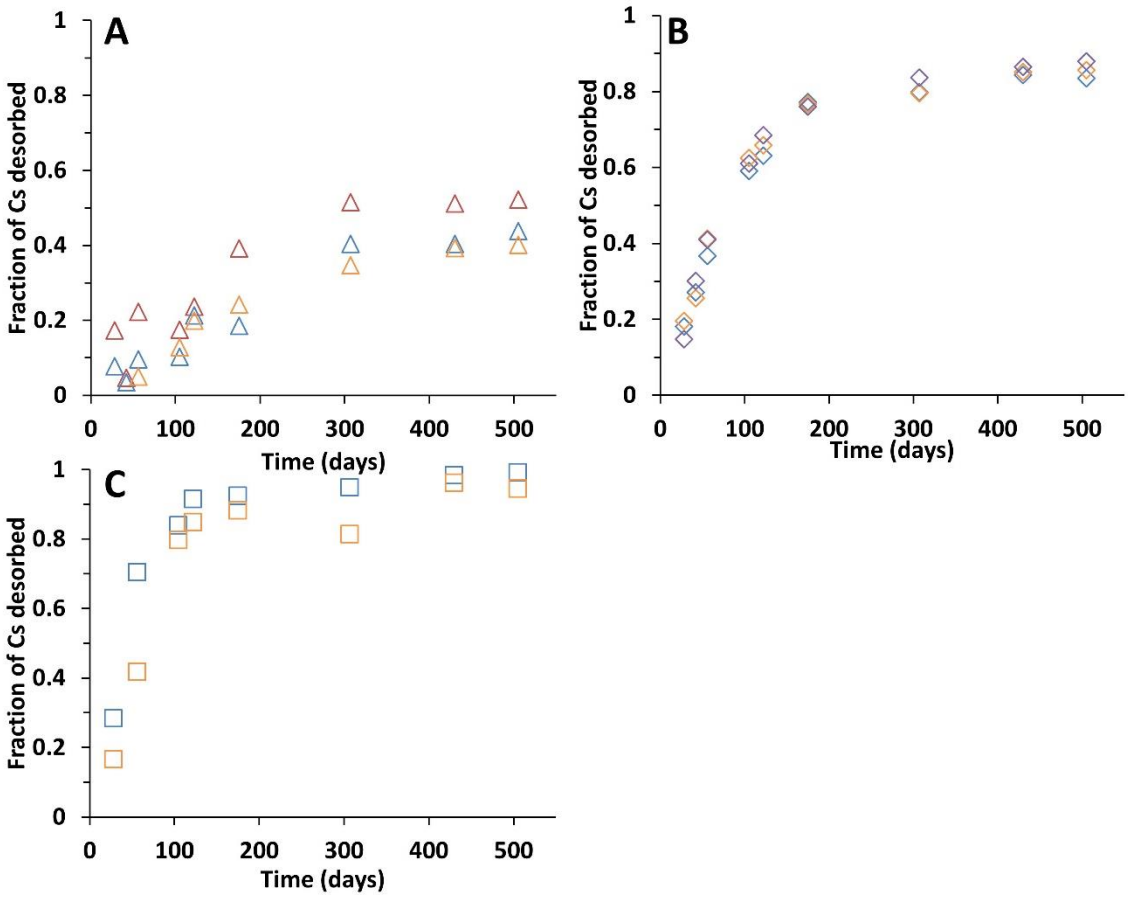

Figure 2-13. The fraction of Cs desorbed from the (A) illite, (B) montmorillonite and (C) kaolinite mineral suspensions outside the dialysis membrane over time is shown. Red, blue, orange and purple colors represent initial [Cs] of 10^{-6}, 5×10^{-7}, 10^{-7} and 5×10^{-8} M, respectively. Error bars based on propagation of 2s % LSC uncertainties are removed for clarity.

Cesium desorption from illite in the 2-mineral systems was also greater than that obtained from binary batch desorption. After a single binary desorption 6, 2 and less than 1 percent of the Cs desorbed from the mineral surface for initial Cs concentrations of 1 x 10^{-6}, 5×10^{-7} and 1 x 10^{-7} M, respectively. For the same concentrations in the 2-mineral system, 52, 44 and 40 percent of the Cs desorbed from the mineral surface, respectively. Sequential binary batch desorption also resulted in much less Cs removed from illite in contrast to the kaolinite and montmorillonite where sequential desorption significantly increased the desorption of Cs from the mineral surface, 40 and 55 percent desorbed from montmorillonite and kaolinite after a single binary desorption and 70 percent desorbed cumulatively after three binary desorptions (see Appendix Figure A-4 and Figure A-5). In the 2-mineral systems, the Cs that desorbed from the illite outside the Float-A-Lyzer is rapidly sorbed in the Float-A-Lyzer. This gradient combined with long-time scales likely produced an environment where more Cs could desorb in the 2-mineral system compared to the binary batch desorption experiments.

A higher desorbed fraction of Cs in the 2-mineral experiments is similar to results from the work by De Koning, et al., (2004) who also found greater desorption or reversibility of Cs from illite in a ternary system using ammonium hexacyanoferrate inside a dialysis membrane [64] as opposed to a batch desorption. De Koning et al., (2004) posit that Cs is reversibly sorbed to illite in specific conditions including a short equilibration time of 5 minutes [64]. However, the more likely environmental scenario is a longer equilibration time where some Cs diffuses into the interlayer and becomes fixed [91]. The plateau in Figure 2-13-A likely indicates that some of the Cs is irreversibly sorbed to illite as expected due to a long contact time with illite.

Distribution coefficients for the ternary system were predicted from the binary sorption models. The predicted K_d values for the ternary system were determined by combining the binary sorption models for illite and the mineral outside the Float-A-Lyzer. Next the appropriate initial Cs concentrations and mineral masses were added and then the combined model was applied to each case. The model determined the equilibrium Cs concentration and the total Cs concentration expected on each mineral surface at equilibrium, from which a total mineral K_d value was determined for each case. The predicted amount of Cs desorbed from the mineral outside the Float-A-Lyzer was determined by the difference of the final Cs concentration sorbed to that mineral surface as predicted by the sorption model and the initial Cs concentration sorbed to that mineral surface when the Float-A-Lyzer was added. The equilibrium aqueous Cs concentration was also determined by the combined binary sorption model and the predicted log K_d values, percent desorbed and equilibrium aqueous Cs concentrations for each case are presented in Table 2-4. The experimentally measured aqueous Cs concentrations, and calculated log K_d values and percent desorbed values are also included in Table 2-4.

The errors listed in Table 2-4 represent two standard deviations. For the experimental results this error is propagated from the counting error. For the predicted values, the error was determined by adjusting the selectivity coefficients obtained from the binary sorption experiments by two standard deviations and taking the difference between the resulting values and the values obtained without changing the selectivity coefficients. Comparing the experimental values with the model predicted values for the three montmorillonite systems show that while the predicted K_d values and expected Cs to desorb were higher than experimentally determined values, they are within two

standard deviations. Also, nearly all of the Cs was expected to desorb from the montmorillonite according to model predictions and the experimental results confirm the reversibility of Cs sorption to montmorillonite. The values for the predicted K_d and percent Cs desorbed for kaolinite are congruous with the experimentally determined values. The large errors associated with the kaolinite values are most probably the result of the small amount of Cs initially sorbed to kaolinite before the Float-A-Lyzer was added. Thus, even small variations in the fraction of Cs to desorb from the kaolinite can lead to large errors when propagated to the calculated K_d and percent desorbed values. Despite the large variance, the predicted and experimental values appear to confirm that Cs sorption to kaolinite is also reversible.

The uncertainties reported in Table 4 represent two standard deviations. For the experimental results, this error is propagated from the counting error. For the predicted values, the uncertainty was determined by accounting for the uncertainty in the fitted selectivity coefficients (Table 2-2).

For the ternary montmorillonite experiments, the predicted K_d and percent desorption values were higher than the experimentally determined values. However, the differences are not statistically significant. Nearly all of the Cs was predicted to desorb from the montmorillonite and the experimental and modeling results confirm sorption reversibility.

Table 2-4. The measured and predicted values for aqueous Cs concentration (mol/L), K_d (mL/g) and percent of Cs desorbed from the mineral outside the Float-A-Lyzer.

		Experimental			Predicted		
Outside Mineral	[Cs]*i* mol/L	log[Cs]$_{eq}$	log(K_d)	Desorbed %	log[Cs]$_{eq}$	log(K_d)	Desorbed %
Montmorillonite	5×10^{-7}	-7.48±0.01	3.7±0.1	84±7	-8.3±0.1	4.0±0.1	98±10
Montmorillonite	10^{-7}	-8.31±0.01	3.8±0.1	86±7	-9.1±0.1	4.2±0.1	99±8
Montmorillonite	5×10^{-8}	-8.78±0.01	4.0±0.1	88±7	-9.4±0.1	4.2±0.1	99±7
Kaolinite	5×10^{-7}	-8.01±0.01	4.2±0.1	99±23	-8.3±0.1	4.0±0.1	99±10
Kaolinite	10^{-7}	-8.52±0.01	4.0±0.1	94±20	-9.1±0.1	4.2±0.1	99±10
Illite	10^{-6}	-7.46±0.01	3.9±0.1	52±4	-8.0±0.1	4.1±0.1	63±16
Illite	5×10^{-7}	-7.90±0.01	4.1±0.1	44±4	-8.5±0.1	4.2±0.1	65±13
Illite	10^{-7}	-8.68±0.01	4.2±0.1	40±4	-9.3±0.1	4.3±0.1	66±12

For the ternary kaolinite experiments, the predicted K_d and percent desorption values were in agreement with the experimentally determined values. The large errors associated with the kaolinite values result from the small amount of Cs initially sorbed to kaolinite before the Float-A-Lyzer was added. Thus, even small variations in the fraction of Cs to desorb from the kaolinite can lead to large errors when propagated to the calculated K_d and percent desorbed values. Despite the large variance, the predicted and experimental values confirm that Cs sorption to kaolinite is completely reversible.

Unlike montmorillonite and kaolinite, the predicted K_d and percent desorption values for the illite ternary experiments do not agree with the experimental values. At the highest initial Cs concentration (10^{-6} M Cs) the predicted and experimental values are statistically equivalent. However, as the initial Cs concentration decreases the predicted and experimental percent Cs desorbed values diverge and the difference between the predicted and experimental K_d increases. This suggests that Cs sorption to illite exhibits an irreversible or kinetically limited sorption behavior, thus leading to the discrepancy between the predicted and experimental values. This conclusion appears to contradict the earlier results of the batch desorption experiments that indicated reversible sorption behavior at these Cs concentration (Figure 2-10). However, in the batch desorption experiments, a much smaller fraction of Cs desorbed from illite. Thus, batch desorption experiments only accessed a small fraction of the most labile Cs component on the surface. By performing ternary experiments, a much larger fraction of the sorbed Cs would need to desorb to preserve the equilibrium behavior. As a result, the effect of Cs diffusion into the interlayer of illite and the potential collapse of the FES sites over the long time period of the experiment become more prominent in these data [91]. These

experimental results show that in solution concentrations with a low cation concentration and over long time periods, significantly more Cs can desorb from illite than the few percent that was initially determined from batch experiments over the shorter time of weeks [43], The results do indicate some irreversibility which contradicts the suggestion that Cs sorption is reversible under these conditions [64].

2.5 Cs Sorption Conclusions

Cs binary sorption and desorption experiments were conducted for illite, montmorillonite, and kaolinite over an initial Cs concentration range of 10^{-3} M to 10^{-11} M.. In addition, a set of long-term ternary, 2-mineral experiments were conducted to assess the competition for Cs between two different clay minerals using a membrane (Float-A-Lyzer) to separate the minerals. By using the Float-A-Lyzer the Cs sorption behavior between two minerals could be studied in a dynamic manner more representative of the conditions that would be found in the environment. This allowed for the study of competition between minerals, sorption reversibility, and the effectiveness of the component additivity approach. The results of the batch sorption experiments were then used to compare the sorption results obtained from ternary system experiments. Predictions of the ternary system equilibrium were made using the sorption models developed from the batch sorption experiments and then compared to the measured data from the ternary systems. This comparison shows that Cs is reversibly sorbed to montmorillonite and kaolinite, even after an equilibration period of two weeks. The addition of a mineral with strong affinity for Cs such as illite was sufficient to drive

the desorption of Cs from montmorillonite and kaolinite. However, for the Cs that is initially equilibrated with illite, it is unlikely to be completely reversible due to fixation of Cs in the interlayer caused by the collapse of the FES sites. Still, over long time frames where the Cs is in low concentrations a significant fraction (more than 40 percent) of Cs may desorb from illite. This finding suggests that Cs cannot be transported significant distances if sorbed to mineral clay colloids under the geochemical conditions investigated.

Chapter 3

Plutonium Sorption/Desorption between common minerals

The worldwide inventory of plutonium (Pu) in the environment can be attributed to contamination resulting from the production and testing of nuclear weapons, nuclear accidents and intentional radionuclide discharges [92] [93] [94] [95]. Storage of nuclear waste in repositories may also ultimately introduce large quantities of Pu to the environment due a combination of its long half-life (24100 years for ^{239}Pu) [96] and the ultimate degradation of any engineered barrier system designed to isolate the Pu from the environment. The radiological toxicity and long half-life of Pu poses a serious health risk necessitating an understanding of the mobility of Pu contamination in the environment.

Plutonium has low solubility in groundwater and a high affinity for mineral surfaces and for a long time it was thought to be immobile in the subsurface. Field studies showed that low concentrations could be transported, but the mechanisms were unknown, until more recent work showed that colloids (< 1 micron particles) could transport Pu significant distances [97] [98] [99] . Colloids are naturally occurring particles made up of inorganic, organic or microbial particles that consist of components of the soil and rock matrix and due to their small size are transported in groundwater. Although colloid-facilitated transport of Pu can occur, it is not yet understood how much, how long, or under what geochemical groundwater conditions this process operates. In addition, not only is it necessary to understand the competition of Pu between the solid and the aqueous phase, but also between different colloid material, e.g. minerals, organic

or microbial material. In addition, once Pu is sorbed to a solid particle, it is the desorption rate that will ultimately determine its mobility in the subsurface.

Pu mobility in the environment is affected by a number of phenomena including: redox processes [100] [101], colloid-facilitated transport processes [97] [98] [99], solubility effects [102] [103], groundwater chemistry, sorption/desorption rates and affinities for natural mineral surfaces [104] [105] [106] and interactions with natural organic matter (including bacteria) [107] [108]. Each of these phenomena may increase or decrease the mobility of Pu in the environment. Currently our understanding of how Pu migrates in the subsurface is not sufficiently well understood to develop robust predictive transport models. Yet, dependable Pu transport models are essential for predicting the risk environment contamination and ensuring the safety of long-term nuclear waste disposal options.

The redox behavior of Pu in environment is complex and can significantly impact its mobility. Plutonium can exist in multiple oxidation states in groundwater at the same time (e.g. III, IV, V, VI). Each oxidation state is associated with unique solubilities [102] and mineral sorption affinities [104] [109] [110] [111] that ultimately determine its mobility. Generally, the mineral sorption affinity of an actinide will increase accordingly: An(V)<An(VI)<An(III)<An(IV) [113] and Pu follows this trend with Pu(V) and Pu(IV) displaying the lowest and highest sorption affinities for minerals respectively [113] [114] [111]. Although Pu(VI) has been found in highly oxic groundwaters, it is rapidly reduced to Pu(V) under most conditions [115] [114]. For surface waters Pu(V) is the most common Pu oxidation state to occur and it is also the most mobile. Under more reducing groundwaters, aqueous Pu(IV) is the most likely oxidation state to be found [115] [100]

[114]. Although Pu(V) is thermodynamically favored in near neutral groundwaters, in the presence of solid minerals or organic material, it is easily reduced to Pu(IV) on those surfaces [116] [117] [118] [119] [120]. Pu(V) exhibits a lower affinity for adsorption to organic and inorganic (i.e. mineral) surfaces than Pu(IV) [100].

Understanding the sorption behavior of Pu on aluminosilicate clays, such as montmorillonite, is important because these minerals are ubiquitous in the environment. The aluminosilicate clay montmorillonite is a 2:1 dioctohedral mineral from the smectite group. Aside from its presence in the environment, montmorillonite is also a primary component of bentonite, a rock that has been proposed to use as a backfill material for nuclear waste repository designs [112].

The aqueous mobility of Pu in the subsurface environment is largely determined by its oxidation state. In the presence of the sorption behavior of Pu on minerals and the complex redox behavior of Pu impacts the extent of sorption onto various mineral surfaces. A surface-mediated reduction process of Pu(V) sorbed to the mineral surface and then reduced to Pu(IV) has been observed on montmorillonite and this reduction drives continued sorption of Pu(V) to the montmorillonite [104] [121]. The surface mediated reduction of Pu(V) to Pu(IV) has been explained by the presence of iron (Fe) in the clay structure as well as other minerals [122]. Montmorillonite has Fe in its clay structure and the oxidation state of the structural Fe is unknown, but the structural Fe in montmorillonite was demonstrated to be redox active [123]. A possible mechanism for the slow reduction of Pu(V) to Pu(IV) is by redox active Fe in the surface of the montmorillonite clay structure [104], and is evidence of the complex redox sorption behavior of Pu on montmorillonite.

The sorption of Pu on smectites such as montmorillonite is also affected by the pH and ionic strength of the solution. The dependency on pH and ionic strength of Pu sorption to montmorillonite are indicative of the role that surface complexation sorption and ion-exchange sorption mechanisms play [121] [112]. Sorption of Pu to montmorillonite in alkaline pHs is dominated by surface complexation [112] [124]; whereas, sorption in acidic pHs is largely controlled by ion-exchange [125]. Sabodina et al., (2006) show that Pu sorption to montmorillonite increases with pH until a maximum of around 8. As the alkalinity of the solution increases above pH 8, the total Pu sorption to montmorillonite decreases [112].

Smectite minerals including montmorillonite have a strong affinity for Pu. The extent of Pu sorption is described in terms of the distribution coefficient, K_d. The K_d values for Pu(IV) sorption to smectite-rich sediments have been reported in the range of 10,000-40,000 mL g^{-1} for pHs from 5 to 12 and a 45 day equilibration time, with a K_d value of ~35,000 mL g^{-1} at pH 8 [126]. Begg et al., (2013) reported K_d values of 1970-6700 mL g^{-1} for Pu sorption to montmorillonite after a 30 day equilibration time [104] and K_d values of 5800 mL g^{-1} at pH 6.9 and 10 days equilibration time [127] and ~10,000 mL g^{-1} pH 8.2-8.3 after a 21 day equilibration time [106]. These sorption values show that the extent of Pu sorption on montmorillonite has some dependency on the equilibration time. Begg et al., (2015) examined this equilibration time dependency and reported Log K_d values for Pu(IV) sorption to bentonite, of which montmorillonite was the primary component, of 4.05, 4.4, and 4.8 after 21, 67, and 120 days of equilibration time respectively (Begg, et al., 2015). This work highlights the importance of long-term sorption experiments when trying to understand environmental sorption behavior of Pu.

Another pervasive mineral of importance to the mobility of Pu in the environment is the iron oxyhydroxide mineral goethite (α-FeOOH). Plutonium sorption to goethite is independent of ionic strength but very strongly dependent on pH. Pu sorption to goethite increases with pH reaching near complete sorption at pH 8 and above within a few hours [110]. Lu et al., (1998) reported K_d values for Pu sorption to goethite at pH 8.4-8.6 of ~200,000 mL g^{-1} after a four-day equilibration time [129]. Wong et al., (2015) reported R_d (similar to K_d without the assumption of equilibrium) values over period of up to 116 days. After 34 days equilibration time, an R_d value of nearly 1,000,000 mL g^{-1} was reported at pH 7 [130]. The affinity for Pu sorption to goethite is nearly two orders of magnitude stronger than for montmorillonite.

The sorption of Pu to minerals has been studied extensively; yet, equally important to mobility of Pu in the environment, especially over time periods of years, is the desorption of Pu from minerals. Desorption studies of Pu from mineral surfaces (typically studied as batch desorption experiments), have shown that the majority of Pu remains sorbed to the surface for minerals such as goethite and montmorillonite. Lu et al., (1998) discovered that less than 1% of the Pu(IV) and Pu(V) that was originally sorbed to goethite was removed during batch desorption experiments [129]; whereas, up to 20% of the solid associated Pu could be removed from montmorillonite after a 293 day batch desorption [106]. Recently Begg et al., (2017) published results of Pu desorption from montmorillonite using a flow cell system, that could simulate constant groundwater flow similar to the field. They found that up to 12% of the surface Pu could be removed from montmorillonite with the percent of Pu desorbed from the surface decreased with decreasing pH and increasing equilibration time [131]. The flow cell may be a better

representation of environmental conditions because it continuously pumps Pu free solution through a mineral suspension until Pu no longer desorbs, similar to a mineral suspension flowing in the environment.

The oxidation state of Pu is also important for determining the amount of Pu that will desorb from a mineral surface. The oxidation state of Pu (either (IV) or Pu(V)) on the mineral may be the driving force behind the desorption of Pu(IV) [132] [133]. Experiments with Pu(IV) initially sorbed to sediments from Aiken, SC [134] and Irish Sea sediments [132] found that Pu(V) was the predominate oxidation state of mobilized Pu found in solution. It is speculated that the photooxidation of Pu(IV) on the mineral surface by sunlight and subsequent desorption is the cause of remobilized Pu(V) in solution [132].

In this study the competition of Pu sorption and desorption between two environmentally common minerals, montmorillonite clay and the Fe-oxide, goethite is explored. The same experimental set-up pioneered in the Cs experiments discussed in Chapter 2 was used here. Specifically, a dialysis bag was used to separate the two minerals, one being pre-sorbed with Pu. The presence of Pu on the second mineral can only occur by desorption of Pu from the initial mineral and diffusion across the dialysis membrane to the second mineral. The experiment is conducted at pH 8 so that the largest amount of Pu will desorb from the montmorillonite, while simultaneously very little Pu should desorb from the goethite after sorption. These results give qualitative understanding to the behavior of Pu in the presence of multiple minerals in the environment.

3.1 Pu Preliminary Experiment

Preliminary experiments examining the effect of the Float-A-Lyzer pore size on the diffusion across the membrane were conducted for both Pu(IV) and Pu(V). Pu was added to the inside of the Float-A-Lyzer and then placed in the centrifuge tube with only buffer solution at pH 8. The Pu that had diffused into the buffer solution was measured and the results are shown in Figure 3-1and Figure 3-2 for Pu(IV) and Pu(V), respectively.

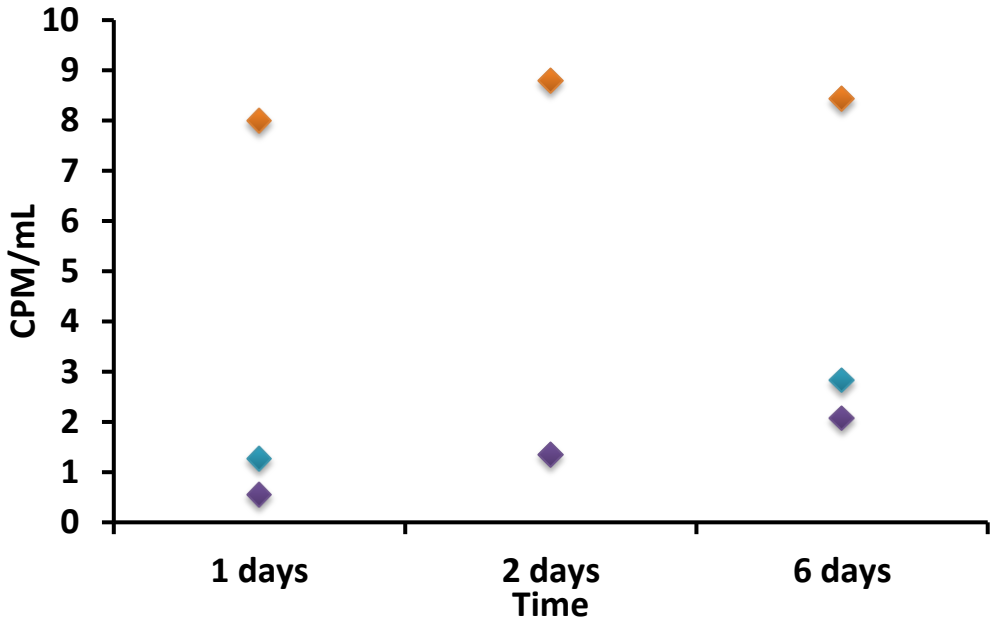

Figure 3-1. A comparison of the diffusion of Pu(IV) through different pore size Float-A-Lyzers (dialysis bags) in a pH 8 buffer solution. The different pore sizes represented by orange, blue, and purple diamonds are 3500-5000 Dalton, 500-1000 Dalton and 100-500 Dalton respectively.

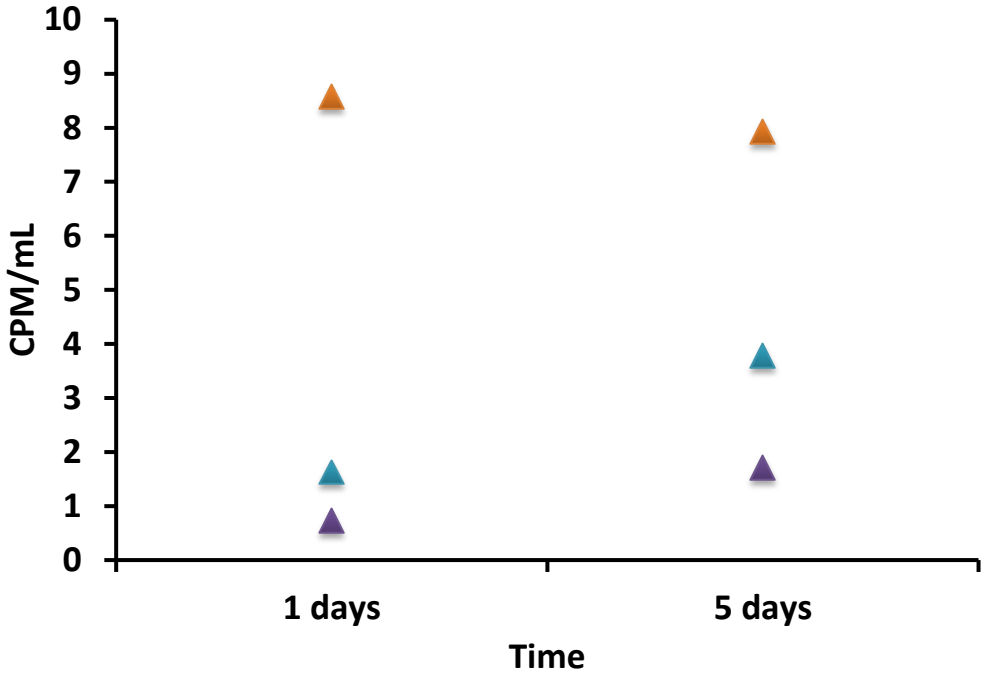

Figure 3-2. A comparison of the diffusion of Pu(V) through different pore size Float-A-Lyzers (dialysis bags) in a pH 8 buffer solution. The different pore sizes represented by orange, blue, and purple diamonds are 3500-5000 Dalton, 500-1000 Dalton and 100-500 Dalton respectively.

These experiments showed that the smaller two pore sizes produced a significant impediment to the diffusion of Pu through the membrane. Correspondingly, the largest pore size allowed for rapid diffusion of Pu, while maintaining a diameter small enough to prevent the intermixing of the minerals used in the ternary experiments. Therefore, the 3500-5000 Dalton size dialysis membranes were used in these experiments.

3.2 Materials and Methods

Materials

ACS grade chemicals without further purification and ultrapure water (Milli-Q Gradient System, > 18 MΩ.cm) were used to prepare all solutions used in this work. A

^{238}Pu stock solution (99.8% ^{238}Pu, 0.1% ^{239}Pu and 0.1% ^{241}Pu by activity) was used. The oxidation state of the Pu stock solution was greater than 99% Pu(III/IV) determined by LaF_3 co-precipitation method [135] [92]. Two different minerals were used in this study, SWy-1 montmorillonite (Clay Minerals Repository) and a synthesized alpha iron oxyhroxide (α-FeOOH) mineral, goethite. Montmorillonite was prepared by treatment with 0.001 M HCl and 0.03 M H_2O_2 in order to remove trace organic matter and iron oxides, respectively. Montmorillonite was then homoionized with sodium and rinsed thoroughly with MQ water. Specifics of the preparation of these minerals were reported previously [104] [121] [136] [137].

Multi-Mineral Experiments

Montmorillonite was initially suspended in a 0.7 mM $NaHCO_3$, 5 mM NaCl background electrolyte buffer solution. A montmorillonite suspension was prepared with a 1.0 g L^{-1} solid-solution ratio. A 150 mL aliquot of the clay suspension was added to a 250 mL centrifuge tube. Plutonium(IV) was added to a final concentration of 1 x 10^{-9} M. This concentration is expected to be below the solubility. Above this concentration, Pu may form intrinsic colloids [136]. The mineral suspensions were adjusted to a final pH of 8 ± 0.1 units using dilute HCl and NaOH. Additionally, a 250 mL centrifuge tube with 150 mL of buffer solution and Pu(IV) adjusted to pH 8 ± 0.1 units was also prepared. The centrifuge tubes were then placed on an orbital shaker in the dark and allowed to equilibrate for at least 21 days in order to establish a steady state prior to the addition of a second mineral.

After the equilibration time, the pH of each centrifuge tube was measured and re-adjusted to pH 8 if necessary. Next aliquots from each suspension or solution were

removed and the Pu activity determined by (LSC(Packard Tri-Carb TR2900 LSA and Ultima Gold scintillation cocktail). A second aliquot from each mineral suspension was removed and centrifuged at 3600 g for 120 minutes to achieve a particle size cut off of 50 nm. The Pu activity remaining in the supernatant was measured by LSC. Spectra/Por Float-A-Lyzers with a 3500-5000 molecular weight cut off (MWCO, less than 2 nm diameter pore size) were filled with approximately 1.1 g of goethite and then added to the 250 mL centrifuge tubes as shown in Figure 3-3.

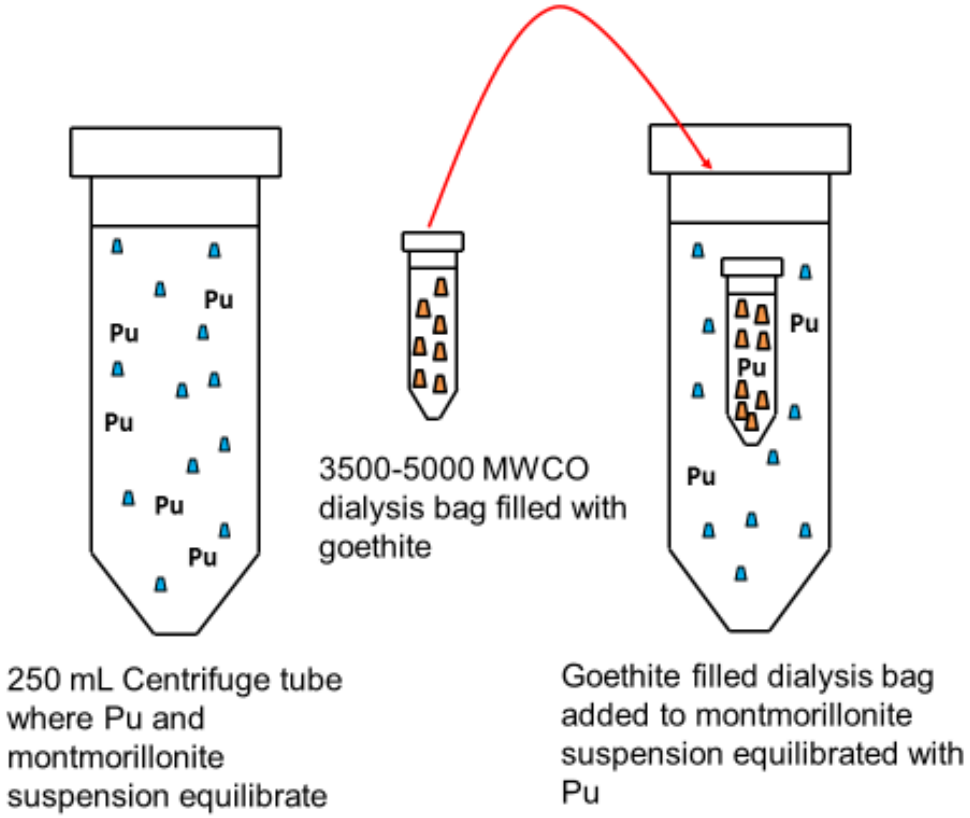

Figure 3-3. The experimental setup for the ternary experiments, showing the Pu equilibration with montmorillonite after which a goethite-filled dialysis bag is added.

The montmorillonite-goethite experiments were performed in duplicate. The 250 mL centrifuge tubes were placed in the dark on the orbital shaker. Periodically, aliquots

were removed and the Pu activities of the suspension outside the Float-A-Lyzer and the supernatant were measured. Aliquots from the buffer solution outside and goethite in the Float-A-Lyzer experiment were also removed and the Pu activities measured. The Pu concentration adsorbed to the goethite or montmorillonite suspension inside the dialysis membrane was calculated as follows:

$$Pu_{id,n} = Pu_0 - Pu_{bulk,n} \qquad \text{Equation 3-1}$$

where $Pu_{id,n}$ is the amount of Pu on the goethite or montmorillonite mineral suspensions inside the dialysis membrane after n days, Pu_0 is the initial amount of Pu added to the montmorillonite suspension prior to the insertion of the dialysis membrane, and $Pu_{bulk,n}$ is the amount of Pu in the suspension outside the dialysis membrane after n days.

Approximately two months after the Float-A-Lyzers were added, three additional 1.5 mL aliquots were removed from the mineral suspension outside the Float-A-Lyzer. These aliquots were also placed in the dark and returned to the orbital shaker. At subsequent one month intervals the aqueous concentration was measured and the oxidation state of Pu in the aqueous phase was determined by the LaF_3 co-precipitation method [135] [92].

3.3 Results and Discussion

After the initial 21-day equilibration period where Pu(IV) was sorbed to the montmorillonite, aliquots were taken and the aqueous and solid Pu concentrations measured. Of the initial 1.3 x 10^{-9} M Pu concentration added to the mineral suspension,

greater than 99 % had sorbed to the montmorillonite. The aqueous Pu remaining after the Float-A-Lyzer was added was 9.8 x 10^{-13} M. This distribution of aqueous and solid Pu in the montmorillonite suspension after the 21-day equilibration time produced an average log K_d value of 4.04 mL g^{-1}. This is comparable to the log K_d value of 4.1 reported by Begg et al. (2015) for Pu sorption to bentonite under the same experimental conditions and equilibration time (Begg, et al., 2015). After the addition of the goethite filled Float-A-Lyzer, two aliquots of the mineral suspension outside the dialysis bag were taken and measured at each sampling time. One was centrifuged to remove the montmorillonite and represents the aqueous fraction of Pu and the second sample was the total Pu including both the aqueous and mineral suspension. Plutonium that is sorbing to the goethite inside the dialysis bag represents the aqueous Pu that was initially in solution at the start of the experiment as well as Pu that continues to desorb from montmorillonite. The amount of Pu sorbed to goethite is calculated by subtracting the Pu outside the dialysis bag from the total Pu added to the system initially. The K_d values for Pu sorption to montmorillonite were calculated and given in Table 3-1.

Table 3-1. Log K_d (mL g^{-1}) values for Pu sorption to montmorillonite in the flotation cell for the duration of the experiment.

Days	**21**	**32**	**39**	**46**	**82**	**116**	**148**	**176**	**232**
1	4.06	3.78	4.32	4.37	4.59	4.76	4.83	4.82	4.86
2	4.03	3.70	4.45	4.54	4.74	4.81	4.89	4.88	5.06
Average	4.04	3.74	4.38	4.46	4.66	4.78	4.86	4.85	4.96

Except for a slight decrease about 10 days after the Float-A-Lyzers were added, the K_d values increase by nearly an order of magnitude over more than 200 days. Begg et

al., (2015) also reported log K_d values for Pu sorption to bentonite after 67 and 120 days equilibration time of 4.4 and 4.8 respectively. This is most probably caused by the reduction of trace Pu(V) initially present in the aqueous phase and its subsequent sorption to the montmorillonite [128]. The log K_d values from this work are consistent with what was expected based on the work of Begg et al. (2015) including a 120-day equilibration time. However, Begg et al., (2015) determined that steady state for Pu sorption was reached after 120 days whereas in this work the log K_d values continue to increase. The difference between the experiments in the work of Begg et al., (2015) is the presence of goethite in these experiments. The increasing K_d is due to the decreasing aqueous Pu concentration as result of continued sorption of Pu to goethite in the dialysis bag and the continued sorption of Pu(V) to the montmorillonite.

Once the second mineral is introduced into the system (goethite inside the dialysis bag), the Pu can remain sorbed to the montmorillonite or it can desorb and sorb to the goethite inside the dialysis bag. The aqueous Pu concentration inside the flotation cells at each sampling time are shown in Figure-3-4. The initial Pu concentration added to the montmorillonite suspension is shown at time zero. During the 21-day equilibration time the aqueous Pu concentration decreased by two orders of magnitude to less than 1×10^{-11} M. The total aqueous Pu decreased by approximately an order of magnitude.

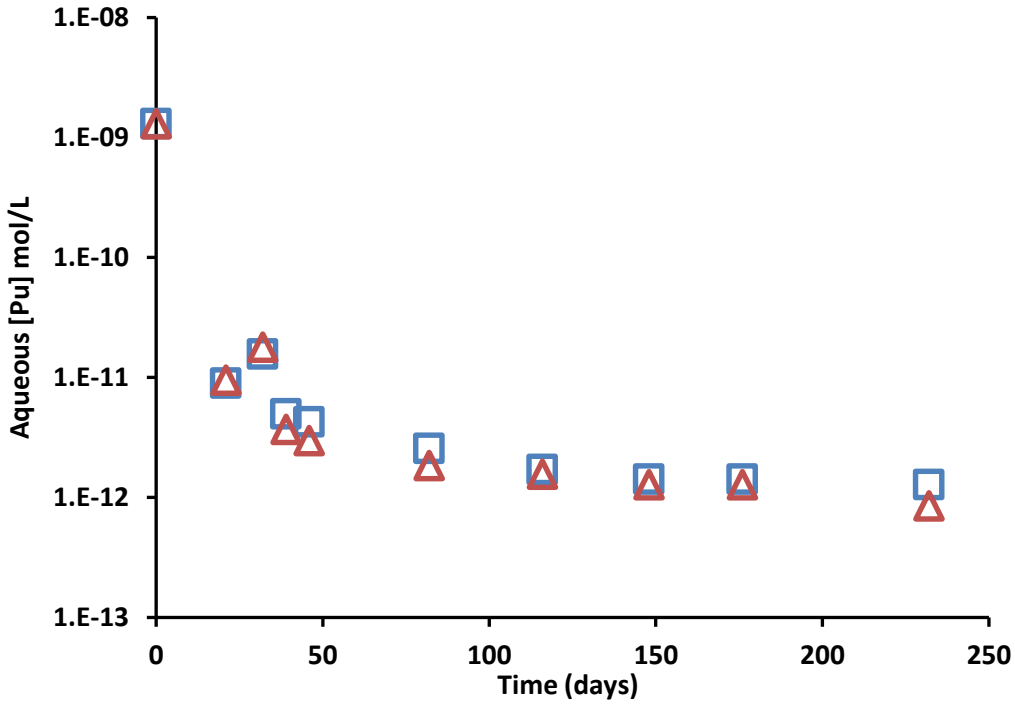

Figure-3-4. The aqueous Pu concentration in the flotation cells for 1 (□) and the duplicate (Δ) given in mol/L plotted against the time in days.

While it is possible that some of the decrease in aqueous Pu concentration may be due to sorption to the walls of the container, this is unlikely to be a significant factor. Begg et al., (2013) showed that only a minimal sorption to the container walls occurred in the presence of montmorillonite suspension [104]. The decreasing aqueous Pu concentration shows that Pu is slowly sorbing to the goethite added in the dialysis bag.

Figure-3-5 represents the calculated percentage of Pu that has sorbed to the goethite. Here the percent of Pu cumulatively desorbed from montmorillonite is plotted against time.

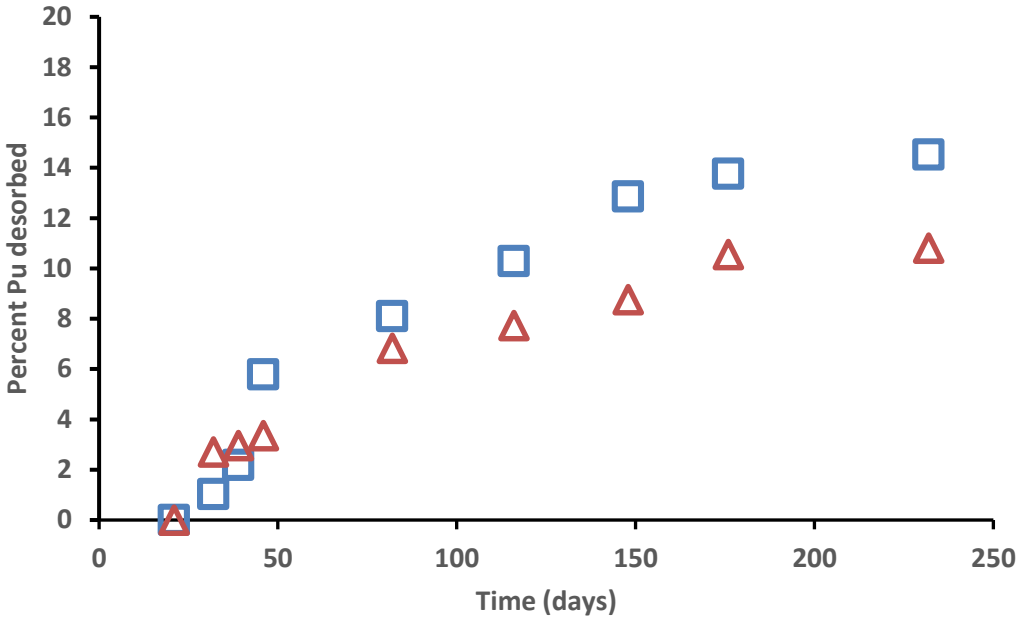

Figure-3-5. The percent of Pu that desorbed from the montmorillonite suspension outside the Float-A-Lyzer for 1 (□) and the duplicate (Δ) plotted against the time in days

The experiments were carried out for 210 days after the goethite-filled dialysis bag was added. At the end of the experiments, 14 % and 10 % of the Pu that was initially sorbed to montmorillonite had desorbed during each experiment. The desorption of Pu from montmorillonite in this ternary system shows that Pu sorption to montmorillonite is not irreversible, but can slowly be removed from the surface. Under constant solution conditions, and pH, the addition of a second mineral with a strong affinity for Pu, affects the desorption. The ternary mineral conditions for this experiment were such that aqueous Pu was expected to sorb to goethite because of the very strong sorption affinity for Pu. The experiment was designed so that there was seven times more goethite than montmorillonite, thus goethite behaved as a sink for aqueous Pu. Also, because the experiments were carried out at pH 8, little Pu was expected to desorb from goethite

[129**]**, whereas appreciable amounts of Pu were anticipated to desorb from the montmorillonite **[**131**] [**106**]**.

Two months after the dialysis bags were added, three additional aliquots were removed from experiment and subsequently placed in the dark on the shaker table. Over the next three months, one aliquot per month was analyzed for its Pu oxidation state using a LaF_3 co-precipitation method. **[**135**] [**92**]** Samples were also used to determine if any desorption occurred in the absence of the goethite. The results are found in Table 3-2.

Table 3-2. The fraction of Pu in each oxidation state for the respective time in days after the aliquot was removed from the flotation cell.

Experiment	Initial [Pu]	Time (days)		
		34	66	94
Total Aqueous Pu	Mol/L 10^{-12}	Mol/L 10^{-12}	Mol/L 10^{-12}	Mol/L 10^{-12}
1	2.56	2.56 ± 0.25	2.56 ± 0.25	2.56 ± 0.25
2	1.85	1.14 ± 0.19	1.14 ± 0.19	1.14 ± 0.19
Pu(V)				
1		0.67 ± 0.39	1.00 ± 0.26	1.00 ± 0.26
2		0.75 ± 0.56	1.03 ± 0.28	0.75 ± 0.56
Pu(IV)				
1		0.33 ± 0.56	0.00 ± 0.26	0.00 ± 0.26
2		0.25 ± 0.56	-0.03 ±0 0.28	0.25 ± 0.56

During the three months during which these aliquots were examined, no additional desorption occurred and some sorption may have occurred in duplicate 2. The oxidation state analysis shows that most, if not all of the aqueous Pu was in the (V) state, consistent with previous studies that have shown Pu and other redox-active radionuclides such as Tc, Np, and U oxidize and then remobilize in solution [138] [139] [140] [141] [142] [132].

3.3 Conclusions

Pu sorption and reversibility in a ternary mineral system with goethite and montmorillonite was examined using a dialysis bag approach. The dialysis bag maintained separation between the goethite and montmorillonite mineral suspensions such that the individual contribution of both phases to the overall sorption could be examined. Throughout the 230 days the K_d values of Pu sorption to montmorillonite increased to a log K_d value of five. The extended increase in K_d is due to the decrease of total aqueous Pu concentration caused by sorption to goethite, and because of trace Pu(V) sorption. Cumulative desorption of 14 and 10 percent of the Pu from the montmorillonite suspension was observed for the two experiments. The desorption occurs over a timescale of months and shows that equilibrium for Pu sorption in a multi-mineral scenario will likely occur over years.

The reversibility of Pu from the montmorillonite surface onto goethite implies that in an environment where there are multiple colloidal minerals present in groundwater, it is important to understand the competitive behavior of different mineral surfaces in order to determine the overall mobility of Pu in the groundwater. Under the experimental conditions explored in these experiments where Pu was present with two different minerals with different reactive surfaces, the goethite surface out competed the montmorillonite for the Pu.

Chapter 4

Automated Chemical Separation of Nuclear Forensic Related Samples

When responding to a nuclear event the primary objective would be assisting with rescue and safety of as many impacted citizens as quickly as possible [143] [1]. The second objective would be gathering data and analyzing the debris so that the responsible party(s) can be identified [5]. Collecting samples and completing their analysis is a labor and time intensive process. The samples are shipped to one of several laboratories throughout the country [144] where complete dissolution, separation and analysis of the samples are undertaken.

A major component of the analysis of the debris is the chemical separation of elements of interest for determining the characteristics of the device including: the sophistication of the device, the yield, efficiency and fuel of the device [5]. Although there are many good portable detectors [145] [146] [147], the high activity and quantity of fission products and activation products from the sample matrix is likely to inhibit their efficiency and effectiveness. Figure 4-2 shows a sample gamma spectrum of a neutron-irradiated ^{235}U foil across the energy range of 0 keV to just under 2100 keV. Figure 4-3 is an enlargement of the spectra from 500 keV to 600 keV and shows the difficulty of resolving the different photopeaks. Without chemical separation it is impossible to obtain the accurate information regarding the composition of the sample needed in order to determine device characteristics. This process is labor intensive and time consuming. Automating any part of the analysis process can reduce the time needed

to complete analysis and increase the throughput of samples to be analyzed. This work focuses on automating the chemical separation of eight elements that can be used to make a preliminary determination of device characteristics: europium (Eu), gadolinium (Gd), neptunium (Np), plutonium (Pu), promethium (Pm), terbium (Tb), uranium (U), and zirconium (Zr). The actinide elements Np, Pu, and U can be used to determine what material was used as the fuel for the device. Determining the fuel type will also inform the subsequent separation procedures that will be carried out in the complete analysis of the samples [148] [5]. The remaining five elements to be separated are fission products produced as a result of fission reactions of the fuel. Four of these five elements, Eu, Gd, Pm and Tb, are members of the lanthanide series of the periodic table. These four elements can be found on the right wing of the fission product yield curve shown in Figure 4-1. Lastly, Zr is a transition metal found in group four of the periodic table and can be found on the left wing of the fission product yield curve in Figure 4-1.

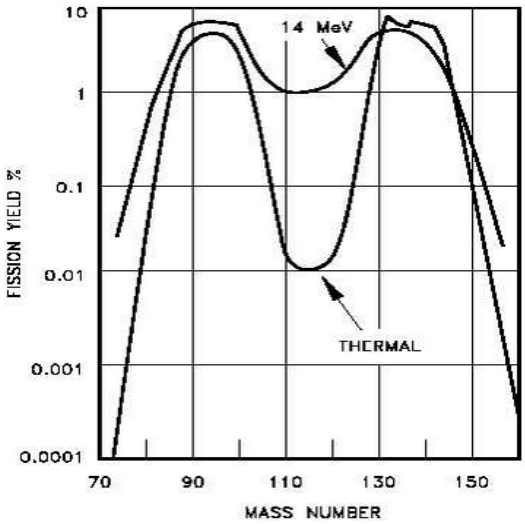

Figure 4-1. The fission product yields for thermal neutron fission of ^{235}U and fission of ^{235}U with 14 MeV neutrons [149].

The long term goal of this automation system is to have it deployable with one or more of the response teams. This system could be used at a base of operations to determine at least the composition of the fuel and potentially give approximate information about some of the device characteristics. Such an automated system could allow individuals with less rigorous scientific and technical backgrounds to operate this portion of the analysis thereby increasing the number of personnel who can contribute and the throughput and rate at which samples can be analyzed. In order to automate the chemical separation of these eight elements a number of factors were considered including: completing the separation as quickly as possible, accounting for the likelihood of matrix interferences, such as cement, that would need to be removed, and simplicity of the system and chemistry involved. The following sections of this chapter will describe the experiments carried out to determine the potential interference effects on the separation of these elements as a result of a cement matrix, the software development of this system and finally the results of using this automated system to separate solutions containing subsets of these eight elements.

In order to facilitate the automated separation of these eight elements, while minimizing the footprint of the system in order to make it amenable to deployment, the chemistry used should be carefully chosen. The chemistry used by the system will have significant impact on the overall design and potential compactness of the system. After potential nuclear forensic samples are dissolved in solution there are numerous methods by which the individual elements could eventually be isolated. However, to isolate individual elements by methods such as crystallization, distillation, and evaporation would require many cycles to achieve sufficient separation. Based on time alone these

separation methods are not conducive to the goal of rapid separations. Extraction techniques such as liquid-liquid extraction and solid phase extraction are more plausible candidates for separating select elements from mixtures of many. Liquid-liquid extraction, also known as solvent extraction, uses the chemical interaction between an aqueous phase and organic phase to selectively extract an element(s) from one phase and into the other. The PUREX process is an example of a liquid-liquid extraction process that uses tributyl phosphate (TBP) as the organic phase to extract Pu and U from dissolved used nuclear fuel in the aqueous phase [150]. Adding additional stages can increase the purity of the extracted species and high yields and high purities are contingent on the number of stages used. Another type of extraction techniques is solid phase extraction which involves the separation of a compound or element in a liquid by contact or interaction with a solid phase. A further subset of solid extraction is ion exchange chromatography, in which a mobile liquid phase flows over a resin, the solid phase, and compounds or elements of interest are selectively extracted on the solid phase. Ion exchange chromatography is the separation method used in the automated chemical separation system developed in this work.

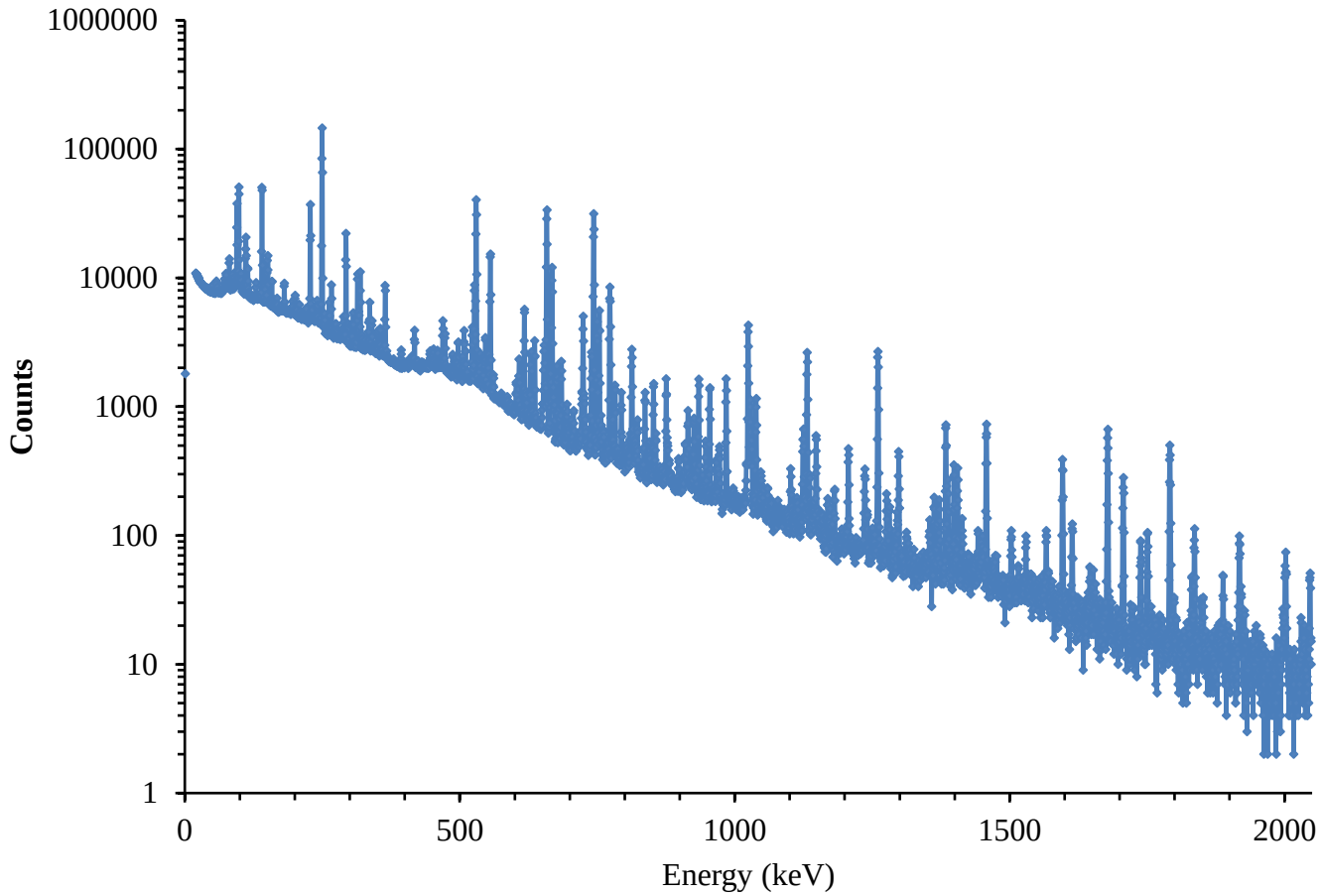

Figure 4-2. A gamma spectrum of the fission products produced from a neutron-irradiated ^{235}U foil counted for 30 minutes on an HPGe detector.

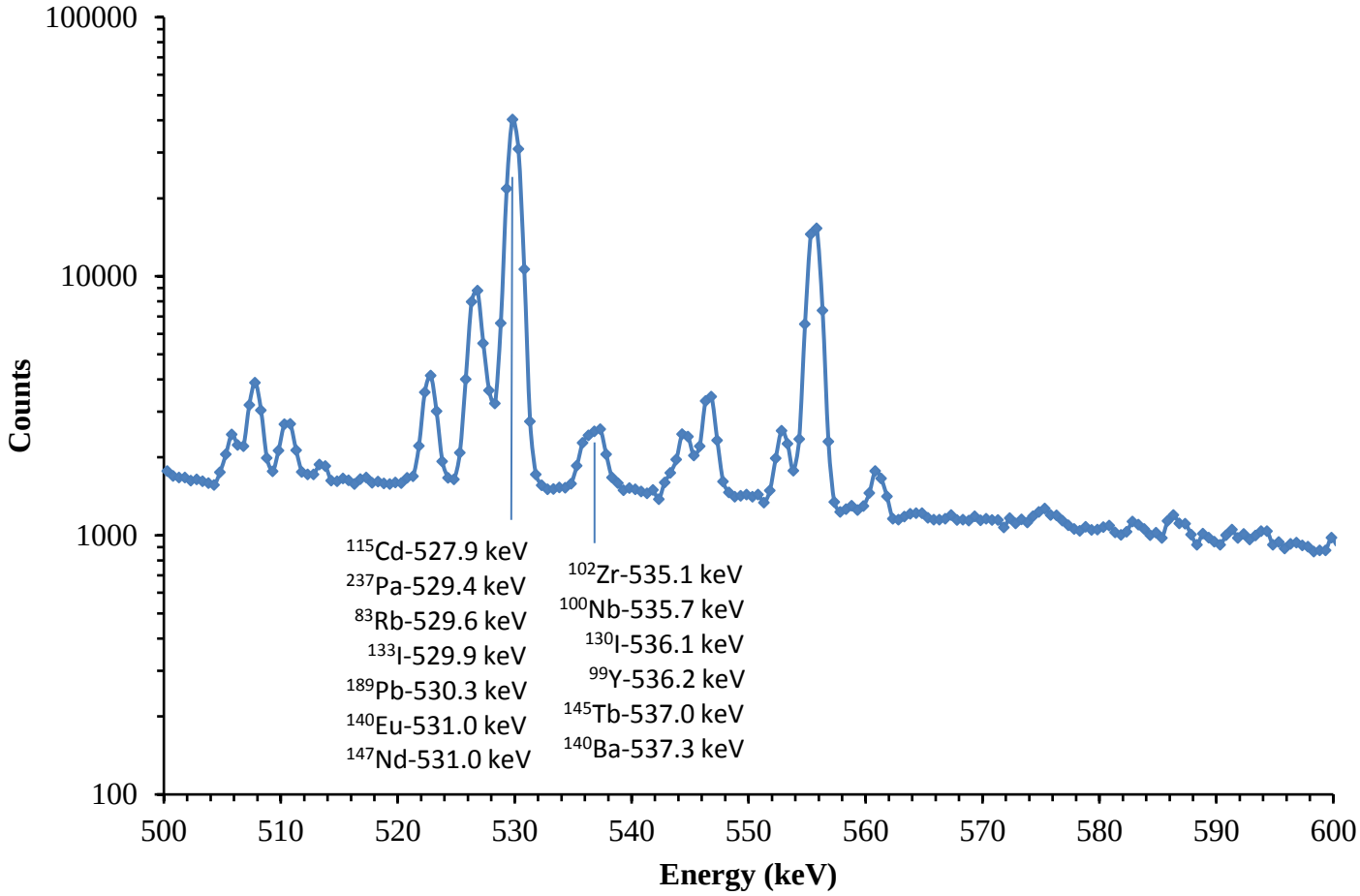

Figure 4-3. An enlarged view of Figure 4-2 from 500 keV to 600 keV. There are multiple isotopes with each peak in this section. For example, in the photopeak with its centroid at 530 keV several isotopes [151] that may contribute to these counts are listed in the box. The same is done for the photopeak with centroid around 536 keV.

4.1 Matrix Interference Effects on Chemical Separability

In the event that a nuclear device is detonated it is likely to occur in or near an urban area. Cement is a ubiquitous material in urban areas and the resulting fireball and fallout from the nuclear device will become mixed with the surrounding materials. In order to determine the effect of cement matrix interferences on the separation of the actinides and lanthanides in the automated chemical separation system a number of batch ion chromatography studies were performed. A brief explanation of ion exchange chromatography is followed by the results of the batch sorption experiments.

4.1.1 Ion Exchange Chromatography

Ion exchange chromatography is a sorption process by which anions or cations in a liquid are exchanged with ions of the opposite charge on the surface of a solid. This exchange is controlled by a reversible, stoichiometric, chemical reaction [152]. The relative strength of this exchange is called the selectivity and is often described in terms of the selectivity coefficient. The selectivity coefficient for the following reaction,

$$A^- + BR_{solid} \leftrightarrow AR_{solid} + B^- \qquad \text{Equation 4-1}$$

is defined as follows,

$$K_{A,B} = \frac{q_{AR} c_B}{q_{BR} c_A} \qquad \text{Equation 4-2}$$

where A and B are both ions with the same charge, q represents the molar concentration of A or B on the solid phase and c represents the molar concentration of A or B in the liquid phase. The selectivity coefficient $K_{A,B}$ refers to A in the liquid phase and its ability to exchange with B on the solid phase. The ion A can then be stripped off of the solid by changing the eluent to one with a much lower selectivity for A on the solid. The solid phase used in ion chromatography often consists of a stable support to which various functional groups are attached. These functional groups provide the reactive sites for ion exchange between the liquid and solid phases. The solid phase is generally also composed of small bead-like particles with porosities between 30-80 percent [152]. Small particles with high porosities increase the effective surface area or the number of potential reactive sites for ion exchange to take place. The ability of an ion exchange resin to selectively sorb one or more elements from solution and then be sequentially eluted is an important characteristic that can be leveraged for the chemical separation of the desired elements pertinent to this work.

The number of sites on the solid phase determines the capacity or total amount of a desired compound or element that can be adsorbed. The capacity of the resin to exchange ions is often represented in terms of milliequivalents per mL (meq/mL). The meq can be determined as follows:

$$meq = \frac{m * valence}{AW, MW} \qquad \text{Equation 4-3}$$

where m is the mass of the element or compound in mg, valence is the valence charge per atom or compound, and AW is the MW of either the atomic weight (AW) of the element, or molecular weight of the compound (MW). The meq of a resin is the theoretical maximum amount of an element of interest that can be adsorbed. In most if not all potential nuclear forensic samples, a large amount of other material may be present that could potentially fill all of the reactive sites on the resin before the desired element can be adsorbed. A number a batch adsorption experiments were carried out to determine the effect of a cement matrix on the adsorption of Pu and U, on an AG 1x8 resin. The adsorption of Eu, to both TRU and LN resin in the presence of significant competition from other ions in a cement matrix.

4.1.2 Plutonium and Uranium Batch Experiments

Based on previously established adsorption and separation procedures [153] [148] [5] an anion-exchange resin AG 1x8 resin will be used to separate the actinides, Np, Pu and U, in the automated chemical separation system. A Bio Rad AG 1x8 100-200 mesh size resin was used for the Pu and U batch experiments. The AG 1 resin is a strongly basic anion exchange resin that has quaternary ammonium functional groups attached to a styrene divinylbenzene copolymer lattice. The 1x8 represents the amount of cross-linking in the resin, eight percent for this resin, and determines the pore size of the resin beads, approximately 1 nm for eight percent cross-linking. The mesh size corresponds to the diameter of the particle size, 150-175 μm diameter for 100-200 mesh. The capacity of AG 1x8 resin is 1.2 meq/mL with a density of 0.75 g/mL. More information about the

resin characteristics can be found in the Bio Rad instruction manual [154]. The purpose of the Pu and U batch experiments was to determine how a dissolved cement matrix may impact the adsorption of Pu, U and other actinides on AG 1x8 resin. All solutions were prepared using ultrapure water (Milli-Q Gradient System, > 18 MΩ.cm), ACS grade chemicals without any further purification.). The cement matrix was prepared by crushing a piece of cement and then dissolving it according to the procedure described in Appendix A7. The dissolved cement solution is hereafter referred to as the pot solution. The composition of the pot solution was measured by via inductively coupled plasma mass spectrometry (ICP-MS) at LLNL and the results are given in Table 4-1.

Also calculated from the ICP-MS results and given in Table 4-1 are the individual meq contributions of each element as determined by average molecular weights and valences of each of the elements. The total meq/mL of the pot solution is ~0.07 meq/mL. Noticeably absent from Table 4-1 is the presence of silica (Si), a major component of cement [155]. While cement chemistry and composition can vary widely [155], this pot solution was used as a representation of the composition of cement that is likely to be seen in urban cement mixtures. Of the 57 elements identified by ICP-MS, Table 4-2 shows the 13 elements responsible for 99.9 percent of the total cation mass of the pot solution and the corresponding weight fraction of each element.

Table 4-1. The elemental composition of the pot solution in PPM and the corresponding meq of each element.

Element	PPM	2σ	meq	Element	PPM	2σ	meq	Element	PPM	2σ	meq
Li	4.4E-2	2.7E-3	6.4E-3	Ge	2.5E-3	2.9E-4	1.4E-4	Sm	4.7E-3	2.6E-4	9.4E-5
Be	3.7E-3	2.0E-4	8.3E-4	As	1.6E-2	9.6E-4	1.0E-3	Eu	2.0E-3	1.1E-4	3.9E-5
B	4.1E+1	2.8	1.1E+1	Rb	1.8E-1	9.5E-3	2.2E-3	Gd	4.7E-3	1.6E-4	9.1E-5
Na	8.7E+1	1.4	3.8	Sr	2.2	8.4E-2	5.0E-2	Tb	6.6E-4	3.9E-5	1.3E-5
Mg	1.2E+1	3.2E-1	1.0	Y	1.4E-2	3.4E-4	4.6E-4	Dy	3.7E-3	1.8E-4	6.8E-5
Al	8..3E+1	2.9	9.2	Zr	3.8E-1	2.0E-2	1.7E-2	Ho	7.5E-4	3.1E-5	1.4E-5
K	6.2E+1	2.6	1.6	Nb	2.0E-2	9.8E-4	1.1E-3	Er	2.1E-3	7.0E-5	3.8E-5
Ca	6.1E+2	3.1E+1	3.0E+1	Mo	1.3E-2	4.7E-4	8.4E-4	Tm	2.9E-4	1.2E-5	5.1E-6
Sc	2.4E-3	4.1E-4	1.6E-4	Ag	1.0E-3	9.9E-5	9.3E-6	Yb	1.8E-3	6.0E-5	3.1E-5
Ti	3.6	2.8E-1	3.0E-1	Cd	2.7E-3	4.2E-4	4.8E-5	Lu	1.3E-2	6.3E-4	2.2E-4
V	1.7E-1	8.9E-3	1.6E-2	Sn	4.3E-3	1.3E-3	7.3E-5	Hf	9.5E-3	8.7E-4	2.1E-4
Cr	7.0E-1	7.8E-2	8.1E-2	Sb	8.5E-3	4.5E-4	2.1E-4	Ta	1.0E-3	7.6E-5	2.8E-5
Mn	4.2	2.3E-1	5.4E-1	Te	6.8E-5	4.8E-5	2.1E-6	W	1.1E-2	8.4E-4	3.4E-4
Fe	4.6E+1	1.6	2.4	Cs	2.6E-3	1.6E-4	1.9E-5	Re	5.3E-6	3.0E-6	1.4E-7
Co	1.5E-2	4.6E-4	7.9E-4	Ba	4.5	3.0E-1	6.5E-2	Tl	1.4E-3	3.7E-5	2.1E-5
Ni	1.6E-1	6.5E-3	5.4E-3	La	3.0E-2	1.2E-3	6.5E-4	Pb	6.8E-2	2.2E-3	6.6E-4
Cu	1.6E-1	4.5E-3	4.9E-3	Ce	4.4E-2	2.1E-3	9.5E-4	Bi	3.6E-4	2.5E-5	5.1E-6
Zn	4.9E-1	2.6E-2	1.5E-2	Pr	6.7E-3	4.5E-4	1.4E-4	Th	1.3E-3	8.4E-5	2.2E-5
Ga	3.8E-2	2.6E-3	1.6E-3	Nd	2.6E-2	1.3E-3	5.5E-4	U	8.2E-3	3.5E-4	2.1E-4

Table 4-2. Summary of the elements with the largest contribution by mass to the chemical composition of the cement matrix.

Element	Weight %
Ca	63.6%
Na	9.1%
Al	8.7%
K	6.4%
Fe	4.8%
B	4.3%
Mg	1.3%
Ba	0.50%
Ti	0.40%
Mn	0.40%
Sr	0.20%
Cr	0.10%
Zn	0.10%
Total	99.9%

Eight of these 13 elements, Ca, Na, Al, K, B, Mg, Ba and Sr are responsible for greater than 94 percent of the total mass. Significantly, these eight elements do not sorb to AG 1x8 resin in HCl regardless of the molarity [153]. The remaining five elements are transition metals that exhibit a range of sorption to AG 1x8 resin from little sorption (10% or less for Mn) to very strong sorption (99.9% or more for Fe) [153]. Thus, a majority of the mass of the pot solution can be removed from the actinides of interest through ion exchange chromatography with AG 1x8 resin.

A ^{239}Pu stock in 8 M HNO_3 with an activity of 75.6 dpm/µL was used. One mL of the ^{239}Pu stock solution was aliquoted into a conical tube and 10 mLs of concentrated HCl were added. The solution was evaporated down until about 1mL of volume remained at which point 10 mL of HCl were added and the process was then repeated four times. After the last evaporation, the solution was adjusted to 2 M HCl and re-assayed using

LSC. A small aliquot, 0.5 mL, of the new ^{239}Pu stock in 2 M HCl was added to 4.5 mL of Ultima Gold scintillation cocktail and counted in a Perkin Elmer Tri-Carb liquid scintillation counter. The new ^{239}Pu stock solution had an activity of 2450 dpm/mL. A ^{233}U in 8 M HCl stock solution was also used such that a 1 mL aliquot was used to make a new stock in 8 M HCl whose activity was verified by LSC to be 6250 dpm/mL. The batch experiments conducted were used to obtain distribution coefficients for Pu and U on the AG 1x8 resin both with and without the pot solution.

The procedure for the batch experiments was adapted from similar batch sorption experiments done in previous work [153] [156] [154]. First, 0.1 g of the dry AG 1x8 resin was added to 1.5 mL microcentrifuge tubes. Then 1 mL of HCl with concentrations ranging from 0.001 M to 12 M in 1 M increments was added to wet the resin in the microcentrifuge tubes. A control with no resin added and 1mL of 2 M HCl was prepared to compare to the other samples and ensure that none of the Pu was unintentionally removed by anything other than the resin. Next 0.1 mL of the ^{239}Pu stock was added to each of the samples and then placed on a rotating shaker table (see Figure 4-4) for three hours. Each sample was prepared in triplicate.

Figure 4-4. A VWR standard orbital shaker table that was used to thoroughly mix the resin-solution slurry.

After three hours, the samples were removed and the resin slurry mixture filtered through a 0.45 µm Whatman polytetrafluoroethylene (PTFE) filter attached to a polypropylene syringe into a new 1.5 mL centrifuge tube. Next, a few µL of HCl were added as needed to ensure the volume, and thereby concentration, was the same before and after filtration. Then a 0.5 mL aliquot of the resin free solution was added to 6.5 mL of Ultima Gold scintillation cocktail and counted by LSC for one hour or until two percent error counting statistics were obtained. The percent of the Pu sorbed by the resin is determined by the following equation:

$$S = 100 * \frac{A_0 - A_f}{A_0} \qquad \text{Equation 4-4}$$

where S is the percent of Pu sorbed to the AG 1x8 resin, A_0 is the initial activity of the Pu that was added to the sample and A_f is the final activity measured by LSC. The percent sorbed can be converted to a K_d value as follows:

$$K_d = \frac{S - R}{100 - S} \qquad \text{Equation 4-5}$$

where S is the percent sorbed from Equation 4-4 and R is the ratio of liquid to resin used, which for these samples was approximately 11. The results of this batch experiment are represented by the blue line in Figure 4-5.

After completing the cement matrix free batch experiment with Pu and AG 1x8 resin, a series of batch experiments with increasing concentrations of pot solution added to the sample were conducted. For the first cement matrix batch experiment 0.01 g of AG 1x8 resin was measured into 1.5 mL microcentrifuge tubes. Then 0.9 mL of HCl

(concentrations varying from 0.001 M to 12 M) was added followed by 0.1 mL of Pu stock, followed by 0.1 mL of pot solution. Five control samples without resin were prepared at HCl concentrations from 2-12 M. Each sample was run in triplicate. Next the samples were placed on the shaker table and the slurry was mixed for three hours. The samples were then filtered and counted in the LSC according to the procedure described above. This process was repeated two more times with 0.2 mL and 0.3 mL of pot solution added to the samples. The last batch experiment involved the addition 1 mL of pot solution to each of the HCl concentrations from 0.001 M to 12 M. Because the HCl concentration of the pot solution was approximately 6 M each sample was adjusted by evaporating the sample until close to dryness or until a precipitate started to form. Then the appropriate HCl concentration was added and the process repeated up to four times. Next 0.1 mL of the Pu stock was added. Each acid-matrix-Pu solution was added to 0.01 g of the resin and the resulting K_d of Pu on the resin in those conditions was determined. The control samples where no resin was added demonstrated one percent adsorption of Pu or less to the container walls or the cement over the course of the three-hour batch experiment. The average activity of these samples was used as the initial activity added to each sample in their respective experiments. The results of these batch experiments are included in Figure 4-5 for ease of comparison with between the cement and cement free experiments.

The results of the Pu batch adsorption to AG 1x8 resin experiments are given in Figure 4-5. The logarithm of the K_d is plotted versus the concentration of HCl that was used in each sample. The log K_d values of 0, 1, 2 and 3 correspond to a percent of Pu sorbed value, S, or 9, 50, 91 and 99 percent sorbed respectively. The blue diamond line

gives the results for adsorption of Pu to resin in the absence of any cement matrix effects. There is essentially no adsorption of Pu to the resin until 6 M HCl, above which there is increasing sorption until greater than log K_d of 2. As increasing amounts of cement matrix are added the HCl concentration at which Pu sorption begins to occur also increases, with the exception of the 100 percent cement matrix which shows Pu adsorption beginning at 5 M HCl. The Pu sorption for the 100 percent cement matrix shows adsorption behavior that is inconsistent with any of the other trends. A possible explanation for the behavior of the 100 percent cement matrix may be a result of the amount of material present that was greater than the operating capacity of the resin as it has been suggested to use less than 25 percent of the capacity [5]. Iron for example shows a corresponding increase in adsorption to the AG 1-x8 resin with increasing HCl concentration until reaching a maximum around 8 M before decreasing. A number of other transition elements show a maximum and then decreasing sorption with a continued increase in the HCl concentration [153]. The total meq of the Pu-cement matrix was approximately 43 percent of the theoretical capacity of the resin. Another possible reason for the behavior may be the result of Pu complexation with the cement matrix constituents, particularly transition metals such as iron. As discussed in Chapter 3 Pu complexes very strongly with the mineral goethite and one of the primary constituents of goethite is iron. However, as there was very little observed sorption of Pu to the cement only, it is not likely that the Pu is complexing with the cement. Each of the batch adsorption experiments leads to 90 percent or more of the initial Pu being adsorbed by the AG 1x8 resin. The adsorption of Pu beginning at 6 M HCl in the absence of cement matrix is consistent with previous work [153]. As the percentage of cement matrix

increases Pu adsorption begins at higher HCl concentrations as might be expected due to an increase in ions competing with Pu to exchange on the resin. The 10 percent cement matrix appears to have a small synergistic effect on the adsorption of Pu at high HCl concentrations compared to the cement matrix free adsorption behavior. The difference in percent sorbed at 12 M HCl is less than 10 percent indicating that a cement matrix should have relatively small impact on the adsorption of Pu to AG 1x8 resin at high HCl concentrations.

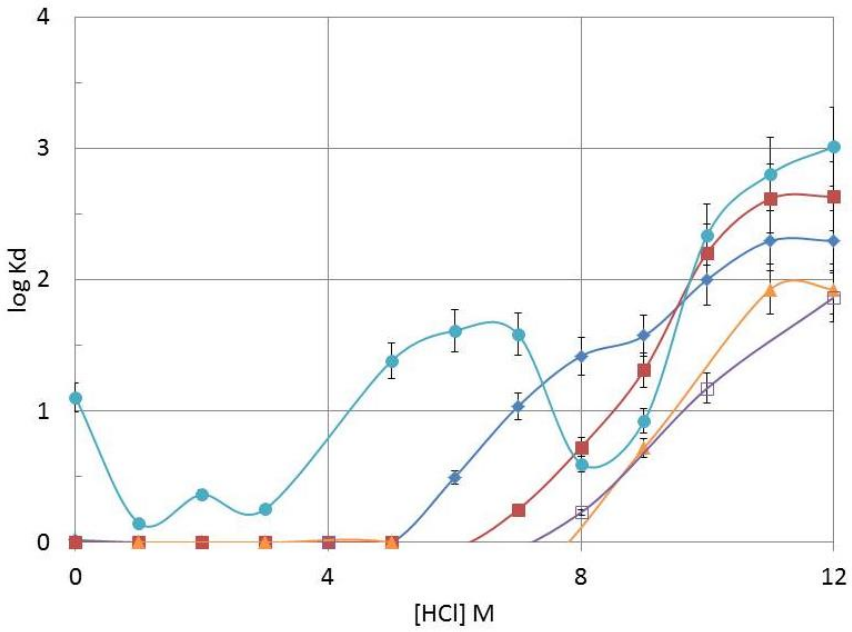

Figure 4-5. Batch experiments for Pu adsorption to AG 1x8 resin versus the [HCl] for (-♦-) no cement matrix, (-■-) 10% cement matrix, (-▲-) 20% cement matrix, (-□-) 30% cement matrix and (-●-) 100% cement matrix. Sorption occurred over three hours. The error bars represent the standard deviation of triplicate samples.

A series of batch U adsorption to AG 1x8 resin experiments were carried out in the same manner as the Pu batch experiments. Initially the adsorption was carried out in the absence of a cement matrix. Then pot solution was added to create 10, 20 and 30 percent mixtures in subsequent batch experiments and the results are given in Figure 4-6

below. In Figure 4-6 the blue diamond line shows the log K_d of U sorption to AG 1x8 resin in the absence of cement matrix and reaches a final log K_d value of 2.6, or greater than 97 percent sorption. Uranium sorption in the absence of cement matrix begins for HCl concentrations greater than 1M. Uranium sorption in the presence of a cement matrix begins at an HCl concentration of 1 M or less. The final log K_d values for the samples with increasing cement matrix concentrations approach three, or the equivalent of 97-99 percent of the U adsorbing to the resin. The presence of the cement matrix appears to provide no hindrance to the adsorption of U and demonstrates possibly a slight enhancement of the adsorption of U onto AG 1x8 resin, particularly for HCl concentrations below 4 M.

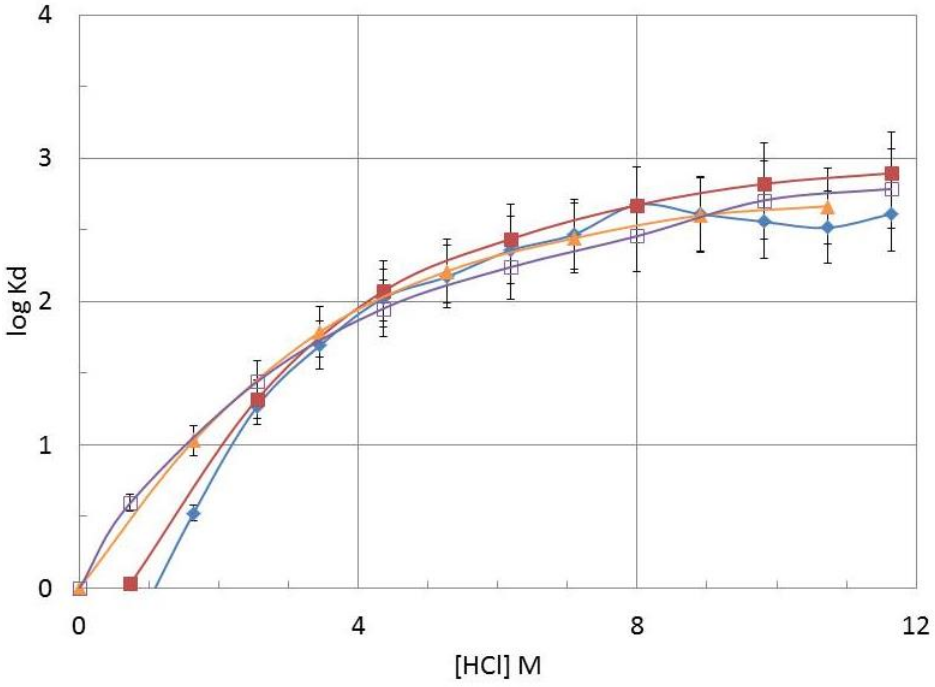

Figure 4-6. Batch experiments for U adsorption to AG 1x8 resin versus the [HCl] for (-♦-) no cement matrix, (-■-) 10% cement matrix, (-▲-) 20% cement matrix and (-□-) 30% cement matrix. Sorption occurred over three hours. The error bars represent the standard deviation of triplicate samples.

After completing the batch sorption experiments gravity based column experiments were conducted to ensure that both Pu and U could be recovered after sorption to the AG 1x8 resin in the presence of the cement matrix.

4.1.3 Plutonium and Uranium Column Experiments

Plutonium and uranium gravity based column experiments were conducted to elute the Pu and U from an AG 1x8 column and determine a suitable HCl/HI acid mixture. The AG 1x8 100-200 mesh resin was previously washed and prepared before loading in the column per the following procedure [157]:

200 g of resin was measured into a 500 mL Nalgene bottle.
The resin was rinsed twice with 200 mL of MQ water.
The resin was rinsed twice with 200 mL of 1M NaOH.
The resin was rinsed twice with 200 mL of MQ water.
The resin was rinsed twice with 200 mL of 1 M HCl.
The resin was rinsed twice with 200 mL of MQ water.
The resin was rinsed with 200 mL of 95 % ethanol
The resin was rinsed twice with 200 mL MQ water.
The resin was stored in a 0.1 M HCl solution.

The column separation of Pu and U is based on published procedures [158] [5]. The column was prepared by placing a PTFE frit in the bottom and then filling with MQ water. The resin was then added drop-wise and allowed to gravity settle in the column until a resin column volume of 2 mL was obtained. Then 5-6 mL of 8 M HCl was used to wash the column. A one mL aliquot of a stock solution with approximately 12500 cpm/mL of ^{233}U and 1500 cpm/mL of ^{239}Pu in 8 M HCl was loaded onto the column. Next the column was washed with 5 mL of 11 M HCl. The Pu was then eluted with an acid mixture containing 10 M HCl and 3 drops of concentrated (7.6 M) HI per mL of

HCl. The HI is added to reduce the Pu from the +4 oxidation state to the +3 oxidation so that it will elute off the column [153]. A total of 6 mL of the HCl/HI acid mixture was added to the column in 1 mL fractions and the eluted Pu was collected in 1.5 mL microcentrifuge tubes. Next 6 mL of 0.1 M HCl was added to the column in 1 mL fractions and the eluted U was collected in 1.5 mL microcentrifuge tubes. A 0.5 mL aliquot was taken from each fraction and added to 6.5 mL of scintillation cocktail and then counted by LSC. The elution curves are shown in Figure 4-7. The total fraction of Pu recovered was 78 percent, which is somewhat lower than expected. This may be due to the HI used that was stored at room temperature and not refrigerated, therefore losing some of its reducing capability. Also, it could result from not enough HI in the HCl/HI mixture. Another factor may be that there was not a complete oxidation state equilibrium before the Pu was added to the column. The total fraction of U recovered was 98 percent.

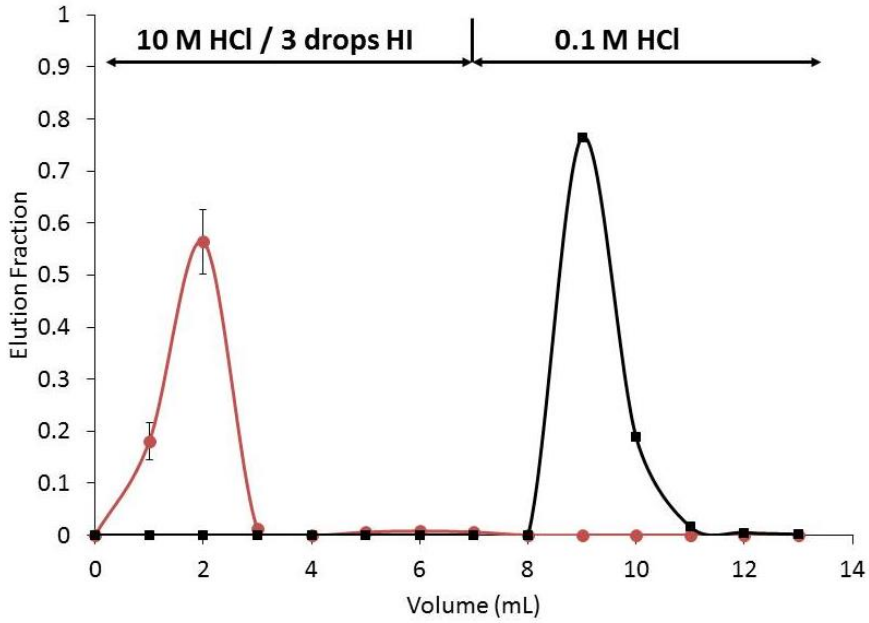

Figure 4-7. The elution curves for the Pu (–●–) and U (–■–) separation on AG 1x8 resin column. The Pu was eluted with a mixture 10 M HCl and 3 drops of HI per mL. The error bars are propagated from counting statistics.

Then a second Pu and U column separation was conducted with a greater volume fraction of HI used to elute the Pu. In the second column separation, a 3:1 ratio of 10 M HCl / HI was used. The fractions were collected in 1.5 mL microcentrifuge tubes and 0.5 mL aliquots were counted by LSC. The elution curves for this separation are given in Figure 4-8. The total Pu eluted from the second column was 82 percent of the total and the total U eluted from the column was 99 percent of the total. Again, the total Pu eluted was a little bit lower than expected but can likely be attributed to using room-temperature HI. These column experiments show that both Pu and U can be sequentially separated using AG 1x8 resin. Also, there appears to be a clear separation between the two elements. This is important for the automation chemistry, where small bleed through of the actinides could lead to significant challenges when counting with LSC.

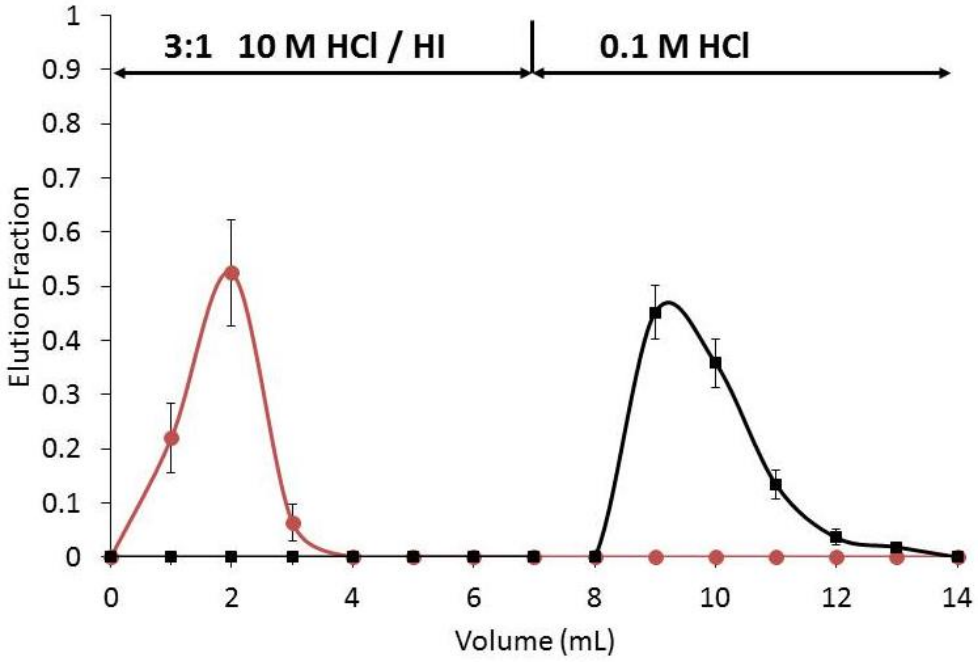

Figure 4-8. The elution curves for the Pu (–●–) and U (–■–) separation on AG 1x8 resin column. The Pu was eluted with a 3:1 mixture of 10 M HCl / HI. The error bars are propagated from counting statistics.

4.1.4 Europium Batch Sorption Experiments

As described in the previous section many elements show no sorption to the AG 1x8 resin in any HCl concentration. The lanthanides series of elements also exhibit no adsorption to the AG 1x8 resin in HCl. The next step in designing a feasible chemistry for use in the automated chemical separation system is determining a suitable approach to separate the lanthanides of interest, Eu, Gd, Pm and Tb. The elements of the lanthanide series exist primarily in the +3 oxidation state and have similar chemical and physical properties that make separation of these elements difficult. In the early 1950s scientists began to explore the separation of individual lanthanides and the first comprehensive study of the separation of the lanthanides using a cation exchange resin and alpha-hydroxyisobutyric acid (α-HIBA) was published in 1956 [159]. For the next 60 years the majority of work involving lanthanide separations has been done with cation exchange chromatography and α-HIBA to elute individual elements [160] [161] [162]. The separation of the lanthanides with cation exchange chromatography and α-HIBA entails a finely tuned gradient in the concentration of α-HIBA [163] [164] [165] or a pH gradient with a low concentration of α-HIBA [148].

While lanthanide separations using α-HIBA has been described extensively, both HNO_3 and low concentrations of HCl have been used to produce individual lanthanide separations. A resin with di-2-ethylhexylorthophosphoric acid (HDEHP) as the functional group has been used to separate the lanthanide series with varying concentrations of HNO_3 [166]. HDEHP is the same functional group used in Eichrom's LN resin and the

extractant molecule is shown in Figure 4-9 [167]. The lanthanides can be eluted from the LN resin using increasing HNO_3 concentrations [166] [167].

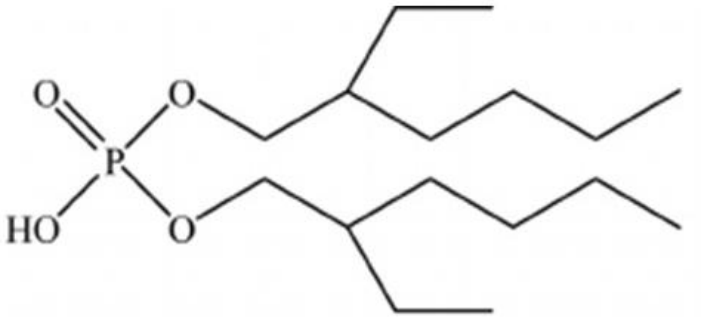

Figure 4-9. HDHEP, the extractant molecule of LN resin.

Separation of the lanthanides from actinides and other elements using both HNO_3 and HCl using Eichrom's TRU resin, which uses octylphenyl-N,N-di-isobutyl carbamoylphosphine oxide (CMPO) dissolved in tri-n-butyl phosphate (TBP) as the functional group for extraction (see Figure 4-10), has also been shown [168] [169].

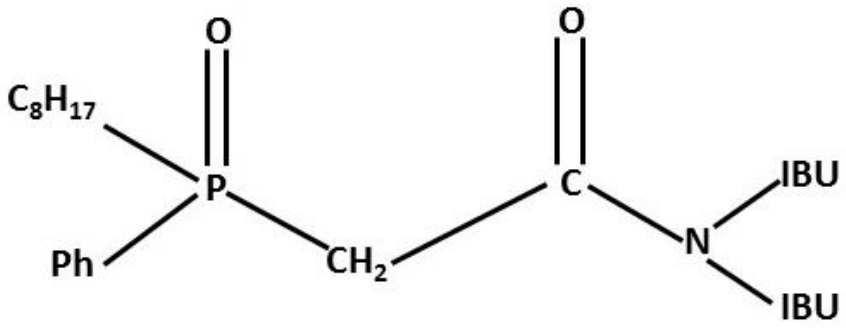

Figure 4-10. CMPO, the extractant molecule of TRU resin.

Earlier work has shown the separation of lanthanides by using TRU resin and LN resin in tandem, where the lanthanide containing eluent of the TRU resin was used as the load solution for the LN resin [170]. The lanthanides will sorb strongly to TRU resin at HNO_3 concentrations above ~3 M and then can be eluted with an HNO_3 concentration of 0.05-0.1 M [145] [147]. Using TRU resin and LN resin in tandem offers the potential to be more robust in separating the lanthanides when trying to eliminate the time required for evaporating and re-suspending the pot solution to use with a finely tuned cation exchange and α-HIBA gradient column. Batch sorption studies were conducted to determine the ability of TRU resin to sorb Eu from an 8 M HCl concentration, slightly higher than the expected HCl concentration of the pot solution, when it is diluted with varying concentrations of HNO_3. Also, batch Eu sorption experiments on TRU resin were conducted with varying cement matrix interference concentrations as most the cement matrix is expected to follow with the lanthanides after loading and washing from an AG 1x8 resin column. Batch Eu sorption experiments onto LN resin were also performed and the results are discussed after the batch sorption onto TRU resin experiments.

For the batch Eu sorption onto TRU resin experiments a stock solution of ^{152}Eu in 8 M HCl was acquired and a one mL aliquot was counted using an Ortec HPGe detector with an efficiency of around 10 % shown in Figure 4-11. Ortec's MAESTRO software was used to collect and analyze the gamma spectra obtained from each sample counted. The ^{152}Eu stock solution had an activity of ~53 counts per second (cps) and the gamma spectra obtained is given in Figure 4-12 as an example of the gamma spectra obtained in this work. The detector was not calibrated for efficiency or geometry and care was taken to count all subsequent samples in the same geometry as the initial sample.

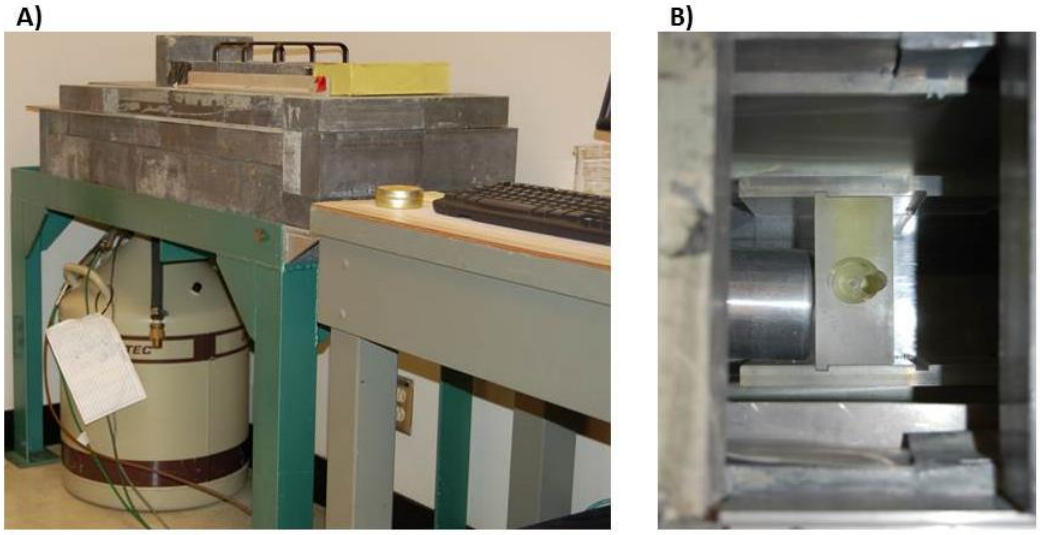

Figure 4-11. The Ortec HPGe detector setup that was used to count solutions with gamma-emitting radionuclides including: A) the detector surrounded by lead shielding and B) an overhead view of the sample holder next to the detector face.

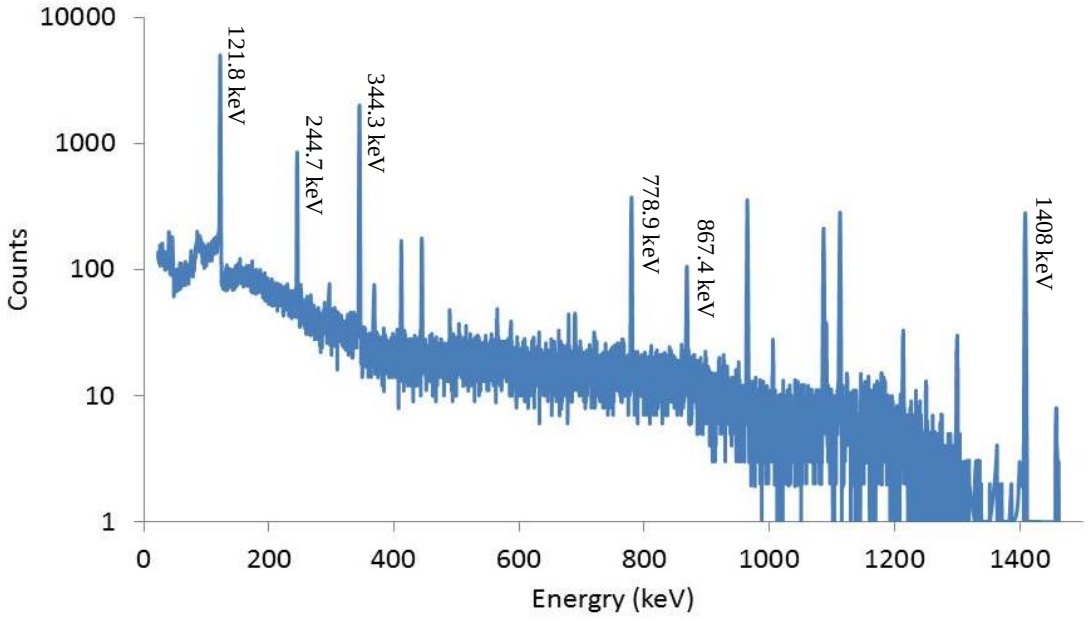

Figure 4-12. The gamma spectra obtained from a 10-minute count of the ^{152}Eu stock solution. Identifying peaks can be found at the following energies: 121.8 keV, 244.7 keV, 344.3 keV, 778.9 keV, 867.4 keV and 1408 keV.

The Eu sorption onto TRU resin batch experiments were performed like the Pu and U batch experiments described in section 4.1.2 Plutonium and Uranium Batch Experiments. For these batch experiments 0.01 g of TRU resin was weighed into 1.5 mL microcentrifuge tubes after which 1 mL of HNO_3 with concentrations varying from 0.001 M to 6 M is added followed by 0.1 mL of ^{152}Eu in 8 M HCl stock solution. Three samples without resin were also used as controls to confirm that no Eu was removed through sorption to cement. Each sample was placed on the orbital shaker for 10 minutes, then removed and filtered. One mL of the remaining filtrate was counted on the HPGe for 10 minutes and the activity was used to determine the percent sorbed K_d values of each sample. All samples were performed in triplicate. The results of the batch sorption experiment are given in Figure 4-13.

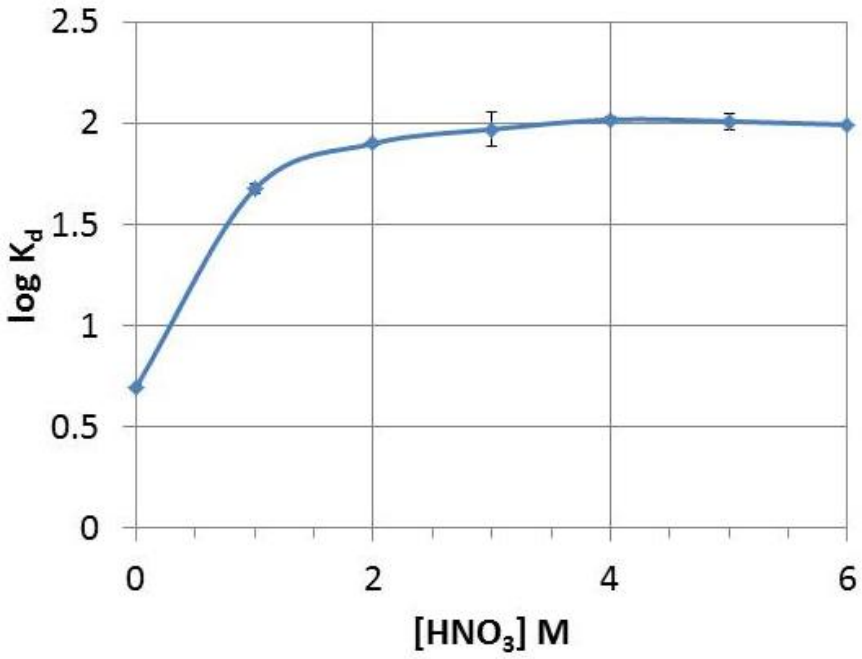

Figure 4-13. Batch Eu sorption onto TRU resin in a 10 % 8 M HCl with 90 % HNO_3 at varying concentrations. Sorption occurred over 10 minutes. The error bars represent the standard deviation of triplicate samples.

There is very little Eu adsorption to the TRU resin when there is no HNO_3 in the slurry mixture. The amount of Eu adsorption to the resin increases with increasing HNO_3 concentration until reaching a K_d value of a little more 2. From Figure 4-13 it is apparent that diluting a pot solution mixture in 6-8 M HCl with HNO_3 between 3-6 M by a factor of 10 should induce adsorption of the lanthanides onto the TRU resin.

After confirming the sorption of lanthanides on TRU resin in an HCl-HNO_3 acid mixture, the next step was to determine any potential matrix effects on the sorption of the lanthanides in the presence of the dissolved cement. A batch Eu sorption onto TRU experiment with increasing concentrations of cement matrix added was conducted. In order to negate some of the decreasing HCl-HNO_3 dilution ratio the ^{152}Eu stock solution was converted from 8 M HCl to 4 M HNO_3. The cement matrix was in 8 M HCl and diluted with 4 M HNO_3. Again 0.01 g of TRU resin was weighed into 1.5 mL microcentrifuge tubes. Then 0.7-0.95 mL of 4 HNO_3 was added to wet the resin followed by a corresponding amount of 0.3-0.05 mL of cement matrix in 8 M HCl and 0.1 mL of the 4 M HNO_3 ^{152}Eu stock solution was added to each microcentrifuge tube. The slurry was placed on the orbital shaker for 10 minutes to thoroughly mix the slurry and then removed and filtered. The sorption results are given in Figure 4-14 in terms of the log K_d values plotted against the volume percent of cement matrix. Figure 4-14 shows a decrease in the K_d value of ~0.1 with an increase in the volume percent of the cement matrix from zero to five percent. Over the next five percent increase in the volume percent of the cement matrix the K_d values decrease by another 0.25. As the volume percent of the cement matrix increases until 28 percent by volume, the K_d only decreases by another 0.1. The TRU resin capacity for 0.01 g was about an order of magnitude lower than the

~0.007 meq present in the cement matrix at 10 volume percent. The initial decrease in the ^{152}Eu sorption K_d is likely a result of increased competition from stable lanthanides and other cations present in the cement matrix. However, as increasing amounts of the cement matrix were added the K_d only decreases slightly. This extended decrease in the K_d may be a result of increased competition from species present in the cement matrix. However, the K_d decreases very slightly with each successive increase in the volume percent of the cement matrix and is possibly the result of the increasing volume percent of the cement matrix gradually increasing the HCl concentrations of the HCl-HNO_3 ratio in the slurry mixtures.

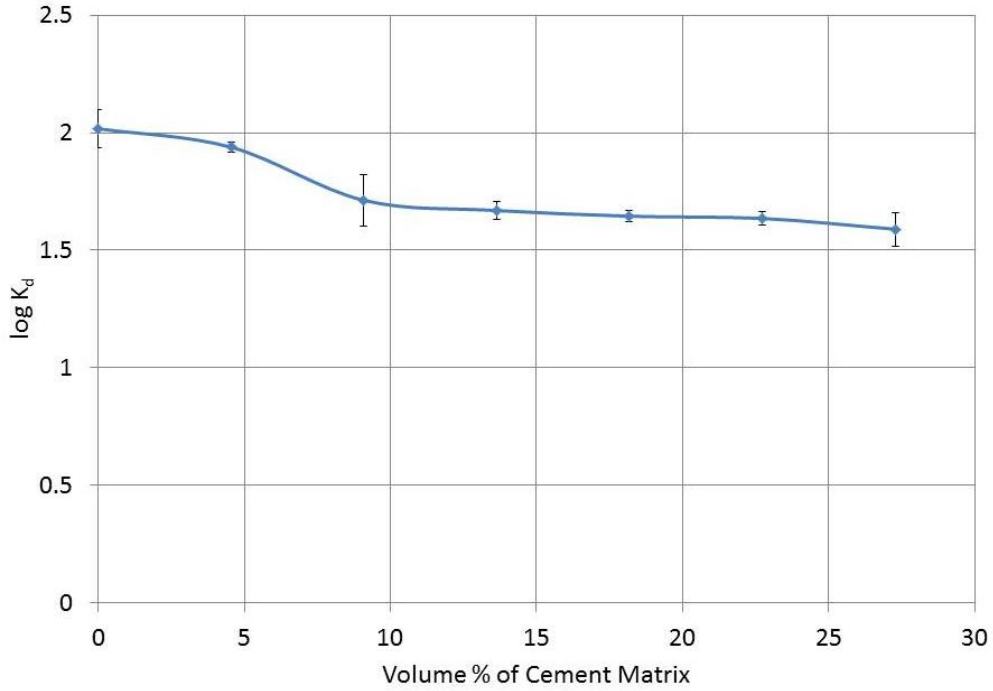

Figure 4-14. Batch Eu sorption to TRU resin experiments in the presence of differing volume percent of cement matrix (8 M HCl) and corresponding volume percent of 4 M HNO_3. Sorption occurred over 10 minutes. The error bars represent the standard deviation of triplicate samples.

Batch Eu sorption on LN resin was also investigated. A ^{152}Eu stock solution in 0.05 M HNO_3 was prepared and then counted with the Ortec HPGe detector. LN resin (0.01g) was weighed into 1.5 mL microcentrifuge tubes and then one mL of varying concentrations of HNO_3 was added to wet the resin followed by 0.1 mL of the ^{152}Eu stock solution. Three control samples at HNO_3 concentrations of 0.05, 1 and 4 M were also prepared and each sample was prepared in triplicate. The microcentrifuge tubes were placed on the orbital shaker and thoroughly mixed for 10 minutes. The tubes were then filtered and 1 mL aliquots were counted with the Ortec HPGe detector. The results are given in Figure 4-15, which shows very strong sorption at very low concentrations of HNO_3 (less than 0.5 M) and decreasing sorption with increasing HNO_3 concentration. This trend of strong sorption at low HNO_3 concentration that decreases with increasing concentration was the expected result based on results from literature [166] [156].

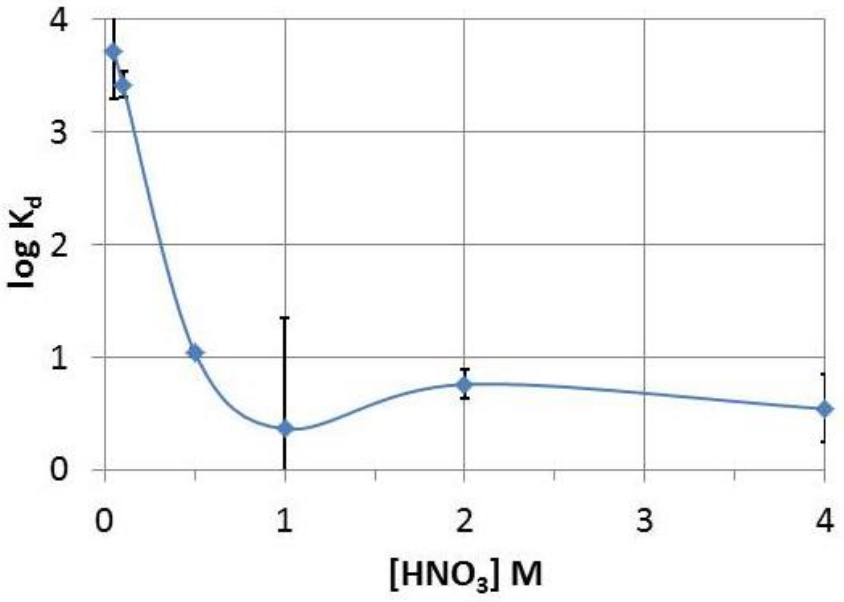

Figure 4-15. Batch Eu sorption to LN resin experiments in the presence of differing concentrations of HNO_3. Sorption occurred over 10 minutes. The error bars represent the standard deviation of triplicate samples.

After completing several batch sorption experiments for U, Pu, and Eu, a potential chemical separation procedure using a combination of AG-1x8, TRU and LN resins was determined that may be suitable for use in an automated system to separate the desired elements: Eu, Gd, Np, Pm, Pu, Tb, U, and Zr. First, the sample(s) is dissolved using the rock dissolution procedure (see Appendix A7) to prepare a load solution in 6 M HCl. The load solution is added to an AG-1x8 column and washed with 11 M HCl. This should remove Np, Pu, U and Zr from the load solution along with a few species, such as Fe from the matrix. If there is a disproportionately large amount of the matrix that is removed a second AG-1x8 column could be added. The elements that are not sorbed with the AG-1x8 resin are then diluted by at least a factor of 10 with 4 M HNO_3 and then become the load solution for a TRU resin column where the lanthanides should be removed from the load solution. The TRU resin is column is then flushed with 4 M HNO_3 to wash the remainder of the pot solution. The elements on the AG-1x8 resin column can be eluted sequentially as follows: Pu is eluted with a 10 M HCl and 7.6 M HI mixture, then Zr is eluted with a 9 M HCl/0.03 M HF mixture, followed by Np eluted with a 4 M HCl/0.1 M HF mixture and finally U is eluted with 0.1 M HCl. After eluting all the elements from the AG-1x8 resin column the lanthanides are eluted from the TRU resin column with 0.05 M HNO_3 and then loaded on the LN resin column where they can be eluted with progressively higher HNO_3 concentrations. First, Pm is eluted with 0.5 M HNO_3 followed by Eu and Gd using 1 M HNO_3 and lastly Tb is removed with 3 M HNO_3. After all the separations are complete a series a washing steps are used to prepare the columns for another separation. A more thorough discussion of the design of the automated system can be found in the following sections.

4.2 Automated System and Program Development

High performance/pressure liquid chromatography (HPLC) is a separation technique that is used to separate the species in a liquid sample by the chemical and physical interaction of those species with porous particles packed in a column. These species are forced through the column with one or more eluents at a high pressure. The eluted fraction is then analyzed in a spectrophotometer. The most common types of spectrophotometry associated with HPLCs are UV-Vis spectroscopy, mass spectroscopy, and refractive index detection. The injection sample is usually of small volume (typically in µL volumes) and there are several different column sizes ranging from < 0.1 mm inner diameter (i.d.) to > 4.6 mm i.d. and up to 250 mm in length. There are several different types of HPLC systems commercially available and more detailed information is available through commercial websites [171] [172] [173].

HPLC is commonly used for preconcentration of trace components, water purification, and ion exchange chromatography of proteins among many other specific applications. Among the applications relevant to this work HPLC has been applied to the separation of lanthanides and actinides [174] [175] [176]. The group and individual separation of lanthanides from actinides as well as the separation of actinides from lanthanides have been demonstrated using HPLC primarily for the purpose of nuclear fuel burn-up calculations or waste characterization analysis [177] [178] [179] [180] [181] [182] [183] [184] [185] [186]. These separations are carried out after dissolving various fuel matrices (uranium, thorium or plutonium) and are diluted before injecting volumes of 20-200 µL to be separated. After dissolution and injection, the actual column

separations are usually completed on timescales of minutes, but if more than one column is used typically one or more intermediate preparation steps that require several hours to complete is necessitated. This work uses a design similar to HPLC and applies the process to the separation of elements relevant to nuclear forensic analysis of a post-detonation scenario.

In a post-detonation scenario, the faster a sample(s) can be analyzed the better. There are likely to be many samples and each sample may contain mg of material. Key differences in applying HPLC to these post-detonation nuclear forensics samples include: these samples are likely to be in either cement or soil type matrices as opposed to nuclear fuel matrices, injection volumes may be many times larger, it removes intermediate steps in order to decrease the overall time for separation, and individual separation of multiple actinides and lanthanides in series from the original injection solution can be obtained. In an effort to address these differences the fundamental HPLC design was tailored for a chemical separation scheme that can separate eight of the elements of interest to possible post-detonation nuclear forensics sample analysis. A schematic of the system developed for this work is shown in Figure 4-16. The sample is injected into valve V1 which has a 1 mL injection loop, and then can be loaded on 1-3 columns before exiting to either the waste stream or fraction collector for analysis. The automated system is controlled using the software program LabVIEW. The hardware and software used to develop this system is described in the following paragraphs.

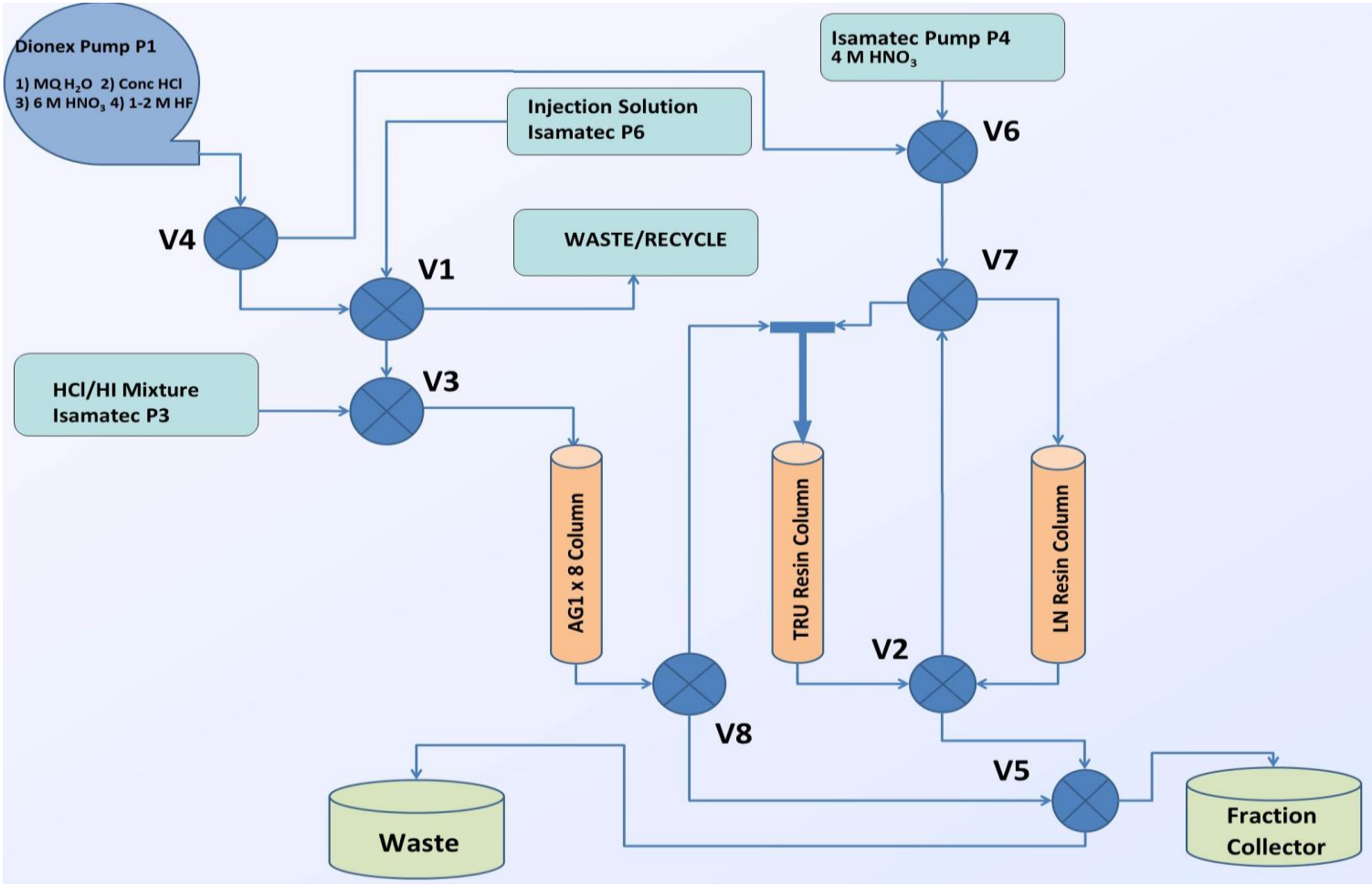

Figure 4-16. A flow chart for the automated system. V1-V8 are multi-position valves. The sample is injected with pump P6 into valve V1 and eluent eventually exits from V5 to either the fraction collector or the waste stream.

A number of different pieces of hardware were incorporated in order to design the automated chemical separation system. A listing of each piece of hardware used in the automated system is given in Table 4-3 along with the company that produces the part.

Table 4-3. A table of the hardware used for the automated chemical separation system

Name	Part	Company
Gradient Pump P1	ICS-5000 DP	Dionex
Pumps P3, P4, P6	Reglo Digital 2 channel	Isamatec
Valves V1-V3, V5-V8	Cheminert 4,6,8 port 2-position valves	VICI
Valve V4	Cheminert 7 port multi-position valve	VICI
Fraction Collector	Amersham RediFrac	GE Healthcare

The gradient pump P1, shown in Figure 4-17, is a standard pump for Dionex HPLC systems. The pump can mix up to four different eluents in the gradient mixer which comes in two sizes depending on the size of the column(s) to be used.

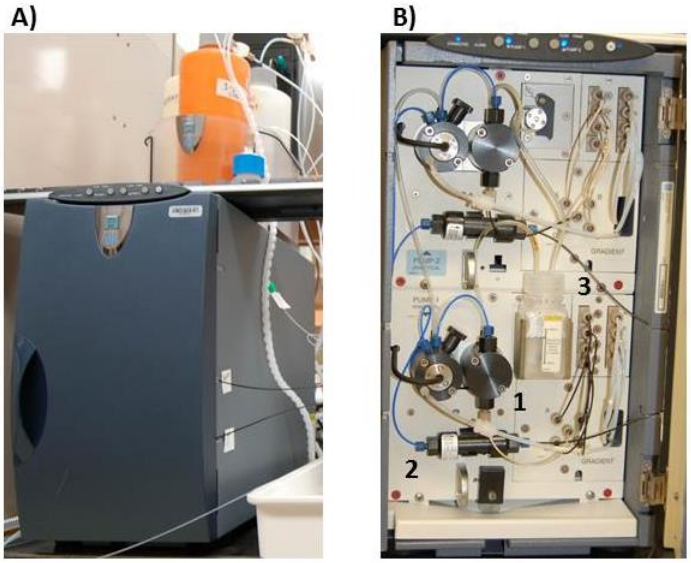

Figure 4-17. The ICS-5000 DP gradient pump viewed from: A) outside with eluent bottles seen on top and B) with the front over open showing the pump (1), the gradient mixer (2) and the inlets from the eluent bottles (3).

The pump may be used at pressures up to 5000 psi and flow rates from 0-10 mL/min. The gradient pump came with polyetheretherketone (PEEK) tubing that is generally resistant to a wide range of eluents. The gradient pump is controlled by Chromeleon software program that has a software development kit that makes the pump amenable to control by other programs. The Reglo Digital pumps (P3, P4 and P6 shown in Figure 4-18 A) from Isamatec came with a LabVIEW driver that was used to control the pumps.

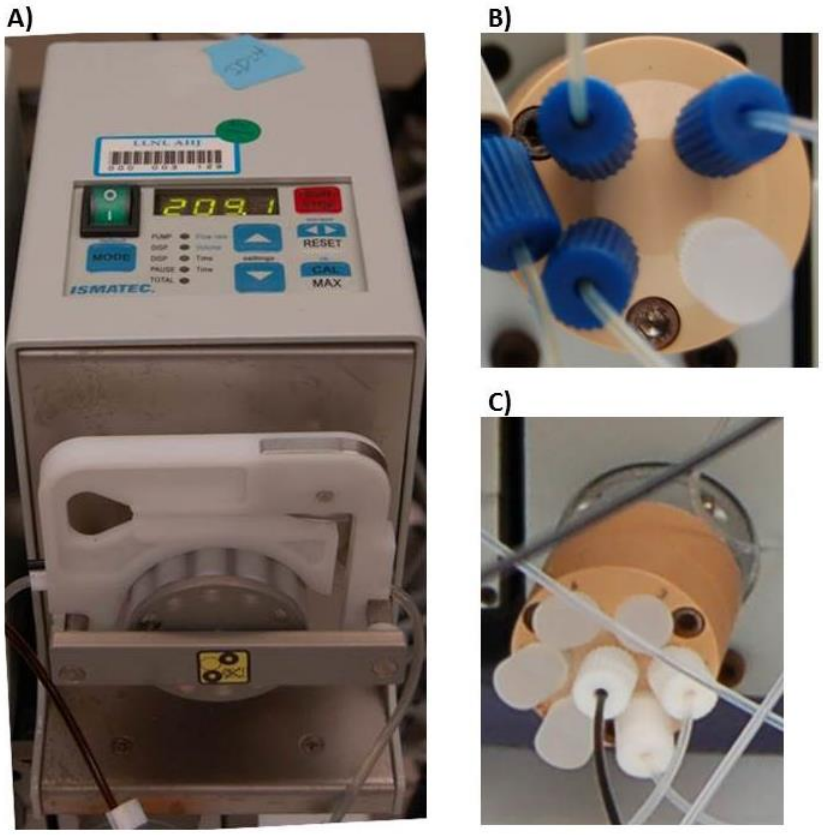

Figure 4-18. (A) One of the Reglo Digital pumps, P4, from Isamatec used in the automation system. Two of the VICI cheiminert valves with (B) a 2-position valve with four ports, and (C) the multi-position valve where the inlet is the center port surrounded by six outlet ports.

The adjustable parameters of the Isamatec pumps include the total pumping time, flow rate, and total volume pumped. There were two different VICI valves used, 2-position valves (Figure 4-18 B) that can be switched back and forth between A and B positions, and a multi-position valve (Figure 4-18 C) that can send fluid from an inlet port to one of six different outlet ports. The 2-position valves have 4, 6 or 8 ports and an example of the flow for the two positions on the 6-port valve V1 is shown in Figure 4-19. The sample, in red, is injected into the 1 mL injection loop on V1 via pump P6 when the V1 is in position B. Also, while in position B eluent from P1, in black, is pumped to the AG 1x8 column via V3. When the valve is changed to position A, the load eluent from P1 is used to push the sample out of the injection loop and onto the first column.

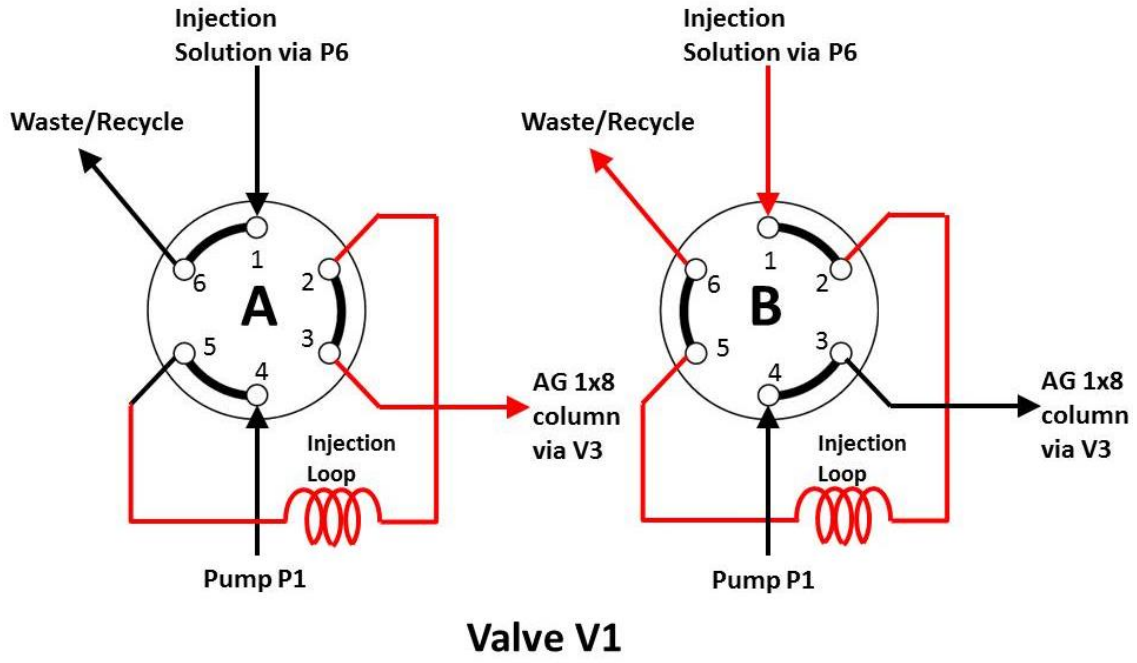

Figure 4-19. A schematic showing the sample flow for the 2-position VICI valve V1. The sample solution is represented by the red lines. When V1 is in position B, the sample is being pumped into the 1 mL injection loop via P6. When V1 is in position A, eluent from P1 flows through the injection loop and loads the sample solution onto the AG 1x8 column.

The fraction collector (Figure 4-20) is pre-programmed to collect fractions based on time in minutes or volume in number of drops. The fraction collector fraction tray can hold up to 95 of the 15 mL polyethylene centrifuge tubes.

The entirety of the automated chemical separation system minus the fraction collector is shown in Figure 4-21. The fraction collector was placed in the fume hood directly to the right of the system in Figure 4-21 as a safety precaution because the liquid fraction contained potentially dispersible radioactive material.

Figure 4-20. The Amersham Redifrac fraction collector that was used to collect eluted fractions from the automated chemical separation system.

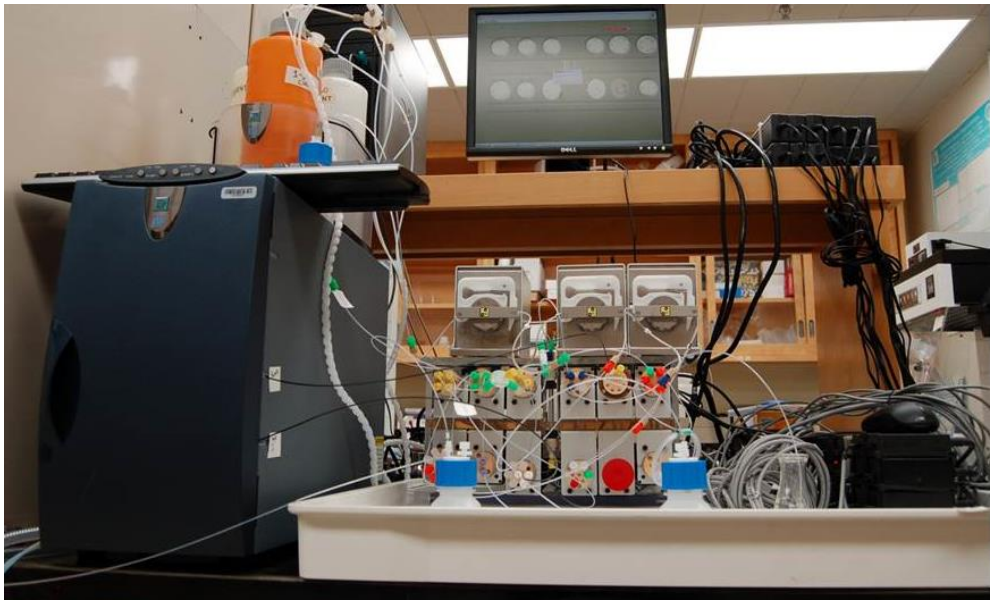

Figure 4-21. The automated chemical separation system that was used to separate surrogate nuclear forensics samples. Not pictured is the fraction collector located in a fume hood directly to the left.

The hardware used for the automated chemical separation system was controlled by the software program LabVIEW. LabVIEW is a graphical based programming language as opposed to text based programming languages such as C/C++ or FORTRAN and it is available through National Instruments. LabVIEW is available on multiple platforms including Windows, OS X and Linux. Some of the key features of LabVIEW include the ease of parallel computing or running multiple processes simultaneously and the ability to interface with a wide variety of devices and instruments. Many of the drivers for those devices and instruments are available through National Instruments. The user programs LabVIEW within virtual instruments (VIs) and subroutines (sub-VIs) are called within the main VI. More information about LabVIEW can be found through the National Instruments website [187].

A LabVIEW program was written to control the hardware and carry out the desired separation(s). Initially some challenges arose when trying to control the Dionex gradient pump, P1, with LabVIEW. Pump P1 uses the Chromeleon software program to determine eluent flow rates, gradient mixing fractions and total volume of eluent delivered. Chromeleon has a software development kit (SDK) specifically for integrating the pump into other systems [188] [189]. The SDK has numerous classes that can be used by another program to read and write various Chromeleon database objects and specific examples of code used to access these classes are given for Visual Basic, C++ and C#. In order to access the classes and functionality of the Chromeleon SDK, an ActiveX control VI was written to log on to Chromeleon and establish an instance of communication between LabVIEW and Chromeleon. Screen shots of the front panel and block diagram are given in Figure 4-22 and Figure 4-23. More screenshots of the code can be found in Appendix A6. After logging on to Chromeleon, LabVIEW could access any of the SDK classes and after integration of the VICI valves a test separation of lead, tin and uranium using a single AG 1x8 column was conducted and the results are discussed in section 4.3.

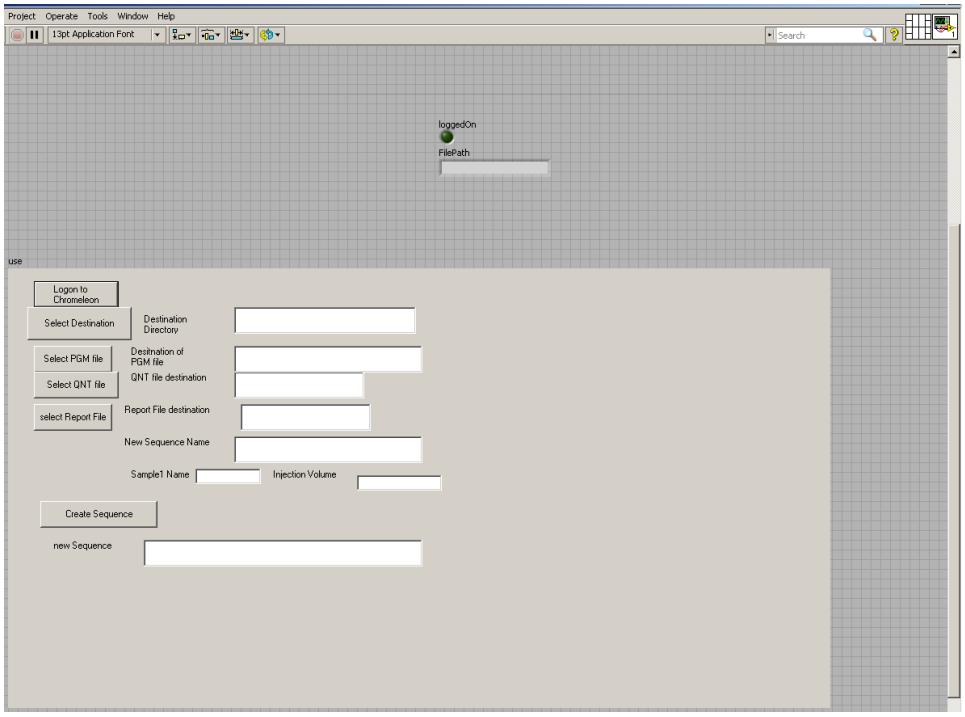

Figure 4-22. The front panel of the ActiveX control that allows LabVIEW to communicate with Chromeleon.

The nuclear forensic sample separation program initially requires user input to determine which of the eight elements to separate. Thus, if a user were only concerned about the actinide elements the user could select Np, Pu and U and accomplish the separation much quicker than separating the whole suite of elements. Currently the chemistry and program are designed for three columns, but if it was determined that the components of the debris matrix were overloading the column(s) then additional columns could be added quickly. Also, additional elements could be added quickly as each element to be separated has its own sub-VI, additional sub-VIs for new elements can be written and then added to the main VI.

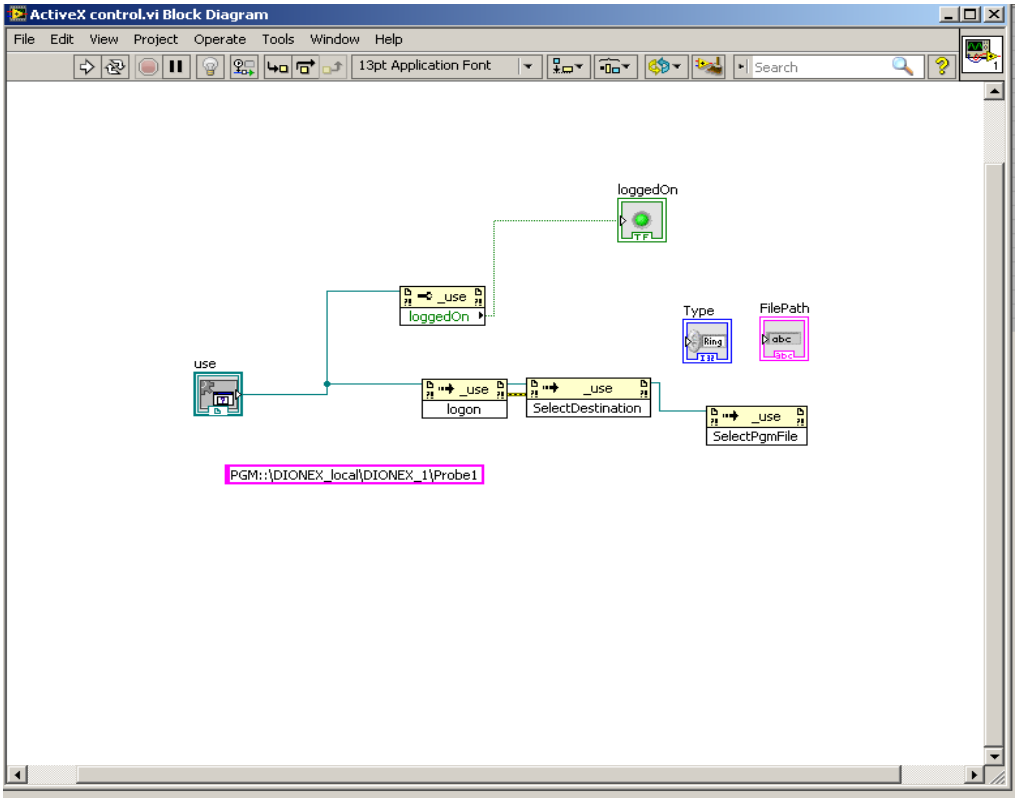

Figure 4-23. The block panel showing the graphical code for the ActiveX control that creates an instance of communication between LabVIEW and Chromeleon.

After determining which elements to separate the user confirms the selection at which point the automated system takes control and the dissolved sample is injected with pump P6 into the 1 mL injection loop. After the injection loop is filled, the valves V1, V3 and V4 are adjusted so that pump P1 can pump the injection out of the loop and onto the AG 1x8 resin column. As described in the previous section the lanthanides pass through the AG 1x8 resin column with no adsorption. Valve V8 is set so that the wash from the AG 1x8 resin column is directed to load the TRU resin column. Simultaneously, valves V6 and V7 are switched to direct HNO_3 to mix with and dilute the HCl based wash from the AG 1x8 resin column. The mixed HNO_3/HCl solution is loaded on the TRU resin

column. The wash from the TRU resin column is directed by valves V2 and V5 to the fraction collector where fractions containing any matrix elements or fission products not sorbed to either the AG 1x8 or TRU resin columns are collected. Then V8 is switched so that raffinate from the AG 1x 8 column is directed to the fraction collector and the Np, Pu, U and Zr element fractions are sequentially eluted from the column. Once the AG 1x8 resin column sequential elutions are complete, V2 is switched so that raffinate from the TRU resin column is directed onto the LN resin column. The lanthanides sorbed to the TRU resin column are eluted with a dilute HNO_3 acid and loaded onto the LN resin column where Eu, Gd, Pm and Tb fractions are eluted and then collected in the fraction collector. At the completion of the separations the user is then given the option to complete another separation, clean/regenerate the resins or stop the program. The total time required from injection of the sample until the completion of the column regeneration step is 160 minutes. This time includes the sample injection, load wash steps, sequential elution steps for each element, and finally column wash steps before the next sample is injected. The total time primarily limited by the flow rate of the eluents from the Dionex pump. The total process time could potentially be shortened if higher flow rates are used, however the recovery and separability of these elements over increased flow rates would need to be examined. The results of the separation system on a number of surrogate samples are given in the following section.

4.3 Automated Separation of Pb, Sn and U

After incorporating Chromeleon, the Dionex gradient pump, one of the Reglo Digital pumps and the valves in the LabVIEW program development a trial separation of three available isotopes, ^{212}Pb, ^{113}Sn, and ^{233}U, was performed to demonstrate the functionality of the designed system and to determine potential issues with the overall flow of the system. The separation sequence was designed based on the chemical interaction of these isotopes with the anion exchange column resin AG 1x8. The chemical behavior, and subsequent program development, was determined by using distribution ratios for these elements in HCl and HNO_3 [190] [191]. The injection solution was a mixture of these three isotopes in 8 M HCl. At this point an injection loop was yet to be incorporated so approximately 1 mL of the injection solution was manually injected into the system. At 8 M HCl the ^{212}Pb did not demonstrate any interaction with the anion exchange resin and was washed through the column in ~9 mL of 8 M HCl. Conversely, both the ^{113}Sn and ^{233}U sorbed strongly to the column. Next, the ^{233}U was eluted from the column in ~9 mL of 2 M HCl. The ^{113}Sn was eluted last from the column using ~9 mL of 4 M HNO_3. In a final step the column was rinsed with ~6 mL of 8 M HCl to remove any traces of HNO_3 from the column in order to preserve the column from degradation by HNO_3. During these test separations, the fraction collector also had not been incorporated therefore each elution fraction was collected manually in ~1 mL fractions and an elution profile for each element fraction was produced. The ^{212}Pb and ^{113}Sn fractions were measured with gamma spectroscopy on the Ortec HPGe and the ^{233}U fraction was determined by LSC.

All the ^{212}Pb samples were counted first because of its short half-live. The half-lives of ^{212}Pb and ^{113}Sn are 10.64 hours and 115.09 days, respectively. The shorter half-lives of ^{212}Pb and ^{113}Sn necessitated decay correction in order to obtain accurate measurements for the elution curves. The injection solution was counted first and then each subsequent fraction was decay corrected to the time that the injection solution was counted per the following equation;

$$A_0 = \frac{A}{e^{-\lambda t}} \qquad \text{Equation 4-6}$$

where A_0 is the decay corrected activity, A is the measured activity, λ is the decay constant and t is the decay time. discussed in Chapter 4.3. An example of the gamma spectra obtained for the ^{212}Pb fractions is shown in Figure 4-24. This spectrum shows the primary ^{212}Pb photopeak at 238.6 keV as well as a secondary photopeak at 300.1 keV. ^{212}Pb x-rays are evident at the lower energy range around 40 keV. There is also an annihilation peak at 511 keV and photopeaks at 583.2 keV and 727.3 keV, which correspond to ^{208}Tl and ^{212}Bi, respectively (radiation decay information was obtained from [169]), both of which are decay products of ^{212}Pb.

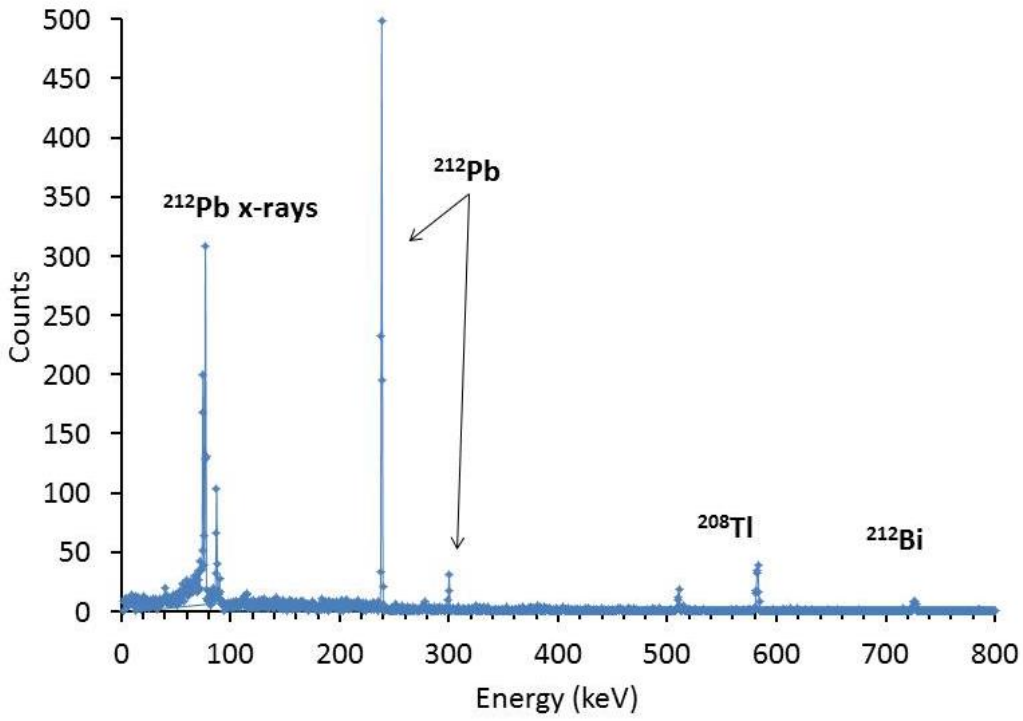

Figure 4-24. A gamma spectra of the 4th sample from the ^{212}Pb fraction.

Each ^{113}Sn fraction was counted on the Ortec HPGe detector for 12 hours to ensure that enough counts were obtained to get reasonable counting statistics. The primary ^{113}Sn photopeak is located at 391.7 keV and there are several ^{113}Sn x-rays below 100 keV that in the spectrum that used to identify and determine the amount of ^{113}Sn present in a fraction. The ^{233}U fraction was determined by LSC and the total elution curves are given in Figure 4-25. The percent of each element eluted in a 1 mL fraction is plotted against the volume that was used for elution. Each element required nine mL to elute from the column and the total volume added is given on the x-axis. The elution curves show a clean separation for each element and the total recovery for each element is given in Table 4-4. The error given in the third column of Table 4-4 is the propagated counting

error. The percent recoveries for this separation are a little lower than were expected; however, there are a few possible explanations. First, the exact amount of injection solution was unknown.

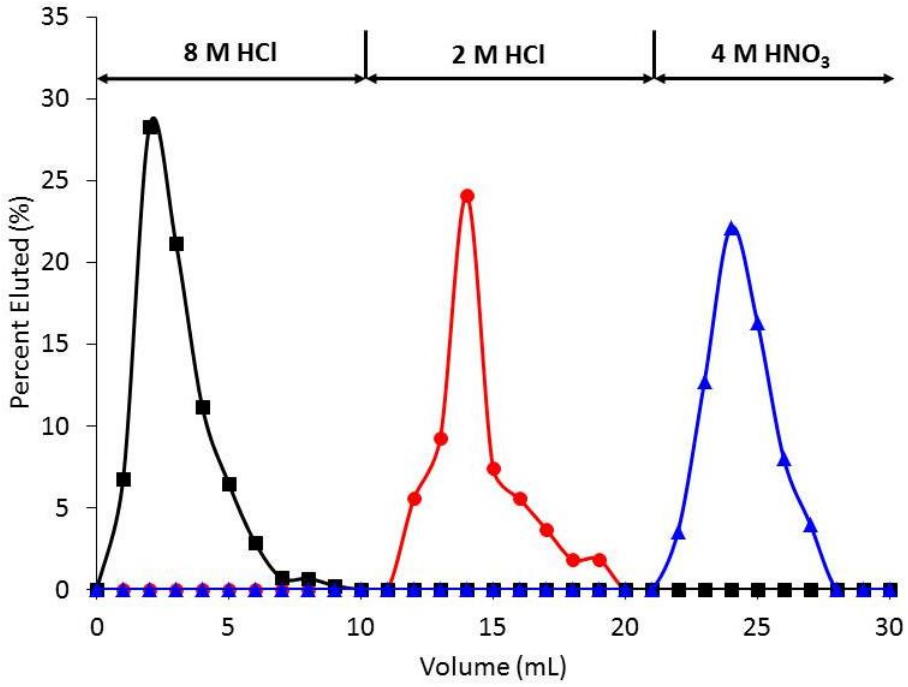

Figure 4-25. The elution curves for the ^{212}Pb (-■-), ^{113}Sn (-▲-), and ^{233}U (-●-) separation with the automated chemical separation system.

Table 4-4. ^{233}U, ^{212}Pb, and ^{113}Sn Percent Recoveries.

Element	% Recovery	% Error
^{233}U	59.3	16
^{212}Pb	78.3	3.5
^{113}Sn	66.8	8

Approximately 1 mL of solution was injected, but based on the design of the injection into the system the actual amount could vary by as much as 30 percent. This is mainly a result due to the absence of an injection loop in the automated chemical separation system. A one mL injection loop was added to the system after this test was completed.

Also, low initial activity was used for both ^{233}U and ^{113}Sn. This impacted the counting error which was then propagated through the recovery error given in the last column of Table 4-4. This error is most pronounced in the ^{233}U error as well as in the ^{233}U elution curve in Figure 4-25. The last two or three data points were close to limit of detection for ^{223}U and if greater activity was used the elution curve likely would have had a more Gaussian distribution similar to the other isotopes. ^{113}Sn forms strong complexes with the chloride form of the quaternary ammonium functional groups of the AG 1x8 resin, and a significant portion remains on the resin even after elution with HNO_3 [193]. These isotopes were readily available and the primary purpose of this experiment was to demonstrate performance of the software program and that a satisfactory separation could be obtained. As such, extensive research and chemistry development for each of these elements was not conducted. After the separation experiments, some of the pre-installed PEEK tubing in the Dionex gradient pump was leaking. The PEEK tubing was removed and fluorinated ethylene propylene (FEP) which has greater chemical resistance to a wider variety of acids was a primary candidate to use as a replacement. Table 4-5 gives the chemical resistance of both PEEK and FEP tubing in terms of suitable, A, not recommended, C, and no available data is denoted by a hyphen.

Table 4-5. A comparison of the chemical resistance of both PEEK and FEP tubing to various acids [171].

Acid	PEEK	FEP
HNO_3 Conc.	C	A
HNO_3 20%	A	A
HF Conc.	C	A
HF 20%	--	A
HCl Any	A	A
HBr Any	C	A
Aqua Regia	C	A

The FEP tubing shows excellent resistance to any of the potential acids that may be used in the automated chemical separation system. Aqua Regia is listed because of potential mixing of HCl and HNO_3. HBr is listed as it is analogous to HI for which there was no data and was also used in the automated system. The PEEK tubing in the Dionex gradient pump was replaced with FEP tubing and FEP tubing was used for all other tubing in the system including the injection loop. The primary objective of this automated separation was to test the performance of the system and identify possible problems that would need to be addressed such as replacing the PEEK tubing with FEP tubing, or adding a fraction collector and injection loop.

4.4 Automated Chemical Separations Results

After completion of the design and programming of the automated chemical separation system, the efficiency and effectiveness of the system to separate the eight elements Eu, Gd, Np, Pm, Pu, Tb, U, and Zr were tested with a number of surrogate samples. A total of five samples, C1-C5, were acquired with varying composition of the desired elements; however, none of them contained Gd or Zr of which there were no isotopes available. The composition of four of the five samples was known at the time they were acquired and the fifth sample was acquired without prior knowledge of the composition. After completing the separation of the fifth sample the actual composition was acquired and the results compared. Of the known samples, three had the same composition in 6 M HCl and the fourth sample also had the same composition but the activity was mixed with one mL of the pot solution produced from the dissolution of 20

mg of puddle glass. Each sample was in about one mL of solution. The actual composition of all five samples, including the fifth sample which was not given until after the separation was complete, is found in

Table 4-6. The total volume of sample required to fill the one mL injection loop is close to three mL because the capillaries and various connections must also be filled as the sample is drawn into the injection loop. As such 6 M HCl was added to samples C1-C5 until they reached a volume of five mL.

Table 4-6. A table of the activities in each of the surrogate samples that were tested in the automated chemical separation system.

Total Elemental Activities (dpm)									
Sample	^{152}Eu	Gd	Np	^{145}Pm	Pu	^{160}Tb	^{234}U	Zr	Matrix
C1	3100	--	^{237}Np-420	2300	^{239}Pu-3200	1400	3300	--	6M HCl
C2	3100	--	^{237}Np-420	2300	^{239}Pu-3200	1400	3300	--	6M HCl
C3	3100	--	^{237}Np-420	2300	^{239}Pu-3200	1400	3300	--	6M HCl
C4	3100	--	^{237}Np-420	2300	^{239}Pu-3200	1400	3300	--	Pot solution
C5	4100	--	^{239}Np-147	--	^{239}Pu-2900 ^{238}Pu-230	--	13000	--	6M HCl

When analyzing the measured activities after separation these isotopes were not decay corrected with the exception of Tb-160 which has a half-life of 72.3 days, and its activity is corrected according to Equation 4-6 to the time when the surrogate samples were received.

In sample C5 the Np isotope ^{239}Np is in secular equilibrium with the americium isotope ^{243}Am and is counted by LSC shortly after separation. The half-lives of the isotopes listed in

Table 4-6 plus the ^{243}Am half-life are given in Table 4-7.

Table 4-7. A table of the half-lives [195] for isotopes and gamma ray energies [196] if applicable, used in this work.

Isotope	Half-life	Detection
^{243}Am	7370 years	LSC
^{152}Eu	13.54 years	121.8, 244.7, 344.3 (keV)
^{237}Np	2140000 years	LSC
^{239}Np	2.36 days	LSC
^{145}Pm	17.7 years	67.2, 72.4 (keV)
^{239}Pu	24100 years	LSC
^{238}Pu	87.7 years	LSC
^{160}Tb	72.3 days	86.8, 298.6 (keV)
^{234}U	245500 years	LSC

Next the three resin columns, AG 1x8, TRU and LN resins, were prepared. The TRU and LN resins were prepared manually as follows:

About 5 grams of resin was weighed in to 50 mL polyethylene bottle.
1 M HNO_3 was added, shaken vigorously and then the resin was allowed to settle completely.
Floating resin was discarded.
The resin washed with MQ water.
Floating resin was again discarded.
The MQ water wash and discarding floating resin process was repeated until no more resin was floating.
A small amount of 1 M HNO_3 was added for storing the resin.

Then each column was filled with MQ water and the resins were then added dropwise and allowed to gravity settle. About 1.5 mL of resin was used for the AG 1x8 and LN resin columns and 2 mL of resin was used for the TRU resin columns which are shown in Figure 4-26. After connecting the columns to the system they were washed with several column volumes of 8 M HCl for the AG 1x8 resin column, 4 M HNO_3 for the TRU resin column and 0.1 M HNO_3 for the LN resin column.

Figure 4-26. The three columns used in the automated chemical separation system. From L to R the AG 1x8 resin column, the TRU resin column and the LN resin column.

Before injecting samples C1-C4 into the automated system they were counted on an HPGe to measure the activities so that the separated fractions could be counted later in the same geometry to determine activities for the gamma ray emitting isotopes, Eu, Pm, and Tb. The wash fractions were also counted to determine if any there was any hold-back that broke through during the resin wash steps. The used resin was also counted on an HPGe to determine if any of the isotopes remained on the resin even after the wash steps. The samples were separated in the following order: C1, C2, C4, C3 and C5. After samples C2 and C3 the columns were replaced with fresh resin. The samples were separated in this order to investigate possible differences in the effectiveness of the separations after running multiple samples on the columns and differences between a sample in pot solution, C4, and one in just HCl, C3. There were no significant differences between the samples and the results are presented for C1-C3 (as an average of the three

samples), C4 and C5. After collecting the separated fractions in the fraction collector they were placed in the water bath evaporator to evaporate the fractions to the same volume as the initial sample. The fractions were then counted on the HPGe and the activities of Eu, Pm, and Tb in each fraction was measured. The characteristic photopeaks and corresponding intensities for the isotopes of these elements are given in Table 4-8. The very low intensities of the ^{145}Pm gamma rays combined with low activity after dilution necessitated counting on a high efficiency (~35%) HPGe in the LLNL counting facility. Then one mL aliquots of each fraction were then taken and counted by LSC to determine the activities of Np, Pu and U. When the column resins were replaced the used resins were collected in 15 mL centrifuge tubes and also counted on the HPGe detector to determine the presence of any residual radioactivity from the lanthanides elements that may be remaining on the resins.

Table 4-8. The gamma ray energies and corresponding intensities for the isotopes identified by gamma spectroscopy [196].

Isotope	E (keV)	I (%)
^{152}Eu	121.78	39.76
	244.7	10.55
	344.28	26.52
^{145}Pm	67.2	0.55
	72.4	1.85
^{160}Tb	86.79	13.15
	298.58	26.13

After all of the fractions were counted, the recovery for each element in the sample was calculated. The average recovery fractions for samples C1-C3 are given in Table 4-9. The first column is a brief description of the fraction being collected and analyzed. The injection fraction represents the amount of each element that was collected

during the initial injection and subsequent loading washes. The La Prep fraction includes elements recovered during loading of the lanthanide elements and ensuing washing steps on the TRU resin and LN resin columns and the Clean fraction represents the amounts of each element recovered while washing and preparing the resin for a subsequent separation. The last column represents a gross alpha percentage recovered in the corresponding fractions. Specific elements could not be determined from LSC spectra and therefore the Injection, La Prep and Clean fractions are stated as total alpha fractions. As Pu needs a reducing agent such as HI, the Pu contribution to these fractions is likely minimal. The majority of each lanthanide was recovered in the expected fraction, however as seen by Eu there was likely not a clean separation for Pm or Tb as well. This trend is easier to see in the Eu recoveries because Eu had more activity and stronger intensity gamma ray photopeaks than either Pm or Tb. The total time to separate one sample was 2 hours 20 minutes. The three samples were completed in just over 7 hours and included changing each of the columns once.

Table 4-9. Average recovery of each element in the corresponding fraction for samples C1-C3.

Step	Fraction						
	Pu %	Np %	U %	Pm %	Eu %	Tb %	Alpha %
Injection	--	--	--	< 5	< 5	< 5	3 ± 2
Pu	81 ± 6	--	--	--	--	--	--
Np	--	79 ± 12	--	--	--	--	--
U	--	--	95 ± 6	--	--	--	--
La Prep	--	--	--	< 5	< 5	< 5	4 ± 3
Pm	--	--	--	34 ± 23	14 ± 8	--	--
Eu	--	--	--	--	39 ± 12	--	--
Tb	--	--	--	--	< 5	34 ± 21	--
Clean	--	--	--	21 ± 15	9 ± 8	8 ± 5	8 ± 5

The average recovery fractions for sample C4 is given in Table 4-10. Sample C4 had the same initial composition for the elements of interest as C1-C3 but was dissolved in pot solution instead of 6 M HCl. The addition of a background matrix, the pot solution, made little difference on the separations of sample C4. The primary challenge in determining if there is a difference between the separations for C1-C3 and C4 is the low activity of the lanthanides resulting in large errors. This separation was also completed in 2 hours and 20 minutes. After completion of these four separations the resin from the six columns that had been used were extruded into 15 mL centrifuge tubes and counted with an HPGe to determine if there was any residual activity remaining on the resins. No measurable activity was found on any of the resins.

Table 4-10. Average recovery of each element in the corresponding fraction for sample C4.

Step	Fraction						
	Pu %	Np %	U %	Pm %	Eu %	Tb %	Alpha %
Injection	--	--	--	< 5	< 5	< 5	5 ± 3
Pu	80 ± 7	--	--	--	--	--	--
Np	--	85 ± 15	--	--	--	--	--
U	--	--	92 ± 6	--	--	--	--
La Prep	--	--	--	< 5	< 5	< 5	4 ± 3
Pm	--	--	--	26 ± 19	< 5	--	--
Eu	--	--	--	--	35 ± 11	14 ± 9	--
Tb	--	--	--	--	10 ± 3	22 ± 12	--
Clean	--	--	--	18 ± 14	10 ± 6	--	5 ± 3

Sample C5 was originally of unknown composition and the objective of separating C5 was to determine the original composition. The predicted activities based on the separation of C5 compared to the actual activities are given in Table 4-11. During the analysis a single peak was identified as ^{160}Tb, however the counting error was greater

than the number of counts and there were no other affirming peaks thus it was assumed there was no Tb in the sample. Of the four elements positively identified three of the actual compositions, Eu, Np and Pu, were within the error range of the predicted compositions. The fourth element U over predicted the amount of U in the sample by less than four percent. The least accurate prediction was the composition of Np. This is mostly due to a low initial activity, which in turn caused a high uncertainty of plus or minus nearly 40 percent of the total Np. It is possible that some of the Np sorbed to the walls of the container, tubing, column, or resin. During this sample, separations for all eight elements were performed. The total run time was 2 hours 40 minutes. The activities for alpha emitting elements, Np, Pu and U, were measured by LSC. As mentioned previously this precludes determination of mixed alpha isotopes such as during the injection or clean fractions. Counting by LSC also does not give isotope information within the elemental fraction. For example, for samples C1-C4 the Np isotope present was ^{237}Np whereas in C5 the isotope was ^{239}Np. Also the Pu fraction in C5 had two Pu isotopes, ^{238}Pu and ^{239}Pu. By using LSC only the total amount of activity for an element could be determined.

Table 4-11. The predicted and actual activities of the unknown sample C5.

Element	Predicted dpm	Actual dpm	Predicted/Actual
Pu	2942 ± 565	3130	0.94
Np	121 ± 45	147	0.82
U	13471 ± 249	13000	1.04
Pm	--	--	--
Eu	4258 ± 370	4100	1.04
Tb	--	--	--

The lanthanides consistently had the lowest recovery and most bleed through of the recovered elements. Initially the designed chemistry planned to use the second gradient pump from the DIONEX dual gradient pump to elute the lanthanides with mM concentrations of HCl according to the method used by Pin et al. (1996) and Dry et al. (2005). However, the second pump stopped working likely due to a malfunction in the pressure transducer. As such the design of the system was altered to use varying HNO_3 concentrations to elute the lanthanides. Using mM concentrations of HCl may have increased the recovery of the lanthanides and possibly decrease the bleed through into other fractions.

Chapter 5

Conclusions and Summary of Work

There are many pathways and sources for introducing anthropogenic radioactive materials into the environment. This work focused on identifying and understanding some of the chemical signatures associated with long-term environmental radioactive contamination that may be introduced to the environment intentionally through nuclear waste repositories or unintentionally through nuclear accidents. Cesium sorption behavior on the common clay minerals, illite, montmorillonite, and kaolinite was studied through batch sorption and desorption experiments. From these batch sorption experiments, fundamental characteristics such as percent sorbed/desorbed and K_d values were derived. This information was then used to probe the reversibility of Cs sorption to the minerals illite, montmorillonite and kaolinite in a ternary system. Dialysis bags were used in the ternary system to isolate distinct mineral phases which permitted the study of the individual contribution of each mineral phase to the overall Cs sorption behavior. The ternary experiments using illite, which has a strong affinity for Cs, as a sink for Cs sorption, show complete reversibility for Cs sorption to kaolinite and near complete reversibility for Cs sorption to montmorillonite. The ternary experiments also show some irreversibility for Cs sorption to illite. This irreversibility is most likely a result of Cs sorbing to the FES sites, which in turn collapses over time as Cs diffuses further into the interlayer structure. Over the 17 months of the experiment, 40 percent or more of the Cs eventually desorbed, which is 20% less than predicted by the sorption model. The ternary

experiments also highlight the importance of appropriate timescales when looking at environmental sorption processes.

After successfully demonstrating the use of the dialysis bags in the Cs studies, the approach was used to study Pu reversibility under similar multi-mineral conditions. The aqueous chemistry of Pu is considerably more complex than aqueous Cs chemistry. Some of the factors that can affect Pu sorption are pH, oxidation state, mineral compositions, concentration and time. In order to examine the Pu sorption behavior in a ternary system many variables had to be controlled. The Pu sorption behavior in a ternary system was examined using montmorillonite as the primary mineral with which Pu was equilibrated and goethite as the mineral sink inside the dialysis bag. The pH was held constant at 8 and 10^{-9} M Pu was initially added to the system. Over the course of seven months between 10-14 percent of Pu associated with montmorillonite desorbed. Again, the importance of conducting environmental sorption experiments was confirmed as it is possible that a steady state or equilibrium had still not been achieved even after seven months.

In a post-detonation scenario, there will exist a demand for information about the device used and extent of contamination as quickly as possible. Decreasing the analysis time required for nuclear forensic samples obtained in response to a post-detonation scenario is important. Having an automated system that can analyze samples from a base of operations has the potential to significantly decrease the analysis time required. This study focused on developing an automated chemical separation system that could be integrated into a larger analysis system and demonstrates a proof of concept from experiment using unknown samples.

Prior to developing the automated system, a number of experiments were carried out to determine the matrix interference effects from cement, a prominent component in urban material. These matrix interference studies were performed with Pu and U on an AG 1x8 resin and with Eu on TRU resin and LN resin. The cement matrix concentration had minimal impact on the sorption of U to AG 1x8 resin and Eu to TRU and LN resins. Sorption of these elements to the corresponding resins was consistent for cement matrix concentrations over the range of 0-30 percent. The cement matrix did have some impact on the sorption of Pu to AG 1x8 resin. As the concentration of the cement matrix increased the K_d of the sorption of Pu decreased by as much as an order of magnitude at similar HCl concentrations. The sorption behavior of Pu in 100 percent cement matrix solution was significantly different from the 10, 20 and 30 percent cement matrix solutions. It is possible that Pu complexation with the cement or resin capacity, however, it is likely that automated separations will occur in less 30 percent cement matrix where normal Pu behavior is expected.

Next, the automated system was put together with the hardware described in Chapter 4 and using the LabVIEW software as the primary software to control the hardware. After the automated chemical separation system was assembled, a set of five samples were analyzed. Four of the samples were separated to determine the effectiveness of the system and the approximate recovery yields of six different elements, Eu, Np, Pm, Pu, Tb and U after being separated with the automated chemical separation system. Recoveries of 80 percent or more were achieved for the actinides in the desired fractions while recoveries of around 30 percent were obtained for the lanthanides in the desired fractions. Residual activities for the actinides could be in either the used resin, the

initial sample vials, or the capillaries of the system. While the recoveries of each lanthanide in the corresponding fraction was much lower than the actinides, there was significant bleed through to other fractions. Some residual activity may also be in the capillaries, initial sample vials, or in the resins. The fifth sample was an unknown and the primary objective was to determine the composition of the sample. The composition was determined and four elements, Eu, Np, Pu and U, were identified. The activity of three of the four elements, Eu, Pu and U were identified to within six percent or less of the actual activity. The identified activity of Np was off by about 20 percent most likely because of counting error caused by low activity or residual activity on the walls of the initial sample vial. The experiments with the surrogate samples and unknown sample validate the proof of concept of the automated chemical separation system and that it can complete the separation of the eight elements, cleaning and washing of the resin columns in 160 minutes.

5.1 Future Work

Using the dialysis bag experimental design to studying mineral sorption allows for determining the individual contribution of minerals in a complex system. For the Cs ternary mineral system, one of the next steps may be to use a dialysis bag with more volume and more illite. The rate of Cs desorbing from kaolinite and montmorillonite in the two systems could be compared and used to improve transport models if a difference were found. Another important principle to study in this revised experimental design is the reversibility of Cs sorption illite. Some of the pertinent questions would include: Does

the increase in available mineral sites increase the desorption of Cs from illite or does it reach an equilibrium irreversible limit? Similarly, in the Pu ternary mineral system would adding a dialysis bag with more volume and mineral mass or adding sequential dialysis bags drive continued desorption of Pu? Also, are the rates of desorption in each dialysis bag comparable or will the rate slow down until desorption plateaus? Finally, the dialysis bag approach could be used to study competing kinetic rates of sorption between two or more minerals and determine if a radionuclide will preferentially sorb to one mineral over another.

While this work successfully demonstrated the proof of concept of the automated chemical separation system, there are number of things that can be improved. First, the recovery of the lanthanides at ~30 percent is low. Initially the designed chemistry planned to use the second gradient pump from the DIONEX dual gradient pump to elute the lanthanides with mM concentrations of HCl according to the method used by Pin et al. (1996) [170] and Dry et al. (2005) [197]. However, the second pump stopped working likely due to a malfunction in the pressure transducer. As such the design of the system was altered to use varying HNO_3 concentrations to elute the lanthanides. In the future using mM concentrations of HCl may increase the recovery of the lanthanides and possibly decrease the bleed through into other fractions. Workability of the system has been established, but to gain a better understanding of the limitations, numerous additional samples will need to be analyzed. Initially this includes samples with varying activities and concentrations of cement matrix interferences. Analysis of these samples can answer questions about robustness of the system, such as how many samples can be run before columns must be replaced or determining more reliable error bands regardless

of the initial sample composition. Also during future samples analysis, measuring the initial sample vials and used capillaries to determine the presence of residual activities can help with the preciseness of the separation and recoveries. Finally, over the long term incorporating the automated separation system with online dissolution and counting systems to completely automate the analysis of these samples.

References

[1] US Department of Homeland Security, "National Response Framework Third Edition," US DHS, Washington DC, 2016.

[2] US Department of Homeland Security, "Nuclear/Radiological Incident Annex," US DHS, Washington DC, 2014.

[3] US Department of Energy, "DOE-NNSA/NFO--FRMAC Program," [Online]. Available: http://www.nv.doe.gov/nationalsecurity/homelandsecurity/frmac/default.aspx. [Accessed 25 August 2016].

[4] "American Academy of Forensic Sciences," [Online]. Available: http://aafs.org/students/student-career/what-forensic-science. [Accessed 20 February 2015].

[5] K. J. Moody, I. D. Hutcheon and P. M. Grant, Nuclear Forensic Analysis, Boca Raton: Taylor & Francis Group, 2005.

[6] P. M. Grant, K. J. Moody, I. D. Hutcheon, D. L. Phinney, J. S. Haas, A. M. Volpe, J. J. Oldani, R. E. Whipple, N. Stoyer, A. Alcaraz, J. E. Andrews, R. E. Russo, G. L. Klunder, B. D. Andresen and S. Cantlin, "Forensic analyses of suspect illicit nuclear material," *Journal of Forensic Science,* vol. 43, no. 3, pp. 680-688, 1998.

[7] Lawrence Livermore National Laboratory, "Forensic analyses of a smuggled HEU sample interdicted in Bulgaria," U.S. Department of Energy, Washington D.C., 2001.

[8] G. Capannesi, C. Vicini, A. Rosada and P. Avino, "Characterization of a suspect nuclear fuel rod in a case of illegal international traffic of fissile material," *Forensic Science International,* vol. 199, no. 1-3, pp. E15-E21, 2010.

[9] H. L. Finston and M. T. Kinsley, "The Radiochemistry of Cesium," Brookhaven National Laboratory, Upton, New York, 1961.

[10] United Nations Scientific Committee on the Effects of Ionizing Radiation, "Sources and effects of ionizining radiation," UN, New York, 2000.

[11] J. M. Zachara, S. C. Smith, C. Liu, J. P. Mckinley, R. J. Serne and P. L. Gassman, "Sorption of Cs+ to micaceous subsurface sediments from the Hanford site, USA," *Geochimica et Cosmochimica Acta,* vol. 66, no. 2, pp. 193-211, 2002.

[12] Nuclear Energy Agency OECD, "Chernobyl: Assessment of radiological and health impacts," 2002.

[13] M. Chino, H. Nakayama, H. Nagai, H. Terada, G. Katata and H. Yamazawa, "Preliminary Estimation of Release Amounts of I-131 and Cs-137 Accidentally Discharged from the Fukushima Daiichi Nuclear Power Plant into the Atmosphere," *Journal of Nuclear Science and Technology,* vol. 48, no. 7, pp. 1129-1134, 2011.

[14] Y. Morino, T. Ohara and M. Nishizawa, "Atmospheric behavior, depostion, and budget of radioactive materials from the Fukushima Daiichi nuclear power plant in March 2011," *Geophysical Research Letters,* vol. 38, pp. 1-7, 2011.

[15] A. Stohl, P. Seibert, G. Wotawa, D. Arnold, J. F. Burkhart, S. Eckhardt, C. Tapia, A. Vargas and T. J. Yasunari, "Xenon-133 and caesium-137 releases into the atmosphere from the Fukushima Dai-ichi nuclear power plant: determination of the source term, atmospheric dispersion, and deposition," *Atmospheric Chemistry and Physics,* vol. 12, no. 5, pp. 2313-2343, 2012.

[16] United States Environment Protection Agency, "National Primary Drinking Water Regulations EPA 816-F-09-004," US EPA, 2009.

[17] B. L. Sawhney, "Selective sorption and fixation of cations by clay minerals: A Review," *Clays and Clay Minerals* , vol. 20, pp. 93-100, 1972.

[18] F. Ackermann, H. Bergmann and U. Schleichert, "Monitoring of heavy-metals in coastal and estuarine sediments - a question of grain-size < 20 mu-m versus < 60 mu-m," *Environmental Technology Letters,* vol. 4, no. 7, pp. 317-328, 1983.

[19] F. R. Livens and M. S. Baxter, "Particle-size and radionuclide levels in some West Cumbrian soils," *The Science of the Total Environment,* vol. 70, pp. 1-17, 1988.

[20] R. M. Cornell, "Adsorption of Cesium on Minerals: A Review," *Journal of Radioanalytical and Nuclear Chemistry, Articles,* vol. 171, no. 2, pp. 483-500, 1993.

[21] A. B. Kersting, "Plutonium Transport in the Environment," *Inorganic Chemistry,* vol. 52, no. 7, pp. 3533-3546, 2013.

[22] G. L. Voelz and I. G. Buican, "Plutonium and Health: How Great is the Risk?," *Los Alamos Science,* vol. 26, pp. 74-89, 2000.

[23] EPA, "National Primary Drinking Water Regulation," Environmental Protection Agency, Washington, DC, 2009.

[24] President's Secretary's File, "U. S. Strategic Bombing Survey: The Effects of the Atomic Bombings of Hiroshima and Nagasaki," Truman Papers, 1946.

[25] A. W. J. Klement, "Radioactive fallout phenomena and mechanisms," *Health Physics,* vol. 11, pp. 1265-1274, 1965.

[26] M. Castrillejo, N. Casacuberta, C. F. Breier, S. M. Pike, P. Masque and K. O. Buesseler, "Reassessment of Sr, Cs and Cs in the coast off Japan derived from the Fukushima Dai-ichi nuclear accident," *Envrionmental Science & Technology,* vol. 50, no. 1, pp. 173-180, 2016.

[27] G. Steinhauser, T. Niisoe, K. H. Harada, K. Shozugawa, S. Schnieder, H.-A. Synal, C. Walther, M. Christl, K. Nanba, H. Ishikawa and A. Koizumi, "Post-accident sporadic releases of airborne radionuclides from the Fukushima Daiichi nuclear power plant site," *Environmental Science & Technology,* vol. 49, no. 24, pp. 14028-14035, 2015.

[28] A. P. Novikov, F. I. Pavlotskaya, T. A. Goryachenkova, A. K. Posokhov, I. E. Kazinskaya, V. V. Emel'yanov, E. V. Kuzovkina, K. V. Barsukova, E. A. Lavrinovich, P. A. Korovaikov, E. G. Drozhko, S. I. Rovnyi and B. F. Myasoedov, "Radionuclide content in underground waters and rock from observation wells around Lake Karachai," *Radiochemistry,* vol. 40, no. 5, pp. 484-490, 1998.

[29] CTBTO, "General Overview of the Effects of Nuclear Testing," 2012. [Online]. Available: https://www.ctbto.org/nuclear-testing/the-effects-of-nuclear-testing/general-overview-of-theeffects-of-nuclear-testing/. [Accessed 12 August 2016].

[30] M. V. Cheshire and C. Shand, "Translocation and Plan Availability of Radiocesium in an Organic Soil," *Plant and Soil,* vol. 134, no. 2, pp. 287-296, 1991.

[31] A. L. Sanchez, S. M. Wright, E. Smolders, C. Naylor, P. A. Stevens, V. H. Kennedy, B. A. Dodd, D. L. Singleton and C. L. Barnett, "High plant uptake of radiocesium from organic soils due to Cs mobility and low soil K content," *Environmental Science & Technology,* vol. 33, no. 16, pp. 2752-2757, 1999.

[32] F. Strebl, M. H. Gerzabek, V. Karg and F. Tataruch, "Cs-137-migration in soils and its transfer to roe deer in an Austrian forest stand," *Science of the Total Envirionment,* vol. 181, no. 3, pp. 237-247, 1996.

[33] K. Akiba, H. Hashimoto and T. Kanno, "Distribution coefficient of cesium and cation-exchange capacity of minerals and rocks," *Journal of Nuclear Science and Technology,* vol. 26, no. 12, pp. 1130-1135, 1989.

[34] J. Koarashi, S. Nishimura, T. Nakanishi, M. Atarashi-Andoh, E. Takeuchi and K. Muto, "Post-deposition early-phase migration and retention behavior of radiocesium in a litter-mineral soil system in a Japanese deciduous forest affected by the Fukushima nuclear accident," *Chemosphere,* vol. 165, pp. 335-341, Dec 2016.

[35] A. N. Mucciardi, I. J. Booker, E. C. Orr and D. Cleveland, "Statistical investigation of the mechanics controlling radionuclide sorption, part II," *WISAP Task 4,* Vols. PNL-SA-7352, pp. 334-425, 1978.

[36] B. Torstenfelt, K. Andersson and B. Allard, "Sorption of strontium and cesium on rocks and minerals," *Chemical Geology,* vol. 36, no. SI, pp. 123-137, 1982.

[37] B. L. Sawhney, "Potassium and cesium ion selectivity in relation to clay mineral structure," *Clays and Clay Minerals,* vol. 18, pp. 47-52, 1970.

[38] E. Brouwer, B. Baeyens, A. Maes and A. Cremers, "Cesium and Rubidium Ion Equilibria in Illite Clay," *Journal of Physical Chemistry,* vol. 87, pp. 1213-1219, 1983.

[39] R. N. J. Comans, M. Haller and P. DePreter, "Sorption of Cesium on Illite: Non-equilibrium Behaviour and Reversibility," *Geochimica et Cosmochimica Acta,* vol. 55, pp. 433-440, 1991 .

[40] C. Poinssot, B. Baeyens and M. H. Bradbury, "Experimental and modelling studies of caesium sorption on illite," *Geochimica et Cosmochimica Acta,* vol. 63, no. 19-20, pp. 3217-3227, 1999.

[41] S. Staunton and M. Roubaud, "Adsorption of Cs-137 on montmorillonite and illite: effect of charge compensating cation, ionic strength, concentration of Cs, K and fulvic acid," *Clays and Clay Minerals,* vol. 45, no. 2, pp. 251-260, 1997.

[42] M. L. Jackson, "Interlayering of expansible layer silicates in soils by chemical weathering," *Clays and Clay Minerals,* vol. 11, pp. 29-46, 1963.

[43] C. I. Rich and W. R. Black, "Potassium exchange as affected by cation size, pH, and mineral structure," *Soil Science,* vol. 97, no. 6, pp. 384-390, 1964.

[44] G. H. Bolt, M. E. Sumner and A. Kamphorst, "A study of equilibria between three categories of potassium in an illitic soil," *Soil Science Society America Proceedings* , vol. 27, no. 3, pp. 294-299, 1963.

[45] S. Komarneni and D. M. Roy, "Hydrothermal effects of cesium sorption and fixation by clay-minerals and shales," *Clays And Clay Minerals,* vol. 28, no. 2, pp. 142-148, 1980.

[46] Y. Kim, R. T. Cygan and R. J. Kirkpatrick, "133Cs NMR and XPS investigation of cesium adsorbed on clay minerals and related phases," *Geochimica et Cosmochimica Acta,* vol. 60, no. 6, pp. 1041-1052, 1996.

[47] Y. Kim, R. J. Kirkpatrick and R. T. Cygan, "Cs-133 NMR study of cesium on the surfaces of kaolinite and illite," *Geochimica et Cosmochimica Acta,* vol. 60, no. 21, pp. 4059-4074, 1996.

[48] L. Bergaoui, J. F. Lambert and R. Prost, "Cesium adsorption on soil clay: macroscopic and spectroscopic measurements," *Applied Clay Science,* vol. 29, no. 1, pp. 23-29, 2005.

[49] C. N. Hsu and K. P. Chang, "Study of factors dominating sorption-desorption of Cs in soil," *Radiochimica Acta,* vol. 68, no. 2, pp. 129-133, 1995.

[50] S. Komarneni and D. M. Roy, "Shale as a radioactive-waste respoitory-importance of vermiculite," *Journal of Inorganic & Nuclear Chemistry,* vol. 41, no. 12, pp. 1793-1796, 1979.

[51] S. L. Swartzen-Allen and E. Matijevic, "Surface and colloid chemistry of clays," *Chemical Reviews,* vol. 74, no. 3, pp. 385-400, 1974.

[52] T. Ohnuki and N. Kozai, "Adsorption behavior of radioactive cesium by non-mica minerals," *Journal of Nuclear Science and Technology,* vol. 50, no. 4, pp. 369-375, 2013.

[53] E. Reinoso-Maset and J. Ly, "Study of major ions sorption equilibria to characterize the ion exchange properties of kaolinite," *Journal of Chemical & Engineering Data,* vol. 59, pp. 4000-4009, 2014.

[54] A. Benedicto, T. Missana and A. M. Fernandez, "Inter layer collapse affects on caesium adsorption onto illite," *Environmental Science & Technology,* vol. 48, no. 9, pp. 4909-4915, 2014.

[55] A. J. Fuller, S. Shaw, C. L. Peacock, D. Trivedi, J. S. Small, L. G. Abrahamsen and I. T. Burke, "Ionic strength and pH dependent multi-site sorption of Cs onto a micaceous aquifer sediment," *Applied Geochemistry,* vol. 40, pp. 32-42, 2014.

[56] K. Norrish, "The swelling of montmorillonite," *Discussions of the Faraday Society,* no. 18, pp. 120-134, 1954.

[57] J. A. Kittrick, "Forces involved in ion fixation by vermiculite," *Soil Science Society of America Proceedings,* vol. 30, no. 6, pp. 801-803, 1966.

[58] I. Shainberg and W. D. Kemper, "Hydration status of adsorbed cations," *Soil Science Society of America Proceedings,* vol. 30, no. 6, pp. 707-713, 1966.

[59] R. K. Schulz, R. Overstreet and I. Barshad, "On the soil chemistry of cesium 137," *Soil Science,* vol. 89, no. 1, pp. 16-27, 1960.

[60] K. Fukushi, H. Sakai, T. Itono, A. Tamura and S. Arai, "Desorption of intrinsic cesium from smectite: Inhibitive effects of clay particle organization on cesium desorption," *Environmental Science & Technology,* vol. 48, no. 18, pp. 10743-10749, 2014.

[61] J. F. Relyea and R. J. Silva, "Application of a site-binding electrical, double-layer model to nuclear waste disposal," Richland, 1981.

[62] S. Y. Shiao, Y. Egozy and R. E. Meyer, "Adsorption of Cs(I), Sr(II), Eu(III), Co(II) and Cd(II) by Al2O3," *Journal of Inorganic Nuclear Chemistry,* vol. 43, no. 12, pp. 3309-3315, 1981.

[63] T. Shahwan, H. N. Erten, L. Black and G. C. Allen, "TO-SIMS study of Cs+ sorption on natural kaolinite," *The Science of the Total Environment,* vol. 226, no. 2-3, pp. 255-260, 1999.

[64] A. De Koning and R. N. J. Comans, "Reversibility of radiocaesium sorption on illite," *Geochimica et Cosmochimica Acta,* vol. 68, no. 13, pp. 2815-2823, 2004.

[65] R. N. J. Comans and D. E. Hockley, "Kinetics of cesium sorption on illite," *Geochimica et Cosmochimica Acta,* vol. 56, pp. 1157-1167, 1992.

[66] B. L. Sawhney, "Kinetics of cesium sorption by clay minerals," *Soil Science Society of America Proceedings,* vol. 30, no. 5, pp. 565-569, 1966.

[67] I. Neretnieks, "Diffusion in the rock matrix: An important factor in radionuclide retardation?," *Journal of Geophysical Research,* vol. 85, no. NB8, pp. 4379-4397, 1980.

[68] J. Wauters, L. Sweeck, E. Valcke, A. Elsen and A. Cremers, "Availability of radiocaesium in soils: a new methodology," *The Science of the Total Envrionment,* vol. 157, pp. 239-248, 1994.

[69] J. A. Davis, J. A. Coston, D. B. Kent and C. C. Fuller, "Application of the surface complexation concept to complex mineral assemblages," *Environmental Science & Technology,* vol. 32, pp. 2820-2828, 1998.

[70] T. Yanagi, M. Watanabe and K. Yamamoto, "Sorption behavior of cesium and strontium ions on mixtures of clay sorbents," *Journal of Nuclear Science and Technology*, vol. 26, no. 9, pp. 861-864, 1989.

[71] D. A. Palmer, S. Y. Shiao, R. E. Meyer and J. A. Wethington, "Adsorption of nuclides on mixtures of minerals," *Journal of Inorganic Nuclear Chemistry,* vol. 43, no. 12, pp. 3317-3322, 1981.

[72] Packard Instrument Company, "Top Count Topics-Quench and Quench Correction," Packard Instrument Company, Meriden, CT, 1993.

[73] J. Thomson, "Use and preparation of quench curves in liquid scintillation counting," Packard BioScience Company, Meriden, CT, 2001.

[74] M. Zavarin, B. A. Powell, M. Bourbin, P. H. Zhao and A. B. Kersting, "Np(V) and Pu(V) ion exchange and surface-mediated reduction mechanisms on montmorillonite," *Envrionmental Science & Technology,* vol. 46, no. 5, pp. 2692-2698, 2012.

[75] M. Zavarin, S. K. Roberts, N. Hakem, A. M. Sawvel and A. B. Kersting, "Eu(III), Sm(III), Np(V), Pu(V), and Pu(IV) sorption to calcite," *Radiochimica Acta,* vol. 93, pp. 93-102, 2005.

[76] A. P. Vanselow, "Equilibria of the base-exchange reaction of bentonites, permutites, soil coloids and zeolites.," *Soil Science,* vol. 33, no. 2, pp. 95-114, 1932.

[77] H. N. Erten, S. Aksoyoglu and S. Hatipoglu, "Sorption of cesium and strontium on montmorillonite and kaolinite," *Radiochimica Acta,* vol. 44, no. 5, pp. 147-151, 1988.

[78] T. Ohnuki, "Sorption characteristics of cesium on sandy soils and their components," *Radiochimica Acta,* vol. 65, pp. 75-80, 1994.

[79] T. Missana, M. Garcia-Gutierrez, A. Benedicto, C. Ayora and K. De-Pourcq, "Modelling of Cs sorption in natural mixed-clays and the effects of ion competition," *Applied Geochemistry,* vol. 49, pp. 95-102, 2014.

[80] T. Ohnuki and N. Kozai, "Adsorption behavior of radioactive cesium by non-mica minerals," *Journal of Nuclear Science and Technology,* vol. 50, no. 4, pp. 369-375, 2013.

[81] E. Reinoso-Maset and J. Ly, "Study of major ions sorption equilibria to characterize the ion exchange properties of kaolinite," *Journal of Chemical & Engineering Data,* vol. 59, pp. 4000-4009, 2014.

[82] M. H. Bradbury and B. Baeyens, "A generalised sorption model for the concentration dependent uptake of caesium by argillaceous rocks," *Journal of Contaminant Hydrology,* vol. 42, pp. 141-163, 2000.

[83] K. Iijima, T. Tomura and Y. Shoji, "Reversibility and modeling of adsorption behavior of cesium ions on colloidal montmorillonite particles," *Applied Clay Science,* vol. 49, pp. 262-268, 2010.

[84] T. Missana, M. Garica-Gutierrez and U. Alonso, "Kinetics and irreversibility of cesium and uranium sorption onto bentonite colloids in a deep granitic environment," *Applied Clay Science,* vol. 26, no. 1-4, pp. 137-150, 2004.

[85] R. G. Gast, R. Van Bladel and K. B. Deshpande, "Standard heats and entropies of exchange for alkali metal cations on Wyoming bentonite," *Soil Science Society of America Proceedings,* vol. 33, no. 5, pp. 661-664, 1969.

[86] R. J. Pruett and H. L. Webb, "Sampling and analysis of KGa-1B well-crystallized kaolin source clay," *Clays and Clay Minerals,* vol. 41, no. 4, pp. 514-519, 1993.

[87] H. van Olphen and J. J. Fripiat, Eds., Data Handbook fro Clay Minerals and Other Non-metallic Minerals, New York: Pergamon Press, 1979.

[88] A. B. Hird and D. L. Rimmer, "Total caesium-fixing potentials of acid organic soils," *Journal of Environmental Radioactivity,* vol. 26, pp. 103-118, 1995.

[89] J. P. McKinley, C. J. Zeissler, J. M. Zachara, R. J. Serne, R. M. Lindstrom, H. T. Schaef and R. D. Orr, "Distribution and retention of Cs-137 in sediments at the Hanford Site, Washington," *Environmental Science & Technology,* vol. 35, no. 17, pp. 3433-3441, 2001.

[90] B. C. Bostick, M. A. Vairavamurthy, K. G. Karthikeyan and J. Chorover, "Cesium adsorption on clay minerals: An EXAFS spectroscopic investigation," *Environmental Science & Technology,* vol. 36, no. 12, pp. 2670-2676, 2002.

[91] A. J. Fuller, S. Shaw, M. B. Ward, S. J. Haigh, J. F. W. Mosselmans, C. L. Peacock, S. Stackhouse, A. J. Dent, D. Trivedi and I. T. Burke, "Caesium incorporation and retention in illite interlayers," *Applied Clay Science,* vol. 108, pp. 128-134, 2015.

[92] D. M. Nelson and M. B. Lovett, "Oxidation state of plutonium in Irish Sea," *Nature,* vol. 276, no. 5688, pp. 599-601, 1978.

[93] P. R. Montero and A. M. Sanchez, "Plutonium contamination from accidental release or simply fallout: Study of soils at Palomares (Spain)," *Journal of Environmental Radioactivity,* vol. 55, no. 2, pp. 157-165, 2001.

[94] D. K. Smith, D. L. Finnegan and S. M. Bowen, "An inventory of long-lived radionuclides residual from underground nuclear testing at the Nevada test site, 1951-1992," *Journal of Environmental Radioactivity,* vol. 67, no. 1, pp. 35-51, 2003.

[95] K. Morris, J. C. Butterworth and F. R. Livens, "Evidence for the remobilization of Sellafield waste radionuclides in an intertidal salt marsh, West Cumbria, UK," *Estuarine, Coastal and Shelf Science,* vol. 51, no. 5, pp. 613-625, 2000.

[96] A. Schwenk-Ferrero, "German spent nuclear fuel legacy: Characteristics and high-level waste management issues," *Science and Technology of Nuclear Installations,* p. 11, 2013.

[97] A. B. Kersting, D. W. Efurd, D. L. Finnegan, D. J. Rokop, D. K. Smith and J. L. Thompson, "Migration of plutonium in ground water at the Nevada Test Site," *Nature,* vol. 397, no. 6714, pp. 56-59, 1999.

[98] A. P. Novikov, S. N. Kalmykov, S. Utsunomiya, R. C. Ewing, F. Horreard, A. Merkulov, S. B. Clark, V. V. Tkachev and B. F. Myasoedov, "Colloid transport of plutonium in the far-field of the Mayak Production Association, Russia," *Science,* vol. 314, no. 5799, pp. 638-641, 2006.

[99] P. H. Santschi, K. A. Roberts and L. D. Guo, "Organic nature of colloidal actinides transported in surface water environments," *Environmental Sciences & Technology,* vol. 36, no. 17, pp. 3711-3719, 2002.

[100] G. R. Choppin, "Redox speciation of plutonium in natural waters.," *Journal of Radioanalytical and Nuclear Chemistry-Articles,* vol. 147, no. 1, pp. 109-116, 1991.

[101] A. Morgenstern and G. R. Choppin, "Kinetics of the reduction of Pu(V)O-2(+) by hydrogen peroxide," *Radiochimica Acta,* vol. 86, no. 3-4, pp. 109-113, 1999.

[102] V. Neck, M. Altmaier, A. Seibert, J. L. Yun, C. M. Marquardt and T. Fanghane, "Solubility and redox reactions of Pu(IV) hydrous oxide: Evidence for the formation of PuO2+x(s, hyd)," *Radiochimica Acta,* vol. 95, no. 4, pp. 193-207, 2007.

[103] D. W. Efurd, W. Runde, J. C. Banar, D. R. Janecky, J. P. Kaszuba, P. D. Palmer, F. R. Roensch and C. D. Tait, "Neptunium and plutonium solubilities in a Yucca Mountain groundwater," *Environmental Science & Technology,* vol. 32, no. 24, pp. 3893-3900, 1998.

[104] J. D. Begg, M. Zavarin, P. Zhao, S. J. Tumey, B. Powell and A. B. Kersting, "Pu(V) and Pu(IV) sorption to montmorillonite," *Environmental Science & Technology,* vol. 47, no. 10, pp. 5146-5153, 2013.

[105] B. A. Powerll, R. A. Fjeld, D. L. Kaplan, J. T. Coates and S. M. Serkiz, "Pu(V)O2+ adsorption and reduction by synthetic magnetite(Fe3O4)," *Environmental Science & Technology,* vol. 38, no. 22, pp. 6016-6024, 2004.

[106] N. P. Lu, P. W. Reimus, G. R. Parker, J. L. Conca and I. R. Triay, "Sorption kinetics and impact of temperature, ionic strength and colloid concentration on the adsorption of plutonium-239 by inorganic colloids," *Radiochimica Acta,* vol. 91, no. 12, pp. 713-720, 2003.

[107] G. A. Icopini, J. G. Lack, L. E. Hersman, M. P. Neu and H. Boukhalfa, "Plutonium(V/VI) reduction by the metal-reducing Bacteria Geobacter metallireducens GS-15 and Shewanella oneidensis MR-1," *Applied and Environmental Microbiology,* vol. 75, no. 11, pp. 3641-3647, 2009.

[108] P. H. Zhao, M. Zavarin, R. N. Leif, B. A. Powell, M. J. Singleton, R. E. Lindvall and A. B. Kersting, "Mobilization of actinides by dissolved organic compounds at the Nevada Test Site," *Applied Geochemistry,* vol. 26, no. 3, pp. 308-318, 2011.

[109] W. L. Keeney-Kennicutt and J. W. Morse, "The redox chemistry of Pu(V)O-2+ interaction with common mineral surfaces in dilute solutions and seawater," *Geochimica et Cosmochimica Acta,* vol. 49, no. 12, pp. 2577-2588, 1985.

[110] A. L. Sanchez, J. W. Murray and T. H. Sibley, "The adsorption of plutonium IV and plutonium V on goethite," *Geochimica et Cosmochimica Acta,* vol. 49, no. 11, pp. 2297-2307, 1985.

[111] R. J. Silva and H. Nitsche, "Actinide environmental chemistry," *Radiochimica Acta,* Vols. 70-1, pp. 377-396, 1995.

[112] M. N. Sabodina, S. N. Kalmykov, Y. A. Sapozhnikov and E. V. Zakharova, "Neptunium, plutonium and Cs-137 sorption by bentonite clays and their speciation in pore waters," *Journal of Radioanalytical and Nuclear Chemistry,* vol. 270, no. 2, pp. 349-355, 2006.

[113] D. I. Kaplan, B. A. Powell, M. C. Duff, D. I. Demirkanli, M. Denham, R. A. Fjeld and F. J. Molz, "Influence of sources on plutonium mobility and oxidation state transformations in vadose zone sediments," *Environmental Science & Technology,* vol. 41, no. 21, pp. 7417-7423, 2007.

[114] G. R. Choppin, A. H. Bond and P. M. Hromadka, "Redox speciation of plutonium," *Journal of Radioanalytical and Nuclear Chemistry,* vol. 219, no. 2, pp. 203-210, 1997.

[115] K. A. Orlandini, W. R. Penrose and D. M. Nelson, "Pu(V) as the stable form of oxidized plutonium in natural waters," *Marine Chemistry,* vol. 18, no. 1, pp. 49-57, 1986.

[116] A. L. Sanchez, J. W. Murray and T. H. Sibley, "The adsorption of plutonium IV and V on goethite," *Geochimica et Cosmochimica Acta,* vol. 49, pp. 2297-2307, 1985.

[117] B. A. Powell, M. C. Duff, D. I. Kaplan, R. A. Fjeld, M. Newville, D. B. Hunter, P. M. Bertsch, J. T. Coates, P. Eng, M. L. Rivers, S. R. Sutton, I. R. Triay and D. T. Vaniman, "Plutonium oxidation and subsequent reduction by Mn(IV) minerals in Yucca Mountain tuff," *Environmental Science & Technology,* vol. 40, no. 11, pp. 3508-3514, 2006.

[118] B. A. Powell, R. A. Fjeld, D. I. Kaplan, J. T. Coates and S. M. Serkiz, "Pu(V)O2+ adsorption and reduction by synthetic hematite and goethite," *Environmental Science & Technology,* vol. 39, no. 7, pp. 2107-2114, 2005.

[119] G. Lujaniene, P. Benes, K. Stamberg, K. Joksas and I. Kulakauskaite, "Pu and Am sorption to the Baltic Sea bottom sediments," *Journal of Radioanalytical and Nuclear Chemistry,* vol. 295, no. 3, pp. 1957-1967, 2013.

[120] R. A. Buda, N. L. Banik, J. V. Kratz and N. Trautmann, "Studies of the ternary systems humic substances-kaolinite-Pu(III) and Pu(IV)," *Radiochimica Acta,* vol. 96, no. 9-11, pp. 657-665, 2008.

[121] M. Zavarin, B. A. Powell, M. Bourbin, P. H. Zhao and A. B. Kersting, "Np(V) and Pu(V) ion exchange and surface-mediated reduction mechanisms on montmorillonite," *Environmental Science & Technology,* vol. 46, no. 5, pp. 2692-2698, 2012.

[122] A. E. Hixon, Y. J. Hu, D. I. Kaplan, R. K. Kukkadapu, H. Nitsche, O. Qafoku and B. A. Powell, "Influence of iron redox transformations on plutonium sorption to sediments," *Radiochimia Acta,* vol. 98, no. 9-11, pp. 685-692, 2010.

[123] C. A. Gorski, L. Klupfel, A. Voegelin, M. Sander and T. B. Hofstetter, "Redox properties of structural Fe in clay minerals. 2. Electrochemical and spectroscopic characterization of

electron transfer irreversibility in ferruginous smectite, SWa-1," *Environmental Science & Technology,* vol. 46, no. 17, pp. 9369-9377, 2012.

[124] A. M. L. Kraepiel, K. Keller and F. M. M. Morel, "A model for metal adsorption on montmorillonite," *Journal of Colloid and Interface Science,* vol. 210, no. 1, pp. 43-54, 1999.

[125] D. A. Dzombak and R. J. M. Hudson, in *Aquatic chemistry: Interfacial and interspecies processes,* American Chemical Society, Washington DC, 1995, pp. 59-94.

[126] G. Lujaniene, S. Motiejunas and J. Sapolaite, "Sorption of Cs, Pu and Am on clay minerals," *Journal of Radioanalytical and Nuclear Chemistry,* vol. 274, no. 2, pp. 345-353, 2007.

[127] W. Runde, S. D. Conradson, D. W. Efurd, N. P. Lu, C. E. VanPelt and C. D. Tait, "Solubility and sorption of redox-sensitive radionuclides (Np, Pu) in J-13 water from the Yucca Mountain site: comparison between experiment and theory," *Applied Geochemistry,* vol. 17, no. 6, pp. 837-853, 2002.

[128] J. D. Begg, M. Zavarin, S. J. Tumey and A. B. Kersting, "Plutonium sorption and desorption behavior on bentonite," *Journal of Environmental Radioactivity* , vol. 141, pp. 106-114, 2015.

[129] N. Lu, C. R. Cotter, H. D. Kitten, J. Bentley and I. R. Triay, "Reversibility of sorption of plutonium-239 onto hematite and goethite colloids," *Radiochimica Acta,* vol. 83, no. 4, pp. 167-173, 1998.

[130] J. C. Wong, M. Zavarin, J. D. Begg, A. B. Kersting and B. A. Powell, "Effect of equilibration time on Pu desorption from goethite," *Radiochimica Acta,* vol. 103, no. 10, pp. 695-705, 2015.

[131] J. D. Begg, M. Zavarin and A. B. Kersting, "Desorption of plutonium from montmorillonite: An experimental and modelling study," *Geochimica et Cosmochimica Acta*, vol. 197, pp. 278-293, 2017.

[132] D. McCubbin and K. S. Leonard, "Photochemical dissolution of radionuclides from marine sediment," *Marine Chemistry,* vol. 55, no. 3-4, pp. 399-408, 1996.

[133] D. McCubbin, K. S. Leonard and H. S. Emerson, "Influence of thermal and photochemical reactions upon the redox cycling of Pu between solid and solution phases in seawater," *Marine Chemistry,* vol. 80, no. 1, pp. 61-77, 2002.

[134] D. I. Kaplan, B. A. Powell, L. Gumapas, J. T. Coates, R. A. Fjeld and D. P. Diprete, "Influence of pH on plutonium desorption/solubilization from sediment," *Environmental Science & Technology,* vol. 40, no. 19, pp. 5937-5942, 2006.

[135] A. Kobashi, G. R. Choppin and J. W. Morse, "A study of techniques for separating plutonium in different oxidation-states," *Radiochimica Acta,* vol. 43, no. 4, pp. 211-215, 1988.

[136] B. A. Powell, Z. R. Dai, M. Zavarin, P. H. Zhao and A. B. Kersting, "Stabilization of plutonium nano-colloids by epitaxial distortion on mineral surfaces," *Environmental Science & Technology,* vol. 45, no. 7, pp. 2698-2703, 2011.

[137] R. M. Tinnacher, M. Zavarin, B. A. Powell and A. B. Kersting, "Kinetics of neptunium(V) sorption and desorption on goethite: An experimental and modeling study," *Geochimica et Cosmochimica Acta,* vol. 75, no. 21, pp. 6584-6599, 2011.

[138] I. T. Burke, C. Boothman, J. R. Lloyd, F. R. Livens, J. M. Charnock, J. M. McBeth, R. J. G. Mortimer and K. Morris, "Reoxidation behavior of technetium, iron, and sulfur in

estuarine sediments," *Environmental Science & Technology,* vol. 40, no. 11, pp. 3529-3535, 2006.

[139] G. T. W. Law, A. Geissler, J. R. Lloyd, F. R. Livens, C. Boothman, J. D. C. Begg, M. A. Denecke, J. Rothe, K. Dardenne, I. T. Burke, J. M. Charnock and K. Morris, "Geomicrobiological redox cycling of the transuranic element neptunium," *Envirionmental Science & Technology,* vol. 44, no. 23, pp. 8924-8929, 2010.

[140] H. S. Moon, J. Komlos and P. R. Jaffe, "Uranium reoxidation in previously bioreduced sediment by dissolved oxygen and nitrate," *Environmental Science & Technology,* vol. 41, no. 13, pp. 4587-4592, 2007.

[141] J. D. C. Begg, I. T. Burke, J. M. Charnock and K. Morris, "Technetium reduction and reoxidation behaviour in Dounreay soils," *Radiochimica Acta,* vol. 96, no. 9-11, pp. 631-636, 2008.

[142] R. K. Sani, B. M. Peyton, A. Dohnalkova and J. E. Amonette, "Reoxidation of reduced uranium with ironIII) (hydr)oxdies under sulfate-reducing conditions," *Environmental Science & Technology,* vol. 39, no. 7, pp. 2059-2066, 2005.

[143] NNSA, "Testimony on "The Status of U.S. Response Following an RDD Attack" before the House Committee on Homeland Security," 15 November 2007. [Online]. Available: https://nnsa.energy.gov/mediaroom/congressionaltestimony/11.15.07. [Accessed 15 August 2016].

[144] US Department of Homeland Security, "Integrated Consortium of Laboratory Networks," [Online]. Available: https://www.icln.org/. [Accessed 13 August 2016].

[145] Leidos, "Exploranium Radioisotope Identification Device," [Online]. Available: https://www.leidos.com/products/security/gr-135. [Accessed 16 August 2016].

[146] Ortec, "Nuclear Security and Safeguards," Ortec, [Online]. Available: http://www.ortec-online.com/Products-Solutions/Hand-Held-Radioisotope-Identifiers-Overview.aspx. [Accessed 16 August 2016].

[147] Canberra, "Hand held Spectroscopy," [Online]. Available: http://www.canberra.com/products/hp_radioprotection/hand-held-spectroscopy.asp. [Accessed 16 August 2016].

[148] Los Alamos National Laboratory, "LA-1721 Collected Radiochemical Procedures 4th Ed.," Los Alamos, 1982.

[149] J. R. Lamarsh and A. J. Baratta, Introduction to Nuclear Engineering, 3rd ed., Upper Saddle River, New Jersey: Prentice Hall, 2001.

[150] M. Benedict, T. H. Pigford and H. W. Levi, Nuclear Chemical Engineering, 2nd ed., New York: McGraw-Hill, 1981.

[151] Japan Atomic Energy Agency, "Nuclear Data Center," [Online]. Available: http://wwwndc.jaea.go.jp/NuC/sbygame.html. [Accessed 2 November 2016].

[152] J. D. Seader and E. J. Henley, Separation Process Principles, 2nd ed., Hoboken, New Jersey: John Wiley & Sons, Inc, 2006.

[153] S. F. Marsh, J. E. Alarid, C. F. Hammond, M. J. McLeod, F. R. Roensch and J. E. Rein, "Anion exchange of 58 elements in hydrobromic acid and in hydroiodic acid," Los Alamos National Laboratory, Los Alamos, NM, 1978.

[154] Bio-Rad Laboratories, "AG 1, AG MP-1 and AG 2 Strong Anion Exchange Resin Instruction Manual," Bio-Rad Laboratories, Hercules, CA, 2000.

[155] H. F. W. Taylor, Cement chemistry, 2nd ed., New York, NY: Thomas Telford, 1997.

[156] E. P. Horwitz, R. Chiarizia, M. L. Dietz and H. Diamond, "Separation and preconcentration of actinides from acidic media by extraction chromatography," *Analytica Chimica Acta,* no. 281, pp. 361-372, 1993.

[157] W. Rieman and H. F. Walton, Ion Exchange in Analytical Chemistry (Volume 38 of the International Series of Monographs in Analytical Chemistry), Oxford: Pergamon Press, 1970.

[158] U. I. Narayanan, P. B. Mason, J. P. Zebrowski, M. Rocca, I. W. Frank, M. M. Smith, K. D. Johnson, G. J. Orlowicz and E. Dallmann, "The quantitative ion exchange separation of uranium from impurities," New Brunswick Laboratory, Argonne, IL, 1995.

[159] G. R. Choppin and R. J. Silva, "Separation of the lanthanides by ion exchange with alpha-hydroxy isobutric acid," *Journal of Inorganic Nuclear Chemistry,* vol. 3, pp. 153-154, 1956.

[160] K. Robards, S. Clarke and E. Patsalides, "Advances in the analytical chromatography of the lanthanides a review," *Analyst,* vol. 113, pp. 1757-1779, 1988.

[161] M. Kumar, "Recent trends in chromatographic procedures for separation and determination of rare earth elements a review," *Analyst,* vol. 119, pp. 2013-2024, 1994.

[162] K. L. Nash and M. P. Jensen, "Analytical-scale separations of the lanthanides: A review of techniques and fundamentals," *Separation Science and Technology,* vol. 36, no. 5-6, pp. 1257-1282, 2001.

[163] D. H. Sisson, V. A. Mode and D. O. Campbell, "High-speed separation of the rare earths by ion exchange part II.," *Journal of Chromatography,* vol. 66, pp. 129-135, 1972.

[164] D. O. Campbell, "Rapid rare earth separation by pressurized ion exchange chromotography," *Journal of Inorganic Nuclear Chemistry,* vol. 35, pp. 3911-3919, 1973.

[165] Y. Shuheng, L. Fa, H. Zhang, X. Li and S. Zhang, "Application of pressurized cation exchange chromatography for fission yield determination," *Journal of Radioanalytical and Nuclear Chemistry, Articles,* vol. 124, no. 1, pp. 187-195, 1988.

[166] E. P. Horwitz and C. A. A. Bloomquist, "Chemical separation for super-heavy element searches in irradiated uranium targets," *Journal of Inorganic Nuclear Chemistry,* vol. 37, pp. 425-434, 1975.

[167] Eichrom, "Eichrom Technologies Product Catalog for 2013," 2013. [Online]. Available: http://www.eichrom.com/PDF/eic-2013-product-catalog.pdf. [Accessed 10 March 2015].

[168] E. P. Horwitz, R. Chiarizia, M. L. Dietz, H. Diamond and D. M. Nelson, "Separatio and preconcentration of actinides from acidic media by extraction chromatography," *Analytica Chimica Acta,* vol. 281, no. 2, pp. 361-372, 1993.

[169] E. A. Huff and D. R. Huff, "TRU-Spec and RE-Spec chromatography: Basic studies and applications," in *34th ORNL/DOE Conference On Analytical Chemistry in Energy Technology*, Gatlinburg, TN, 1993.

[170] C. Pin and J. F. S. Zalduegui, "Sequential separation of light rare-earth elements, thorium and uranium by miniaturized extraction chromatography: Application to isotopic analyses of silicate rocks," *Analytica Chimica Acta,* vol. 339, pp. 79-89, 1997.

[171] Thermo Scientific, "Liquid Chromatography," [Online]. Available: http://www.dionex.com/en-us/products/liquid-chromatography/lp-71340.html. [Accessed 2016 May 2016].

[172] Jasco Inc, "JASCO," [Online]. Available: http://www.jascoinc.com/. [Accessed 18 May 2016].

[173] aapptec, "HPLC Systems," [Online]. Available: http://www.aapptec.com/hplc-systems-i-105.html. [Accessed 18 May 2016].

[174] R. Morales, C. S. Bartholdi and P. T. Cunningham, "HPLC separation of heterocyclic beta-diketonates of actinide, lanthanide and transition-metals," *Talanta,* vol. 35, no. 6, pp. 461-464, 1988.

[175] T. P. Rao and V. M. Biju, "Trace determination of lanthanides in metallurgical, environmental, and geological samples," *Critical Reviews in Analytical Chemistry,* vol. 30, no. 2-3, pp. 179-220, 2000.

[176] S. P. Verma and E. Santoyo, "High-performance liquid and ion-chromatography: Separation and quantification analytical techniques for rare earth elements," *Geostandards and Geoanalytical Research* , vol. 31, no. 3, pp. 161-184, 2007.

[177] S. Rollin, Z. Kopatjtic, B. Wernli and B. Magyar, "Determination of lanthanides and actinides in uranium materials by high-performance liquid chromatography with inductively coupled plasma mass spectrometric detection," *Journal of Chromatography A,* vol. 739, no. 1-2, pp. 139-149, 1996.

[178] N. Sivaraman, S. Subramaniam, T. G. Srinivasan and P. R. V. Rao, "Burn-up measurements on nuclear reactor fuels using high performance liquid chromatography," *Journal of Radioanalytical and Nuclear Chemistry*, vol. 253, no. 1, pp. 35-40, 2002.

[179] N. M. Raut, P. G. Jaison and S. K. Aggarwal, "Separation and determination of lanthanides, thorium and uranium using a dual gradient in reversed-phase liquid chromatography," *Journal of Chromatography A,* vol. 1052, no. 1-2, pp. 131-136, 2004.

[180] I. Gunther-Leopold, J. K. Waldis, B. Wernli and Z. Kopajtic, "Measurement of plutonium isotope ratios in nuclear fuel samples by HPLC-MC-ICP-MS," *International Journal of Mass Spectrometry*, vol. 242, no. 2-3, pp. 197-202, 2005.

[181] P. G. Jaison, N. M. Raut and S. K. Aggarwal, "Direct determination of lanthanides in simulated irradiated thoria fuels using reversed-phase high-performance liquid chromatography," *Journal of Chromatography A*, vol. 1122, no. 1-2, pp. 47-53, 2006.

[182] M. A. Maheswari, D. Prabhakaran, M. S. Subramanian, N. Sivaraman, T. G. Srinivasan and P. R. V. Rao, "High performance liquid chromatographic studies on lanthanides, uranium and thorium on amide modified reversed phase supports," *Talanta*, vol. 72, no. 2, pp. 730-740, 2007.

[183] C. S. K. Raju, M. S. Subramanian, N. Sivaraman, T. G. Srinivasan and P. R. V. Rao, "Retention studies on uranium, thorium and lanthanides with amide modified reverse phase support and its applications," *Journal of Chromatography A*, vol. 1156, no. 1-2, pp. 340-347, 2007.

[184] A. Datta, N. Sivaraman, T. G. Srinivasan and P. R. V. Rao, "Rapid separation of lanthanides and actinides on small particle based reverse phase supports," *Radiochimica Acta*, vol. 95, no. 5, pp. 277-285, 2010.

[185] D. Das, S. A. Ansari, P. K. Mohapatra, G. Mary, K. Radhakrishnan, S. C. Tripathi and V. Manchnada, "Separation and determination of components of high level waste using IC and dynamically modified reversed-phase HPLC in 'actinide partitioning' studies using synthetic waste solution," *Journal of Radioanalytical and Nuclear Chemistry*, vol. 287, no. 1, pp. 293-298, 2011.

[186] P. Deepika, N. Sivaraman, K. N. Sabharwal, T. G. Srinivasan and P. R. V. Rao, "Separation of lanthanides and actinides on a bistriazinyl prydine coated reverse phase column," *Radiochimica Acta,* vol. 99, no. 6, pp. 325-334, 2011.

[187] National Instruments, "LabVIEW System Design Software," 2016. [Online]. Available: http://www.ni.com/labview/. [Accessed 25 August 2016].

[188] Dionex, "Chromeleon SDK Software Developers Kit User's Guide," Dionex Softron, Sunnyvale, 2006.

[189] Dionex, "Chromeleon SKD Software Developers Kit Reference Manual," Dionex, Sunnyvale, 2006.

[190] S. F. Marsh, J. E. Alarid, C. F. Hammond, M. J. McLeod, F. R. Roensch and Rein, "Anion exchange of 58 elements in hydrobromic acid and in hydriodic acid," Los Alamos Scientific Laboratory, Los Alamos, NM, 1972.

[191] J. P. Faris and R. F. Buchanan, "Anion exchange characteristics of the elements in nitric acid medium," *Analyticl Chemistry,* vol. 36, no. 6, pp. 1157-1158, 1964.

[192] Brookhaven National Laboratory, "National Nuclear Data Center-Chart of Nuclides," 2007. [Online]. Available: http://www.nndc.bnl.gov/chart/. [Accessed 10 March 2015].

[193] W. E. Nervik, "The Radiochemistry of Tin," Lawrence Radiation Laboratory, Livermore, 1960.

[194] VICI, "VICI Jour-Technical Support," 2013. [Online]. Available: http://www.vici-jour.com/support/resistance.php. [Accessed 12 May 2015].

[195] NNDC, Brookhaven National Laboratory, "Chart of Nuclides," [Online]. Available: http://www.nndc.bnl.gov/chart/. [Accessed 5 December 2016].

[196] Idaho National Laboratory, "Online Spectrum Catalogs for Ge and Si(Li)," 16 February 2009. [Online]. Available: http://www4vip.inl.gov/gammaray/catalogs/ge/catalog_ge.shtml. [Accessed 5 December 2016].

[197] D. E. Dry, E. Bauer and L. A. Petersen, "Rapid separation of fresh fission products," *Journal of Radioanalytical and Nuclear Chemistry*, vol. 263, no. 1, pp. 19-22, 2005.

[198] G. F. Knoll, Radiation Detection and Measurement, 4th ed., Hoboken, NJ: John Wiley & Sons, 2010.

A. Appendix

A.1 Float-A-Lyzer pore size chart

A pore size chart

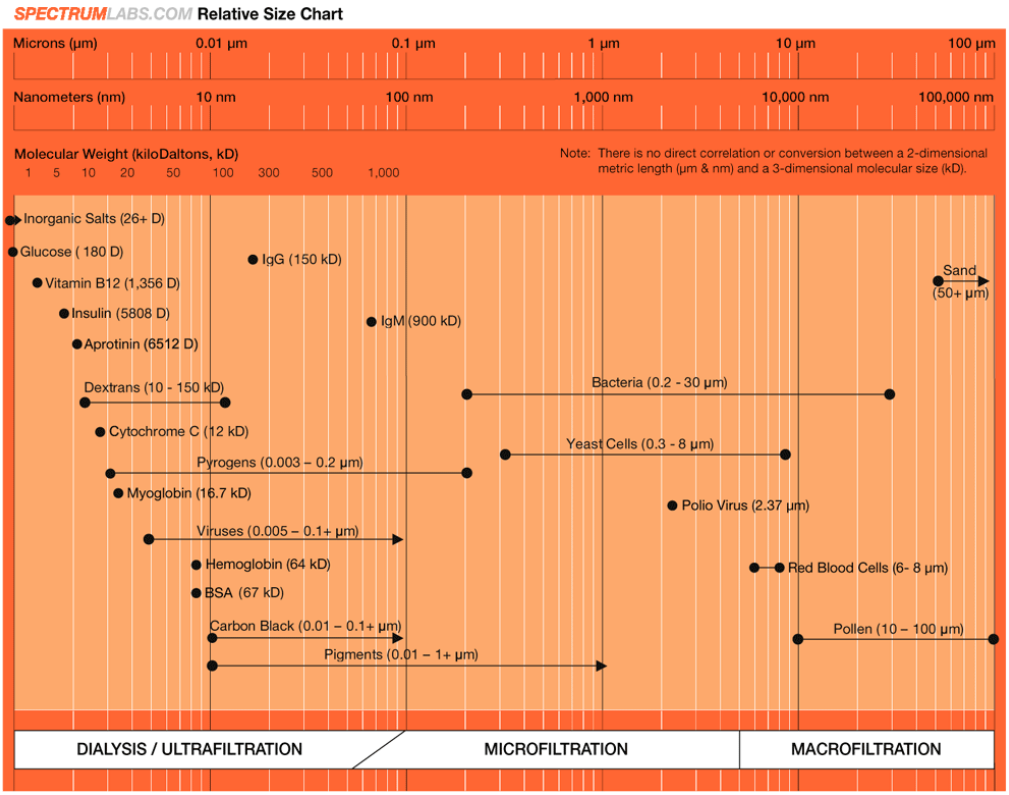

Figure A-1. http://spectrumlabs.com/dialysis

A.2 2-site modeling of kaolinite and montmorillonite

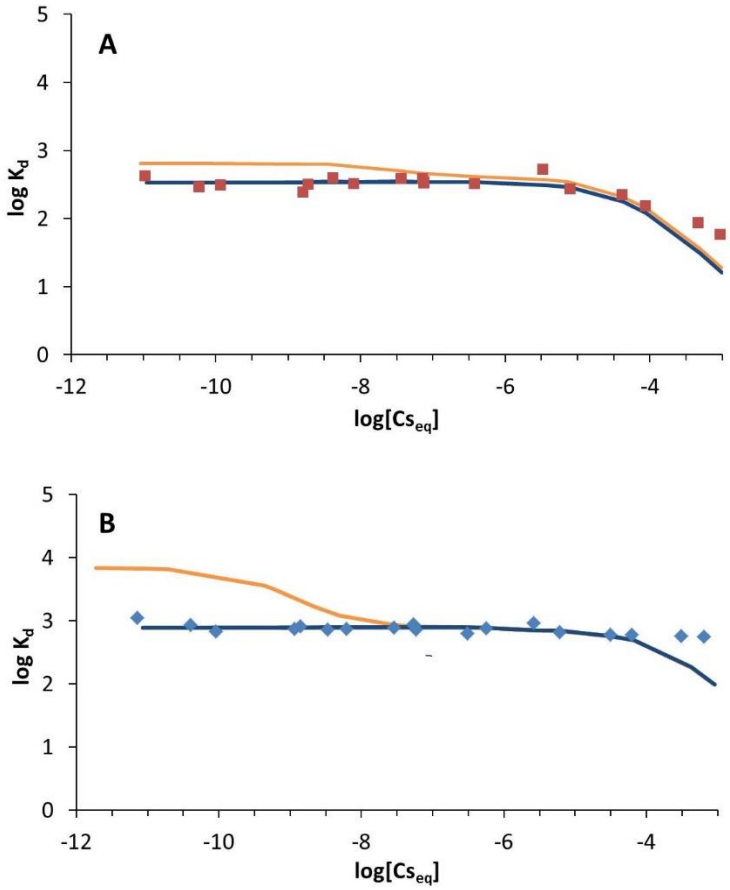

Figure A-2. A comparison of the 1-site (dark blue lines) and 2-site (orange lines) models for (A) Cs-kaolinite sorption and (B) Cs-montmorillonite sorption **[**79**]**.

When developing the sorption models for Cs sorption to kaolinite (Figure A-2) and montmorillonite (Figure A-2) conducted in this work the initial inputs were based on 2-site models from Missana et al., (2014). The 2-site models are the solid orange lines in Figure A5. Next 1-site models, solid dark blue lines) were used to try and fit the sorption data by removing the high affinity sites from the 2-site models. In both cases, the absence

of a high affinity site in the montmorillonite and kaolinite sorption data suggests that the high affinity sites observed by Missana et al. (2014) are likely the result of high affinity mineral impurities in their samples. This was suggested in the analysis reported by Missana et al. (2014) The difference is most pronounced in the montmorillonite models and less so in the kaolinite models, but 1-site models were used to describe Cs sorption to kaolinite and montmorillonite.

A.3 Ternary experiments control samples

Figure A-3 shows the total Cs sorbed to illite inside the dialysis membranes in mol/g with montmorillonite (A), illite (B), kaolinite (C) and no mineral (D) suspensions outside the dialysis membranes. It was assumed that the cause of the decreasing aqueous Cs concentrations (see Figure A-4) was a result of Cs sorption to illite in the dialysis membranes. The horizontal lines in Figure A-3 represent the amount of Cs that would be sorbed to the illite inside the dialysis membrane if all the aqueous Cs present when the dialysis membranes were added to the centrifuge tube was adsorbed. By 200 days in Figure A-3A-Figure A-3C, the illite in the dialysis membrane has sorbed at least as much Cs as was initially present in the aqueous phase. Figure A-3D shows the total Cs on the illite in the dialysis membranes reaching the solid lines, thereby showing that the illite in the dialysis membranes had the capacity to sorb the entirety of the Cs added in each ternary system. As time increases, the amount of Cs on illite in the dialysis membrane in Figure A-3A-Figure A-3C continues to increase above the solid line. In order for the total Cs on illite in the dialysis membrane to surpass the solid line an additional source of Cs

other than the initial aqueous Cs must contribute. As shown in Figure 2-13 Cs desorbs from the mineral outside of the dialysis membrane over time. Cs desorbed from the minerals outside the dialysis membrane and adsorbed by illite inside the dialysis membrane would explain the amount of total Cs sorbed exceeding the solid lines. These results indicate that adding a second mineral, like illite, with a high affinity for Cs can effect desorption of Cs previously sorbed to another mineral.

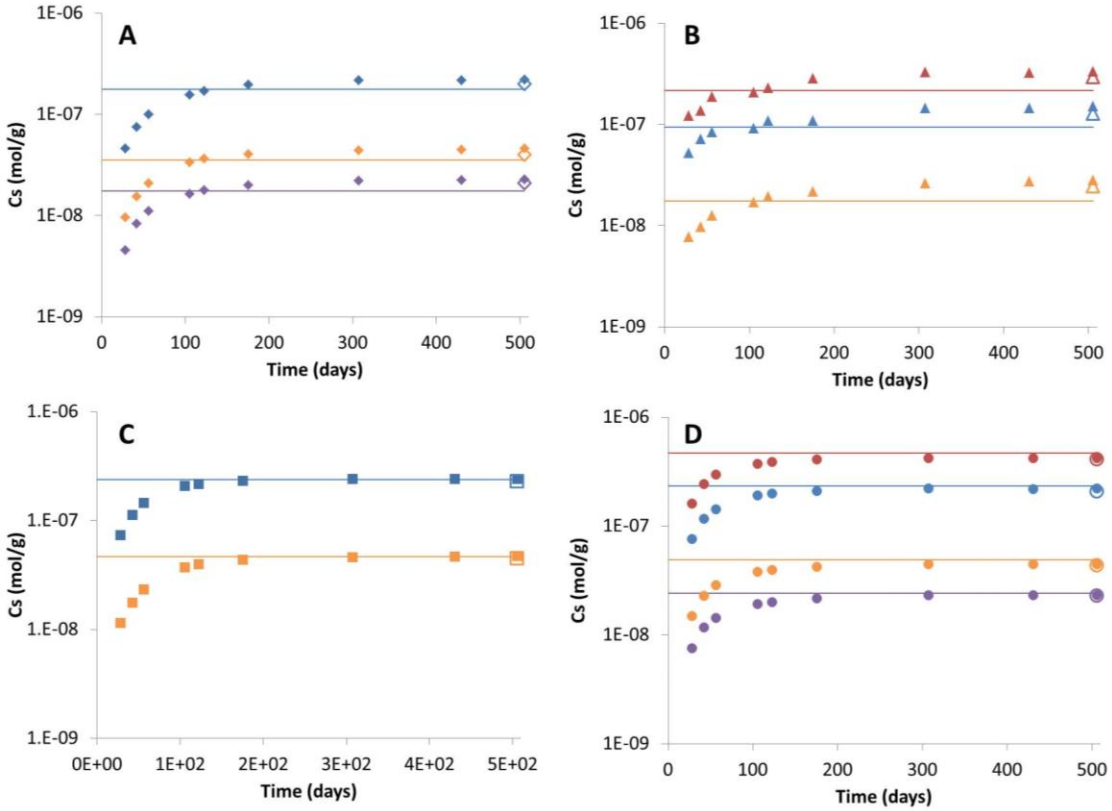

Figure A-3. The calculated (closed shapes) and measured (open shapes at 505 days) sorption of Cs by illite inside the dialysis membranes in mol/g is plotted over time for each (A) montmorillonite, (B) illite, (C) kaolinite mineral suspension experiment. The data plotted in figure D represents the Cs control where no mineral suspension is present outside the dialysis membrane. Red, blue, orange and purple colors represent initial [Cs] of 1 x 10^{-6} M, 5 x 10^{-7} M, 1 x 10^{-7} M and 5 x 10^{-8} M, respectively. The solid lines represent the aqueous Cs available at the start of the experiment that could be sorbed when the illite-containing dialysis membranes were added. Error bars based on propagation of 2s % LSC uncertainties are within the marker size.

A.5 Sequential Batch Extractions

Figure A-4 and Figure A-5 show sequential batch desorptions for illite, montmorillonite and kaolinite respectively. In subsequent batch desorptions from each mineral, proportionally less Cs is desorbed. Figure A-4 shows the cumulative Cs to desorb from illite, montmorillonite, and kaolinite after each batch desorption. The cumulative Cs desorbed is greater for each successive batch desorption. Figure A-4-B and Figure A-5-B show that less than 5% of Cs desorbs from illite in a single batch or cumulatively after multiple batches for Cs equilibrium concentrations below 10^{-7} M. This low desorption of Cs from illite affirms prior findings that Cs is at least partly irreversibly fsorbed on illite. Figure A-4-A and Figure A-5-A show the continued desorption of Cs from montmorillonite over multiple batch desorptions and over more than 200 days. Generally the first batch desorption has the highest fraction of Cs desorbed with each successive batch desorption having less Cs desorbed.

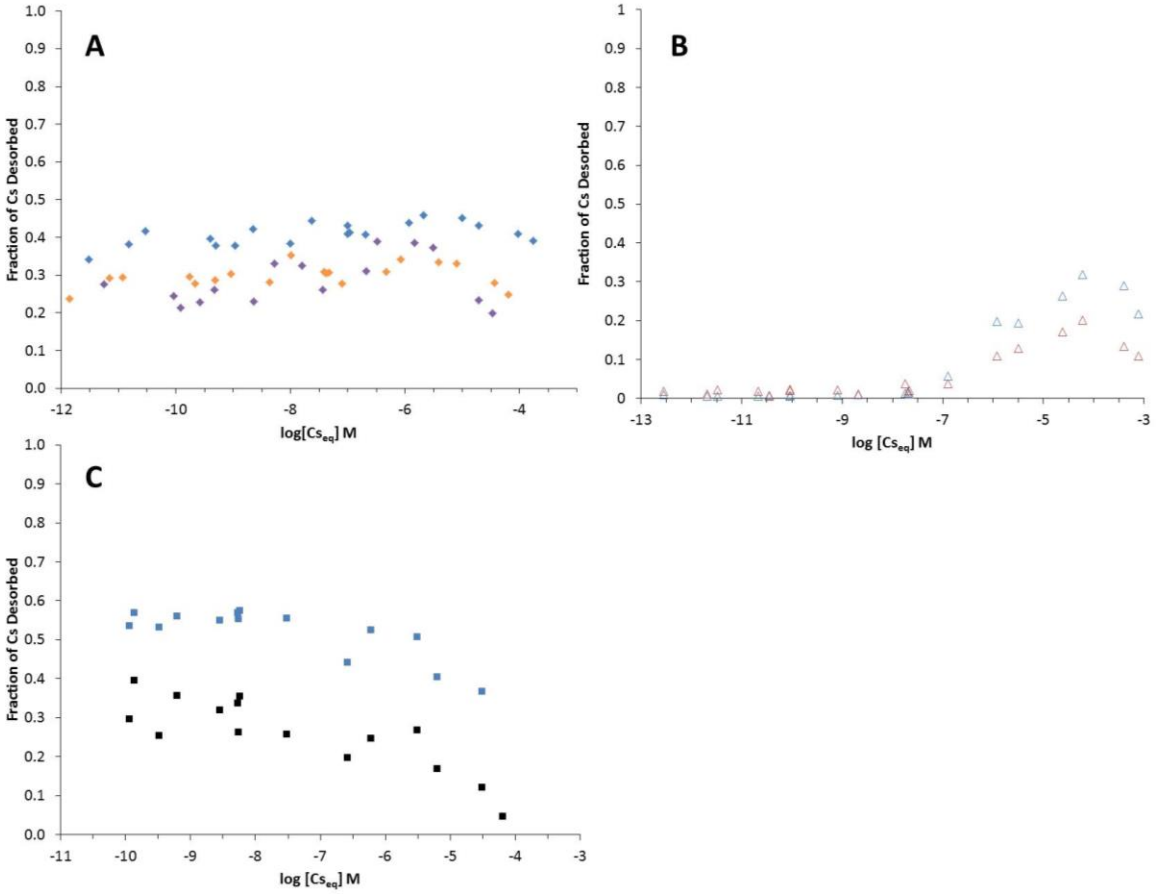

Figure A-4. Sequential Cs batch desorption experiments for (A) for Na-montmorillonite after (♦) 14 days, (♦) 142 days, (♦) 209 days, (B) Na-illite after (Δ) 14 days, (Δ) 197 days and (C) Na-kaolinite after (♦) 14 days, (■) 307 days. All experiments performed in 0.7 mM $NaHCO_3$, 5 mM NaCl buffer solution at pH 8. The solid solution ratio is 1 g/L for each mineral and error bars are removed for clarity.

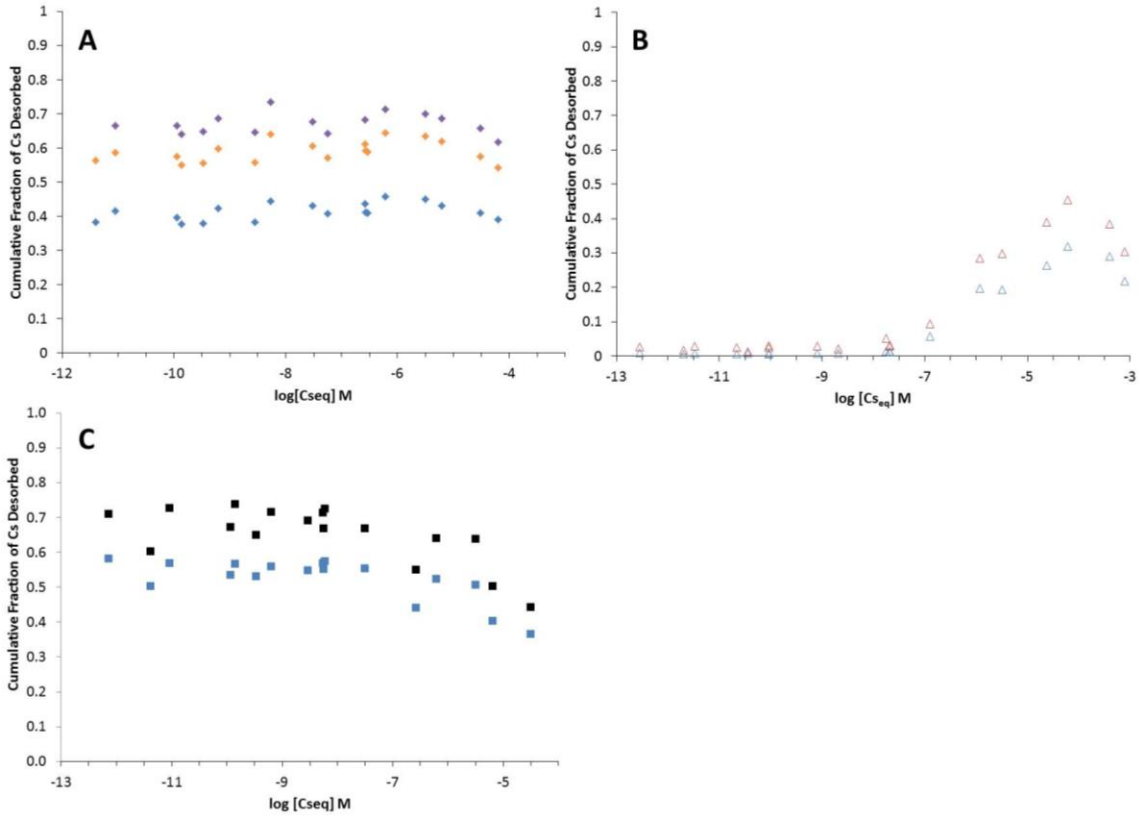

Figure A-5. Cumulative Cs desorbed from sequential Cs batch desorption experiments for (A) Na-montmorillonite after (♦) 14 days, (♦) 142 days, (♦) 209 days, (B) Na-illite after (Δ) 14 days, (Δ) 197 days and (C) Na-kaolinite after (♦) 14 days, (■) 307 days. All experiments performed in 0.7 mM $NaHCO_3$, 5 mM NaCl buffer solution at pH 8. The solid solution ratio is 1 g/L for each mineral and error bars are removed for clarity

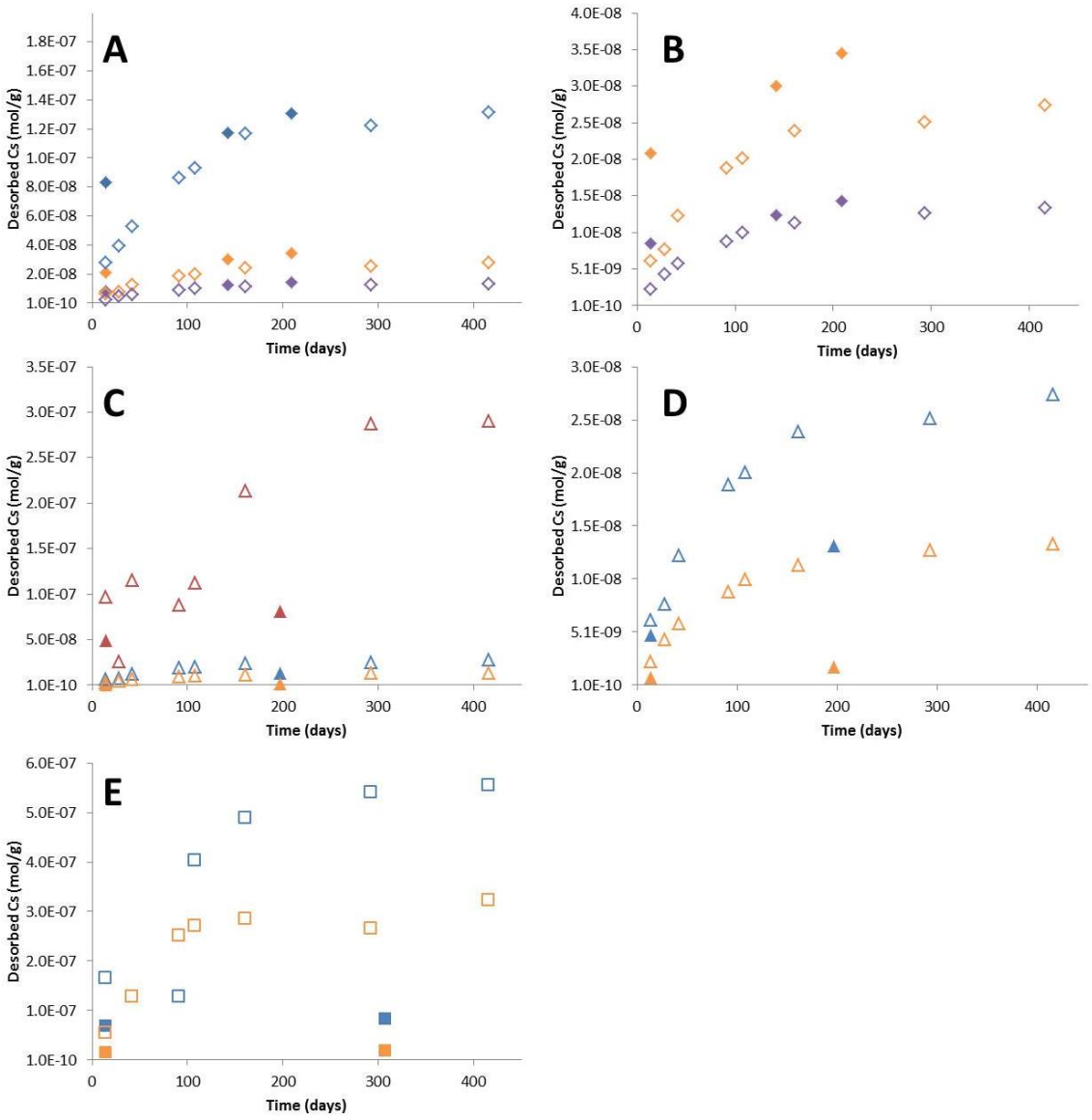

Figure A-6. The desorption of Cs over time from (A and B) montmorillonite, (C and D) illite and (E) kaolinite mineral suspensions in mol/g. Batch desorption experiments are represented by solid shapes and multi-mineral experiments by open shapes. Red, blue, orange and purple colors represent initial [Cs] of 1 x 10^{-6} M, 5 x 10^{-7} M, 1 x 10^{-7} M and 5 x 10^{-8} M respectively. Error bars based on propagation of 2s % LSC uncertainties are within the marker size.

Figure A-6 shows the amount of Cs to desorb from illite, kaolinite and montmorillonite normalized for mass. The open shapes represent the desorption that occurred in the ternary systems and the closed shapes are from the batch desorption

experiments. Figures B and D are on a different scale in order to magnify the desorption behavior of the two lower Cs concentrations from Figures A and C respectively.

A.6 LabVIEW software program

Included here are several screenshots of the LabVIEW software program developed for the automated system.

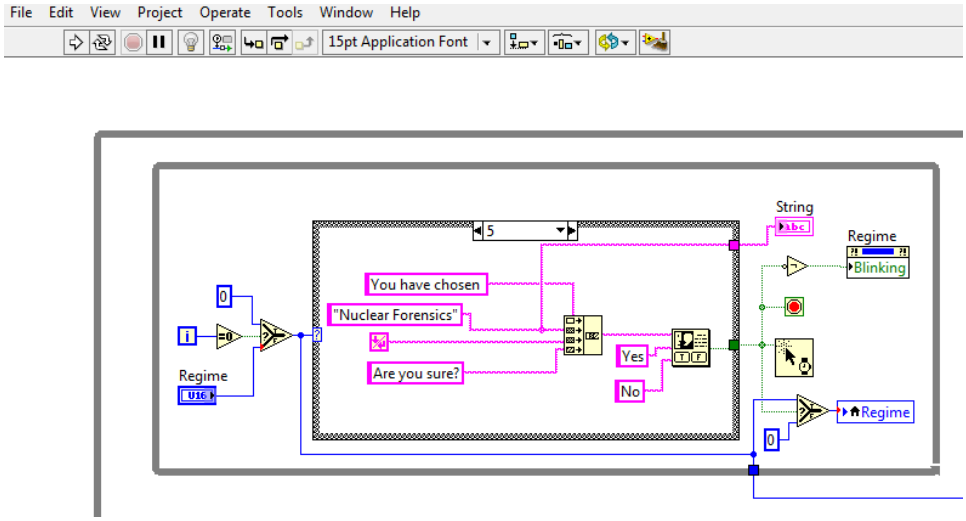

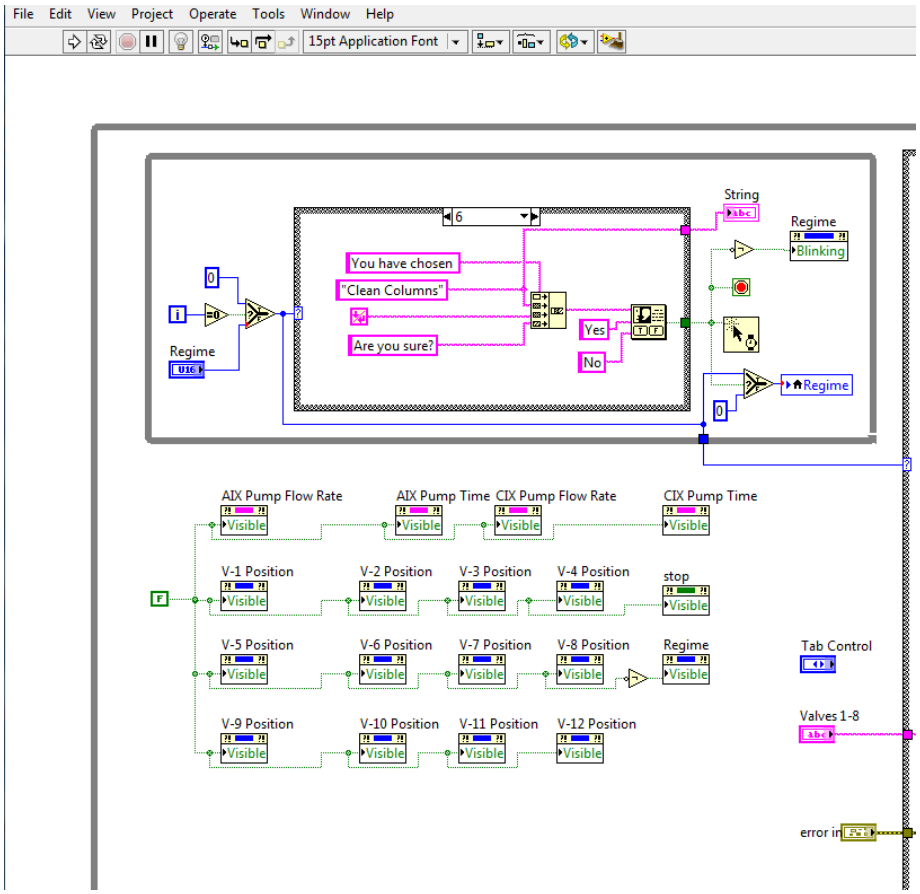
File Edit View Project Operate Tools Window Help
15pt Application Font
String
Regime
Blinking
You have chosen
"Clean Columns"
Are you sure?
Yes
No
Regime
Regime
AIX Pump Flow Rate
AIX Pump Time
CIX Pump Flow Rate
CIX Pump Time
V-1 Position
V-2 Position
V-3 Position
V-4 Position
stop
V-5 Position
V-6 Position
V-7 Position
V-8 Position
Regime
Tab Control
V-9 Position
V-10 Position
V-11 Position
V-12 Position
Valves 1-8
error in

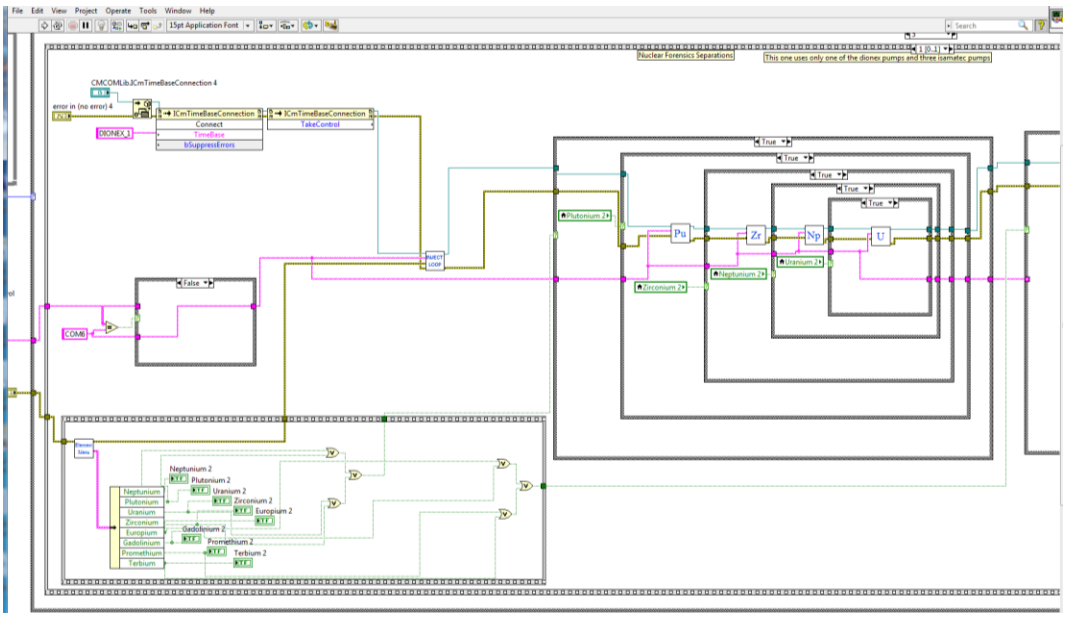

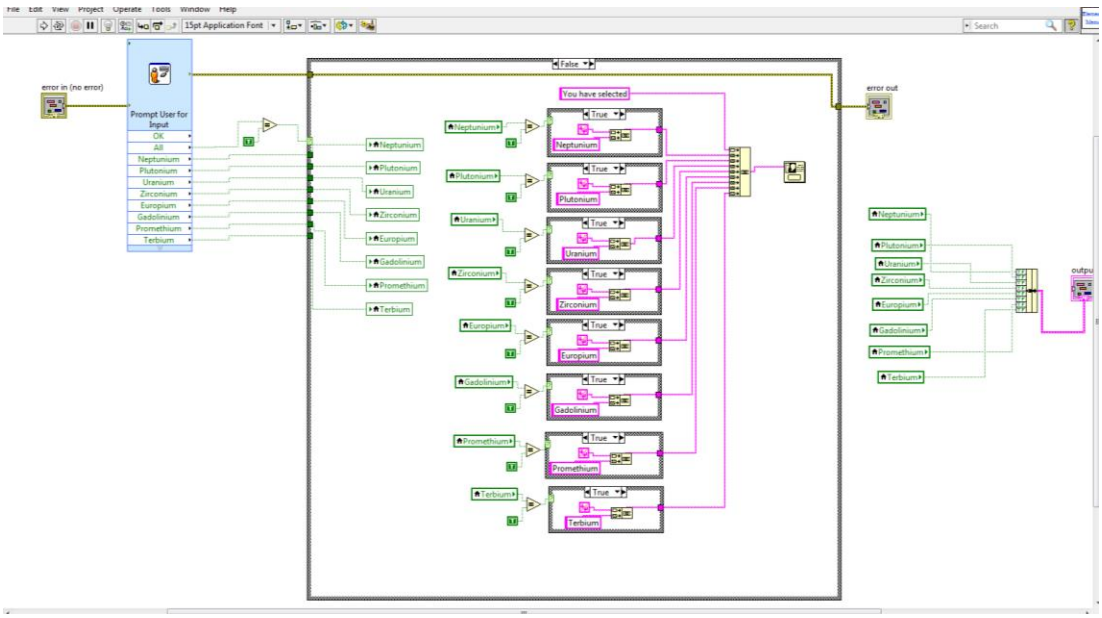
error in (no error)
Prompt User for Input
OK
All
Neptunium
Plutonium
Uranium
Zirconium
Europium
Gadolinium
Promethium
Terbium
False
You have selected
True
error out

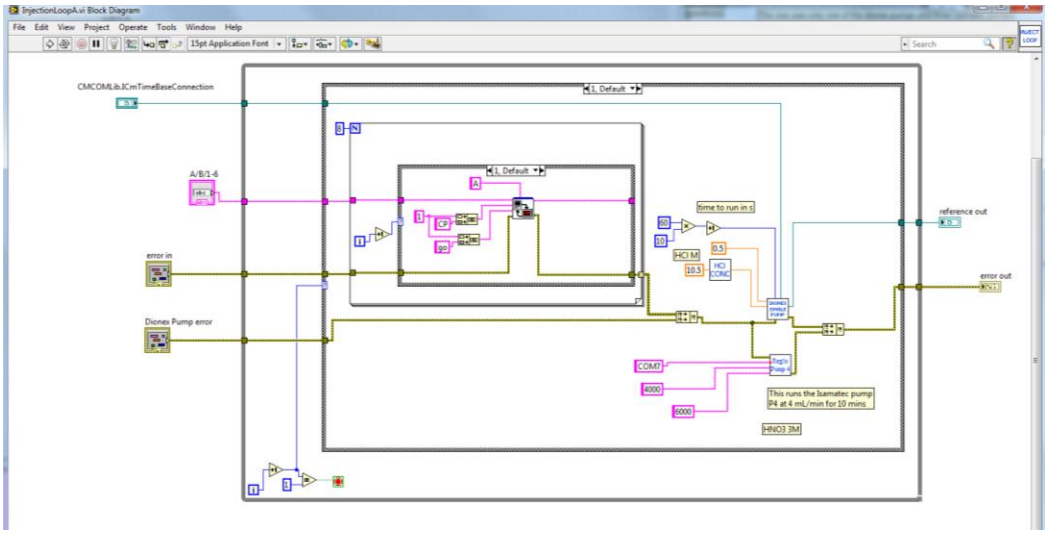
InjectionLoopA.vi Block Diagram
File Edit View Project Operate Tools Window Help
CMCOMLib.ICmTimeBaseConnection
A/B/1-6
error in
Dionex Pump error
time to run in s
reference out
error out
COM7
4000
6000
This runs the Isamatec pump P4 at 4 mL/min for 10 mins
HNO3 3M

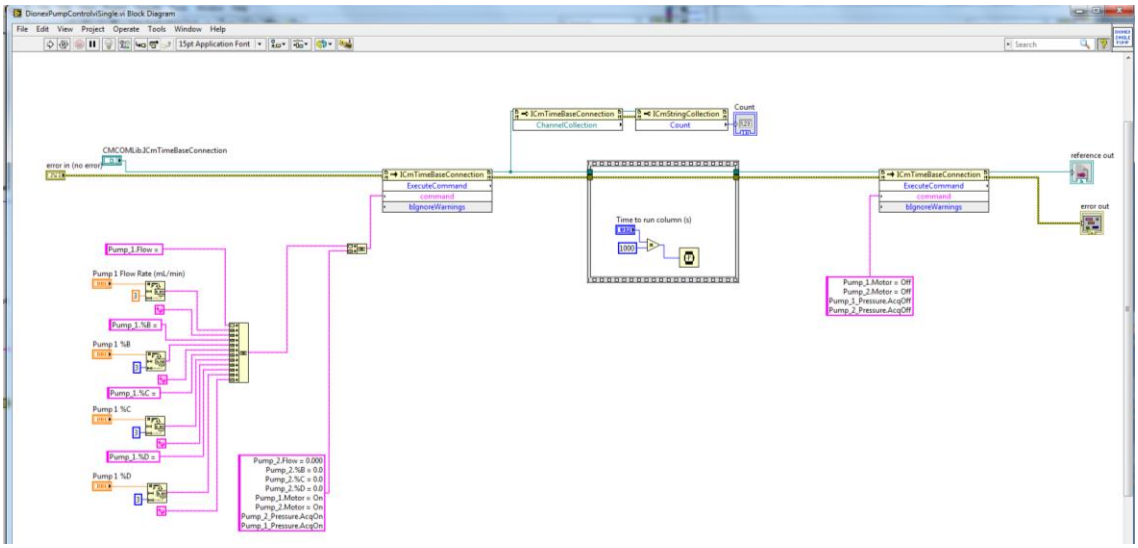

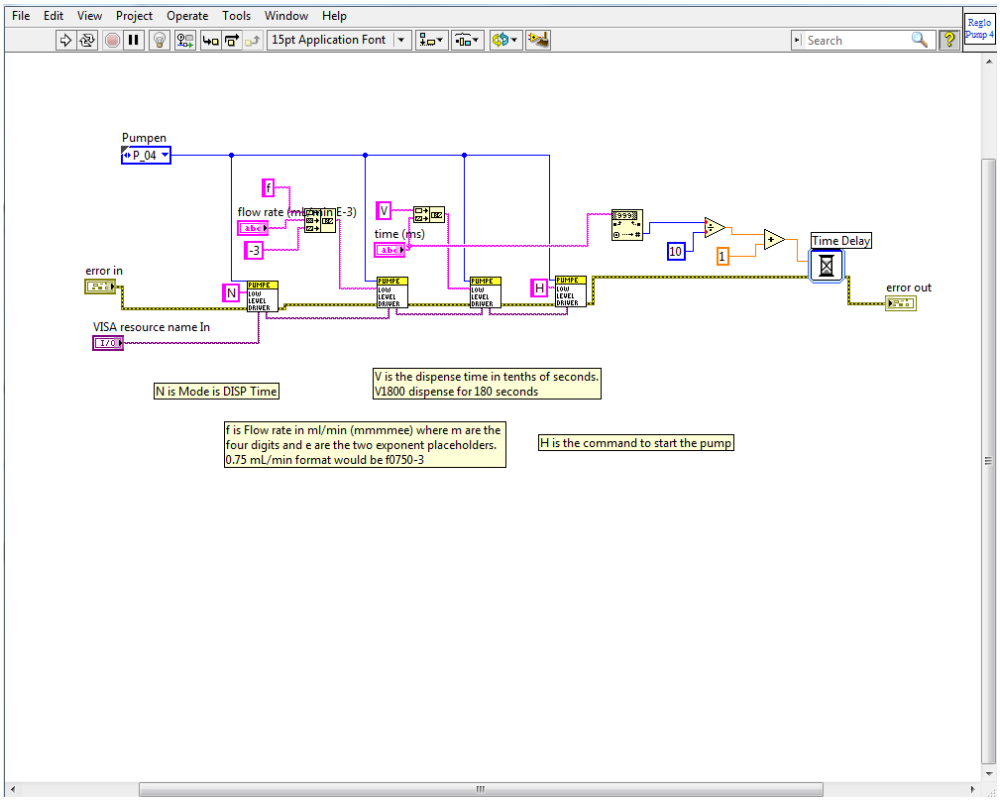
File Edit View Project Operate Tools Window Help
15pt Application Font
Search
Pumpen
P_04
f
flow rate (ml
E-3)
-3
V
time (ms)
10
1
Time Delay
error in
error out
N
H
VISA resource name In
N is Mode is DISP Time
V is the dispense time in tenths of seconds.
V1800 dispense for 180 seconds
f is Flow rate in ml/min (mmmmee) where m are the four digits and e are the two exponent placeholders.
0.75 mL/min format would be f0750-3
H is the command to start the pump

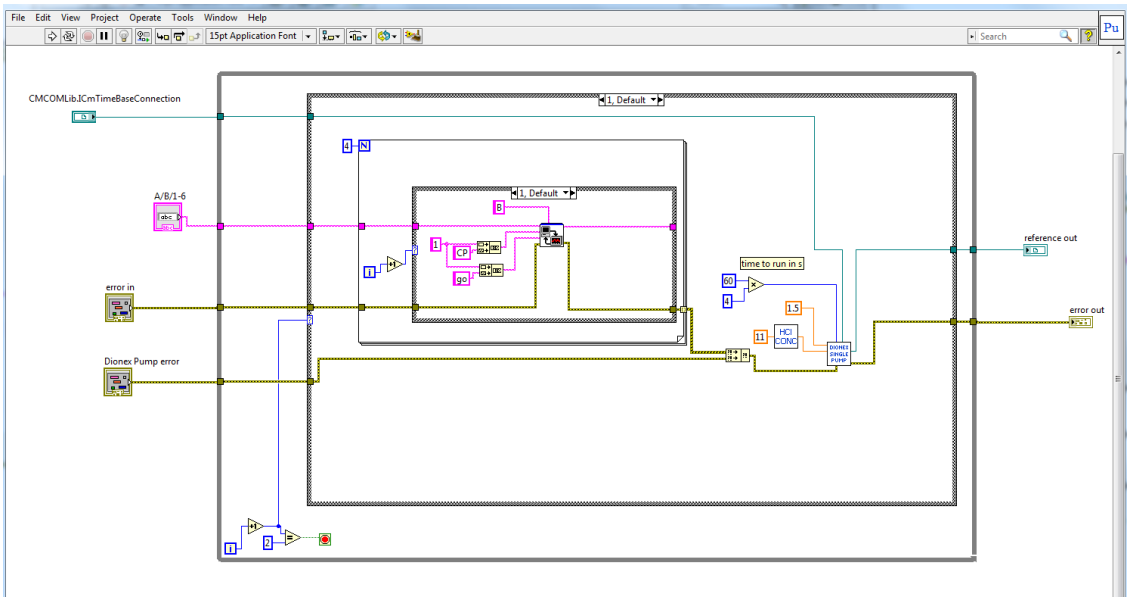
File Edit View Project Operate Tools Window Help
15pt Application Font
Search
CMCOMLib.ICmTimeBaseConnection
A/B/1-6
error in
Dionex Pump error
1, Default
CP
go
time to run in s
60
1.5
HCl
CONC
reference out
error out

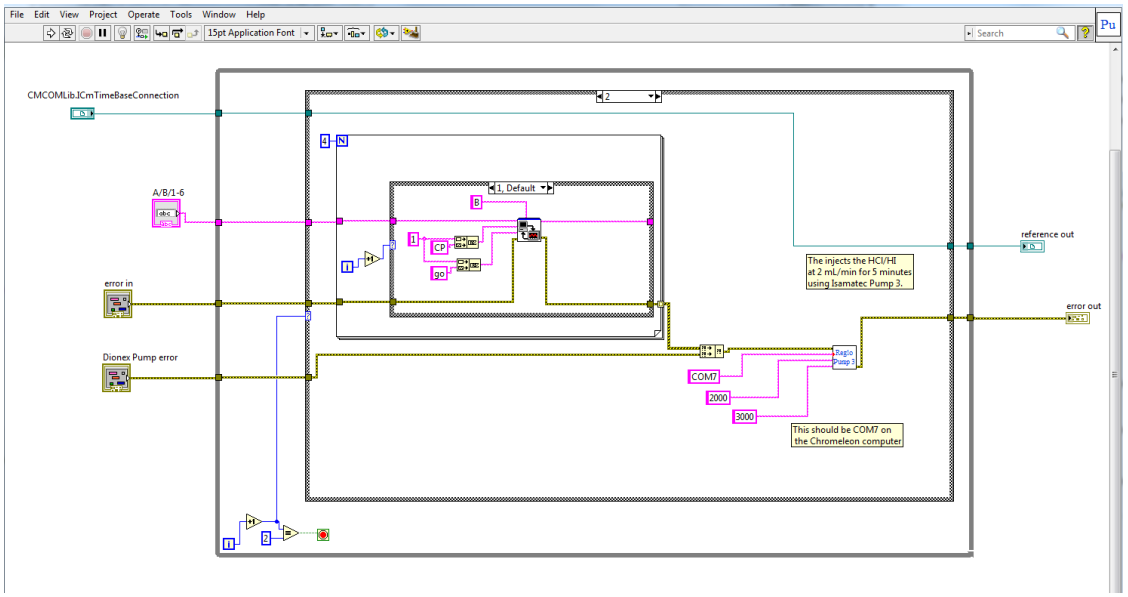
File Edit View Project Operate Tools Window Help
15pt Application Font
Search
CMCOMLib.ICmTimeBaseConnection
A/B/1-6
error in
Dionex Pump error
2
1, Default
CP
go
The injects the HCl/HI
at 2 mL/min for 5 minutes
using Isamatec Pump 3.
COM7
2000
3000
This should be COM7 on
the Chromeleon computer
reference out
error out

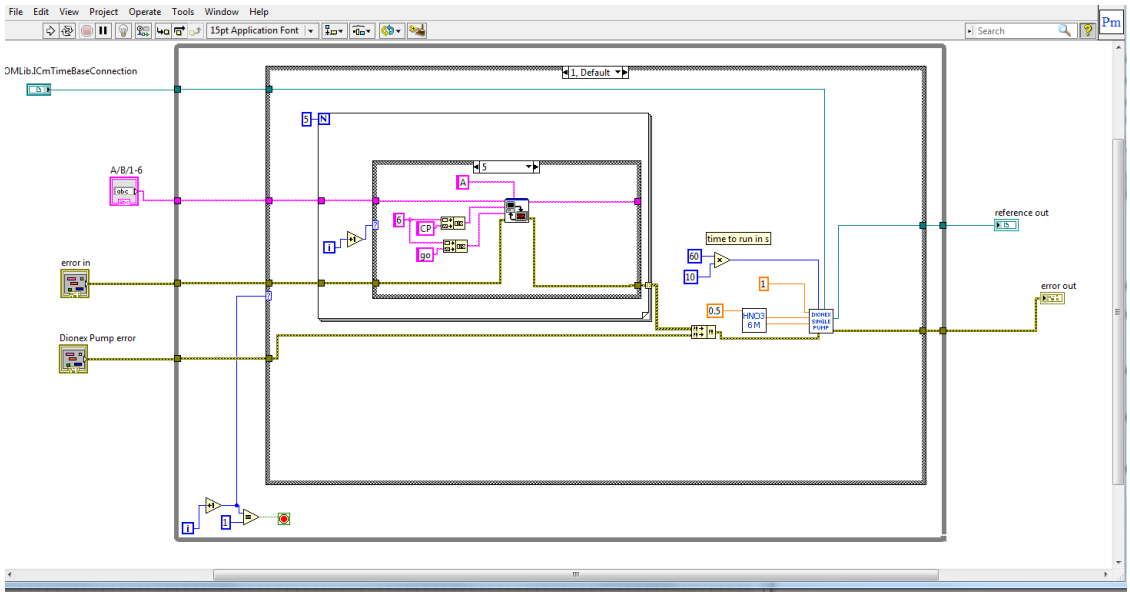
File Edit View Project Operate Tools Window Help
15pt Application Font
Search
OMLib.ICmTimeBaseConnection
1, Default
5
N
A/B/1-6
A
6
CP
go
error in
Dionex Pump error
time to run in s
60
10
1
0.5
HNO3 6 M
reference out
error out

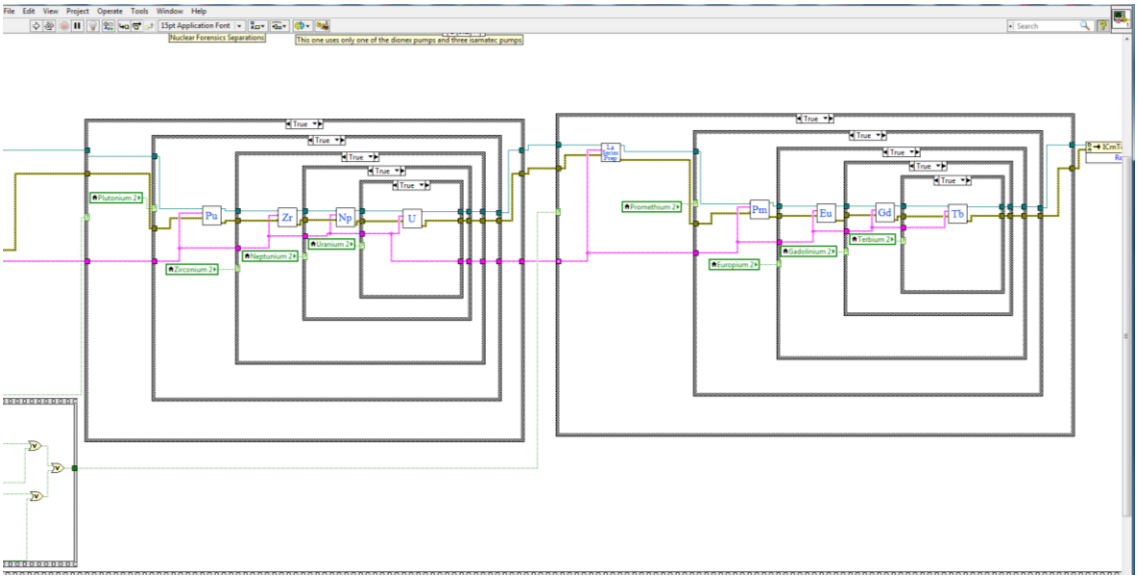
File Edit View Project Operate Tools Window Help
15pt Application Font
Search
Nuclear Forensics Separations
This one uses only one of the dionex pumps and three namatec pumps
Plutonium 2+
Pu
Zr
Np
U
Zirconium 2+
Neptunium 2+
Uranium 2+
Promethium 2+
Pm
Eu
Gd
Tb
Europium 2+
Gadolinium 2+
Terbium 2+

A.7 Procedure for dissolving cement

The procedure used to dissolve the piece of cement for use in the various experiments in Chapter 4 was adapted from a rock dissolving procedure used at LLNL. The procedure is written for 20 grams of material to be dissolved, but this work only used 10 grams and all subsequent volumes and masses were halved. Also the fume hood used for this procedure was not compatible with the use of per chloric acid. Changes are indicated by a strikethrough for removal and the subsequent modification or addition is underlined. The final pot solution volume was purposely left at half of what was expected, meaning that the final pot solution was twice as concentrated as might be normally used.

1. The sample, including about 20 grams of water, in a crucible, is placed on the crucible heater.
2. Add 40 grams conc. HNO3.
3. Add 40 grams conc. HF.
4. 80 grams of solution are evaporated at ~ 2 grams/minute.
5. Add 80 grams conc. HF to bring back to 100 grams.
6. Set heater to a value of 30.
7. Cook solution at setting of 30 for about an hour.
8. 80 grams of solution are evaporated at ~2 grams/minute.
9. ~~HClO4~~ HCl is added until the back to 100 grams.
10. 80 grams of solution are evaporated at ~2 grams/minute.
11. ~~HClO4~~ HCl is added until the back to 100 grams.

12. The solution is cooked at a setting of 35 for about an hour.
13. 80 grams of solution are evaporated at ~2 grams/minute.
14. ~~HClO4~~ HCl is added until back to 100 grams and 1 mL of saturated boric acid in conc. HCl is added.
15. 80 grams of solution are evaporated at ~2 grams/minute.
16. Here ends the automated portion of the dissolving procedure.

    Bring the sample to ~ 60 mL with 6M HCl.

(The following is a revision of "RDP 830928" as written by N. A. Bonner on September, 28, 1983 and revised on September 10, 1991 by E. H. Wiles.)

CARDINAL RULES:

A. Do not put any fluoride ion (HF) in the pot.
B. Never put chloride ion and nitrate ion (HCl-HNO3) together in the Pt crucible.
C. Keep the pot above 3M HCl.
D. Never evaporate the sample to dryness before step 6a.
E. Do not cut short the centrifuging time.

The quality of all the diagnostic measurements depends on the quality of the pot.

PROCEDURE:

The sample in the glove box has been pre-treated by an automatic process and is ready for final dissolution. The sample is in 6M HCl and residual HClO4 from the automatic process.

1. Decant the cooled HCl mixture from the crucible into two 40 mL cones containing 5 to 10 mL water. (Extremely dense solutions tend to plug the filter. The next steps are easier if most of the salts are left in the crucible.) Stir and centrifuge a minimum of 10 minutes at 2250 RPM. Carefully pour the supernatant through a WH 40 filter paper into the pot. Wash filter with a little water.
2. Add about 20 mL of 6M HCl and 40 mL of H20 to the residue in the crucible and boil 5 minutes. While boiling, add 10 mL of water to each cone. At the end of the 5 min boil, allow the crucible to cool for 2 or 3 minutes. Decant into centrifuge cones and stir. Centrifuge 10 minutes at 2250 RPM. (WARNING: Do not cut short either the cooling or the centrifuge time as you may end up with a plugged filter!) Filter supernatant into pot. Repeat until the mass of the residue becomes constant.
3. Wash residue into crucible with about 60 mL of water. Boil briefly. Decant into cones. Stir, then centrifuge 5 minutes at 2250 RPM. Pour supernatant into pot. If any appreciable residue remains check with dissolver personnel. Wash filter several times with water to remove the Cl- from the filter. (No yellow color.)
4. Transfer precipitate quantitatively from both cones into crucible. To make this transfer it is recommended that you bring 20 to 30 mL of water to boiling in the

crucible then divide it between the cones. Mix well with the stirring rod and return it to the crucible. If precipitate is at all gelatinous, contact dissolver personnel for a NaOH treatment. Otherwise, add a little HF to the cones and work it around well with the stirring rod and return it to the crucible. Wash cones with water. Notify the dissolver personnel to check the cones for activity. For all subsequent operations use one cone for the tare and the other for the sample. TIP: Place the tare cone in the centrifuge with the drip tip down to differentiate it from the sample cone.

5. If the NaOH treatment was used, evaporate solutions in the crucible to HClO4 fumes; otherwise, evaporate it to a volume of 5 to 10 mL. Add 25 mL HNO3 to the crucible and THEN put filter in. Thoroughly break up the filter. Then add about 25 mL of HClO4 and if the precipitate was not gelatinous 15 mL of HF. Evaporate nearly to dryness (about 2 mm depth).
6. Add about 30 mL 6M HCl to crucible (Note 1), washing the inside of the crucible thoroughly. Boil 2 minutes, then transfer quantitatively to a single cone and centrifuge 5 minutes at 2250 RPM. Pour supernatant into pot. If there is still a residue which appears:
   A. Gelatinous in any amount: Consult with dissolver personnel,
   B. Like fine powder: transfer residue to crucible with 6M HCl, add 10 mL HF to crucible. (Do not put HF in cone.) Evaporate to dryness (sides of crucible must be dried.) Add 20 mL of 6M HCl and boil 2 minutes. Centrifuge 5 minutes. Pour supernatant into pot. Repeat until counts of residue is

negligible or cleared by the dissolver personnel. If mass of residue ceases to reduce, consult dissolver personnel.

7. Before adjusting final pot volume, check with dissolver personnel.

NOTE 1: If Au carrier is present, notify dissolver personnel and they will add a few crystals of NaClO3 to the 6M HCl. Dissolve the NaClO3 and the HCl and thoroughly wash the sides of the crucible to dissolve the plated Au.

At the end of this procedure there was a small amount of residue (less than one percent of the initial mass) remaining. The remaining residue was discarded and the final pot solution was approximately 250 mL in 6 M HCl.

CURRICULUM VITAE

Chad B. Durrant

EDUCATION

The Pennsylvania State University, University Park, PA **August 2010-Present**

- Dissertation: "Chemical Signatures for Unknown and Interdicted Samples in the Environment for Nuclear Forensic Analysis"
- Advisor: Prof Kenan Ünlü, Dr. Annie B. Kersting, Dr. Dawn A. Shaughnessy
- MSc., Nuclear Engineering, 2014
- Dissertation: "Characterization of Italian Tile Samples Using Comparative Neutron Activation Analysis in the Penn State Breazeale Nuclear Reactor"

Brigham Young University, Provo, UT **August 2003-April 2010**

- B.S., Chemical Engineering, 2010
- B.A., Korean, 2010

EXPERIENCE

Idaho National Laboratory-Intern **May 2010-August 2010**
Rio Tinto-Kennecott Copper-Intern **April 2009-July 2009**
Brigham Young University-Research Assistant **September 2007-May 2010**

PUBLICATIONS

Journals

1. Durrant, C. B., Begg, J. D., Zavarin, M., Ünlü, K., Kersting, A. B. "Reversibility of plutonium in a multi-mineral system" in preparation, 2017
2. Durrant, C. B., Begg, J. D., Zavarin, M., Ünlü, K., Kersting, A. B. "Cesium sorption reversibility and kinetics on illite, montmorillonite, and kaolinite" Sci. Total Environ. 2017. (Submitted)
3. Johnsen, A. M., Heidrich, B. J., Durrant, C. B., Bascom, A. J., Ünlü, K. "Reactor Production of ^{64}Cu and ^{67}Cu Using Enriched Zinc Target Material." *J. Radioanal. Nucl. Chem.* 2015

Conference Proceedings

1. Johnsen, A. M., Durrant, C. B., Ünlü, K. "Characterization of Italian Tile Samples Using Comparative Neutron Activation Analysis." Proceedings of the American Nuclear Society 2013 National Winter Meeting, Washington, DC. November, 2013.
2. Bender, S. E., Durrant, C. B., Heidrich, B. J., Ünlü, K. "Nondestructive Gamma Ray Burnup Analysis of Penn State TRIGA Reactor Used Fuel Rods." Institute of Nuclear Materials Management 2013 National Meeting, Palm Desert, CA. July 2013.
3. Johnsen, A. M., Durrant, C. B., Heidrich, B. J., Ünlü K. "Reactor Based Production and Purification of ^{64}Cu and ^{67}Cu." Proceedings of the American Nuclear Society 2012 National Meeting, Chicago, IL. June 2012.

Other

1. Durrant, C. B. "Characterization of Italian Tile Samples Using Comparative Neutron Activation Analysis in the Penn State Brezeale Nuclear Reactor." *M.Sc. Dissertation*. May 2014.
2. Johnsen, A. M., Heidrich, B. J., Durrant, C. B., Bascom, A. J., Ünlü, K., "Development of Innovative Radioactive Isotope Production Techniques at the Pennsylvania State University Radiation Science and Engineering Center." *DOE Tech. Rep.* 2013. DE-FG02-10ER41689